Propagation Modeling For Land Mobile Satellite Communications

by

W. Scott Bradley

Thesis submitted to the Faculty of the

Virginia Polytechnic Institute and State University

in partial fulfillment of the requirements for the degree of

MASTER OF SCIENCE

in

Electrical Engineering

APPROVED:

W. L. Stutzman, Chairman

C. W. Bostian

T. T. Ha

T. Pratt

July, 1985

Blacksburg, Virginia

Propagation Modeling For Land Mobile Satellite Communications

by

W. Scott Bradley

W. L. Stutzman, Chairman

Electrical Engineering

(ABSTRACT)

Satellite systems are being planned for two-way communication with mobile vehicles using UHF and L-band frequencies. Of special concern in the system design are the characteristics of propagation in suburban and rural areas where fading occurs due to multipath effects and vegetative shadowing. A review of the literature was performed to study these propagation impairments. Available experimental data are examined, compared, and summarized. Propagation through vegetation is studied in order to compare reported modeling efforts and to determine the parameter dependences of path loss. A simple deterministic path model is then presented to estimate vegetative path loss. An overall statistical model is also proposed to describe the signal level fading statistics. The statistical model is compared to data, and the deterministic path model is used to determine the mean of signal level distribution functions in the presence of shadowing.

ACKNOWLEDGEMENTS

I would like to thank my advisor, Dr. Warren Stutzman, for his helpful suggestions, his patience, and his optimism during the changes in the technical and political direction of this project. I would also like to thank the other members of my advisory committee, Drs. Bostian, Ha, and Pratt, for their valuable instruction during my graduate program.

In addition, I am grateful to the following people: the members of the Satellite Communications Group, for their words of encouragement; Dr. Beex, for his helpful comments; the Jet Propulsion Lab, for funding this project; and , for her skill and long hours in preparing this manuscript.

Finally, I wish to thank my family and friends for their support and encouragement. In particular, I am grateful to my fiancee, , for her love and understanding during the discouraging parts of this project.

TABLE OF CONTENTS

I. INTRODUCTION

Telecommunication services to mobile users have become increasingly popular with the advent of cellular mobile radio technology. However, access to these networks is available usually only in metropolitan centers. Providing similar services to rural or remote users with the same technology is not feasible or cost effective. For the past decade NASA has studied the use of a geostationary satellite to fill the gap. Initial concepts for a land mobile satellite system (LMSS) have been discussed by Knouse in [41] and [42]. This system is expected to provide voice and data communications to mobile users over a wide geographical area for applications such as dispatch, emergency rescue, position location, and mobile telephone; it will also extend the range of existing terrestrial based cellular systems.

The first phase of NASA's technology development program for LMSS is called the Mobile Satellite Experiment (MSAT-X) which is managed by the Jet Propulsion Laboratory (JPL). A good overview is given by Naderi et al. in [52] and in [51]. This program is aimed at developing and testing the ground segment technologies required for a more advanced second generation system. These technologies including vehicle antennas, voice processing schemes, spectrally efficient modulation, and fade resistant coding. Current goals are to use 2.4 kbps digital voice or data in a 5 kHz channel with GMSK (Gaussian minimum shift keying) modulation. The experimental part of the program will be two years of testing using the

first generation MSAT satellite; the launch date is around 1988. The operational frequencies will be on four UHF bands (821-825, 845-851, 866-870, and 890-896 MHz) pending FCC allocation; FCC applicants are also requesting allocations at L-band (1.6 GHz) for future growth [51].

The proper selection of modulation and coding schemes requires knowledge of the LMSS channel, and the channel characteristics are a function of the propagation effects. The selection of link margins to provide adequate signal power is also directly dependent upon propagation effects. (See Gardner [31], Reudink [60], and Sandrin [65]) Consequently, the success or failure of LMSS depends heavily upon the knowledge of propagation impairments and the steps taken to defeat them. At present, the propagation problem is not well understood, and its complexity defies simple description. As a result, this topic is becoming an area of active research.

This report is an initial look at the LMSS propagation problem by the Virginia Tech Satellite Communications Group. The major portion of this effort has been a thorough review of the literature in order to determine the state-of-the-art of the problem and to identify the critical issues. After some general study of the entire problem, the focus finally narrowed to a study of propagation through vegetation and ways to model the effects of vegetative shadowing on LMSS signals. The end results are a simple deterministic model to estimate the mean vegetative path loss and a statistical model to describe the overall signal level fading statistics when vegetative shadowing is present in some fraction.

Chapter 2 is intended to be background material. It presents the expected sources of signal degradation and definitions for the signal fading statistics. Chapter 3 extensively reviews reported propagation measurement data from experiments using either simulated or actual satellite sources, and it compares some of the results. Chapter 4 is a brief review of reported modeling and channel simulation efforts. Chapter 5 discusses the results of a study on propagation through vegetation. It includes reported efforts to model vegetative path loss and a summary of parameters affecting propagation. Chapter 6 presents a proposed modeling approach for describing the mean vegetative path loss, the signal level fading statistics, and the relationship between the two. Chapter 7 finishes with conclusions and recommendations for future study.

II. PROPAGATION MECHANISMS AND SIGNAL CHARACTERISTICS

2.1 INTRODUCTION

The propagation effects on a land-mobile satellite system are different from those on a fixed satellite system and those on a terrestrial mobile radio system. A fixed-service satellite utilizes highly directive antennas and is relatively free from the multipath and shadowing effects found in a land-mobile system with smaller, less directive antennas. A terrestrial mobile radio system is typically dominated by multipath fading and blockage by terrain obstacles because of the extremely low elevation angles while propagation impairments for land mobile satellite systems are less severe and unblocked line of sight conditions often prevail.

The received signal arriving at the land mobile antenna has three components: a direct wave, a specularly reflected wave, and diffusely reflected waves. The direct wave is the line of sight (LOS) signal from the satellite. It is affected by tropospheric and ionospheric effects. The specular component is a reflection from an apparently "smooth" surface near the vehicle and combines coherently with the direct component. The diffuse component is basically everything else: all the scattered energy from the rough terrain in the vicinity of the vehicle. These three components are shown in Figure 2.1-1. Finally, there are vegetative and

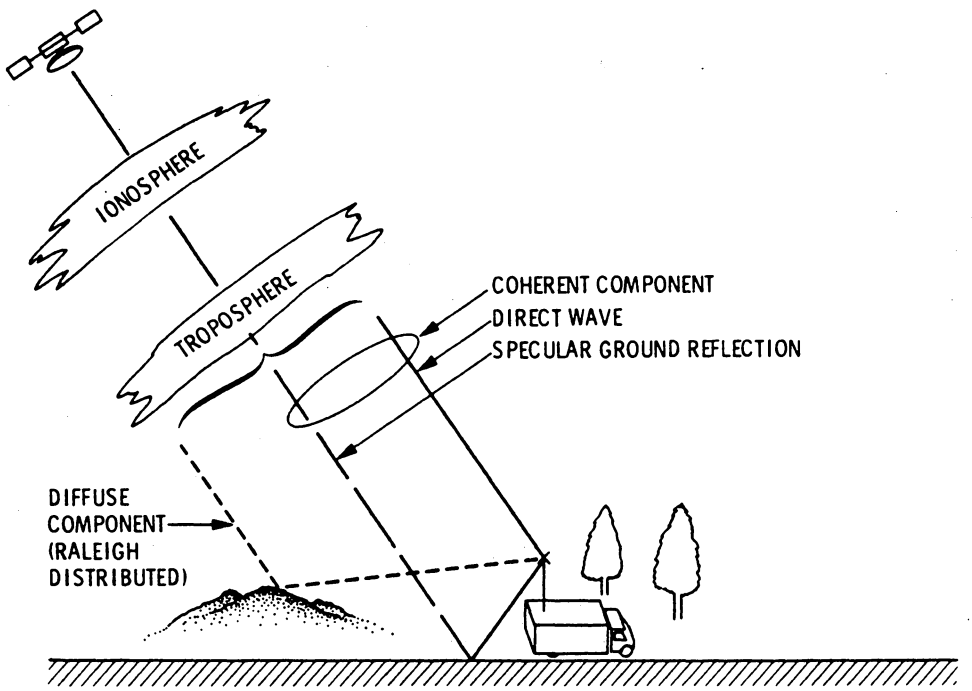

Figure 2.1-1 A physical representation of the LMSS channel showing the direct, specular, and diffuse components. From Vogel and Smith [76]

man-made shadowing effects; these obstacles will attenuate both the direct and specular components.

The first part of this chapter will highlight the current theory for describing the propagation mechanisms affecting LMSS operation. Section 2.2 is a summary of the basic physics with much of the material being drawn from the more complete reports of Smith et al. [69], Flock [28], and preliminary CCIR Study Group 5 documents [21]. Section 2.3 discusses two approaches to describing diffuse scattering and concludes that a statistical model is currently the best choice. The last part of the chapter deviates from propagation issues. Section 2.4 summarizes some of the probability concepts and methods of describing fading signals. This section serves as background for the discussion in later chapters.

2.2 PHYSICS

2.2.1 DIRECT COMPONENT

The direct component is principally affected by shadowing obstacles on the earth's surface, but it may also be degraded by ionospheric and tropospheric effects. In this section we will consider these latter effects first.

As the direct wave passes through the ionosphere, the earth's magnetic field and the ambient electron content combine to cause Faraday rotation, group delay, absorption, dispersion, refraction, and scintillation of the

Table 2.2-1
Estimated maximum ionospheric effects for an elevation angle of 30°, one way propagation, and assuming a zenith electron column of 10^{18} electrons/m^3. From Smith et al. [69]

Effect	Frequency Dependence	Magnitude	
		850 MHz	1600 MHz
Faraday Rotation	$1/f^2$	150°	42°
Propagation delay	$1/f^2$	0.35s	0.1s
Variation in direction of arrival	$1/f^2$	16 sec. of arc	4.7 sec of arc
Refraction	$1/f^2$	> 50"	> 14"
Absorption (mid-lats)	$1/f^2$	>0.014 dB	>0.004 dB
Dispersion	$1/f^3$	0.65 nsec/MHz	0.1 nsec/MHz

signal. Table 2.2-1 summarizes the extreme values for these effects at possible LMSS frequencies assuming an elevation angle of 30°, one way traversal, and a zenith election content of 10^{18} electrons/m^3. The table shows the most significant effect to be Faraday rotation; however, use of circular polarization is expected to minimize this problem. Scintillation effects have typically been ignored for LMSS operation because the problem is seldom serious for elevation angles above 10° and frequencies below 10 GHz [76].

Tropospheric effects on the direct component result from the presence of moisture in the lower atmosphere. Table 2.2-2, from reference [21] and drawn from various CCIR reports, summarizes the predicted tropospheric losses for an elevation angles of 30° and one-way propagation. The table shows that the expected losses are negligible.

In contrast to atmospheric effects, the problem of vegetative shadowing of the LOS component is not well understood. Since analysis of this problem was a larger part of this effort, vegetative shadowing is discussed as a separate topic in Chapter 5.

2.2.2 SPECULAR COMPONENT

The specular component is a coherent ground reflection from the surface in the vicinity of the mobile receiver. While the original theory to describe this component is attributed to Beckmann and Spizzichino [5], several other concise treatments have been reported in the literature.

Table 2.2-2
Estimated tropospheric attenuation for an elevation angle of 30° and one way propagation. From [21]

Effect	Magnitude (dB)	
	850 MHz	1600 MHz
Clear air absorption		
3 g/m^3 (dry)	0.06	0.07
7.5 g/m^3 (average)	0.06	0.07
17 g/m^3 (moist)	0.06	0.07
Cloud attenuation		
0.5 g/m^3, 1 km thick	<0.01	<0.01
1 g/m^3, 2 km thick	<0.01	<0.01
Fog attenuation		
0.05 g/m^3 (average), 0 to 75m ht.	---	---
0.05 g/m^3 (heavy), 0 to 150m ht.	---	---
Rain attenuation		
5 mm/h	<0.01	<0.01
25 mm/h	<0.1	<0.1

These include the references mentioned in the introduction and reports by Butterworth [13], Jamnejad [40], and Salmasi [62].

It is widely agreed that the specular component will be reflected from the region of the first Fresnel zone on the scattering surface. This region is elliptical; its size and location depend upon the height of the antenna, the wavelength, and the grazing angle. (The basic equations for the ellipse size and location are given in Beckmann and Spizzichino [5].) Salmasi [62] has shown that at 850 MHz and a grazing angle of 21°, the major and minor axes of the first Fresnel zone are approximately 9 m and 2 m respectively, and centered 9 m in front of the mobile. For a grazing angle of 57°, the ellipse major and minor axes shrink to 2 m and 1 m, respectively, with the center 1.8 m in front of the mobile. Reference [21] reports Fresnel zone sizes at other grazing angles and frequencies. Generally, the Fresnel zone size will decrease with increasing grazing angle and frequency.

The magnitude of the specular component is determined by the reflection coefficient for the surface in the first Fresnel zone. From a simple model from Beckmann and Spizzichino [5], the specular reflection coefficient, R_s, may be calculated as:

$$R_s = \rho_s \, D \, R_o \qquad (2.2\text{-}1)$$

where ρ_s is the surface roughness factor, D is the curved earth divergence factor, and R_o is the complex voltage reflection coefficient for smooth, plane earth and the appropriate polarization.

The surface roughness factor, ρ_s, accounts for the deviation of the reflecting surface from a truly smooth surface. It is a function of the grazing angle, the wavelength, and the standard deviation of surface irregularities as given theoretically in references [76] and [5]. ρ_s is nearly one for approximately "smooth" surfaces (i.e., those with very small surface irregularities or for small grazing angles), but it drops off rapidly for increasing surface height variations. The curved earth divergence factor, D, is usually only important for high altitude mobiles such as aircraft and is assumed to be unity for LMSS operation. The complex voltage reflection coefficient, R_o, can be calculated from the surface conductivity, the relative permittivity of the reflecting surface, and the grazing angle.

Analysis of the reflection coefficient components for circularly polarized waves shows that reflected waves will be elliptically polarized. For grazing angles below the Brewster angle, which may vary from 6 to 27°, the reflected wave will be elliptically polarized with the incident sense of rotation dominant. For grazing angles above the Brewster angle, the reflected wave will be elliptically polarized with the opposite sense of rotation from the incident wave dominant. Figure 2.2-1 from Butterworth [13] shows the reflection coefficients for the left hand (LHCP) and right hand circularly polarized (RHCP) components for an

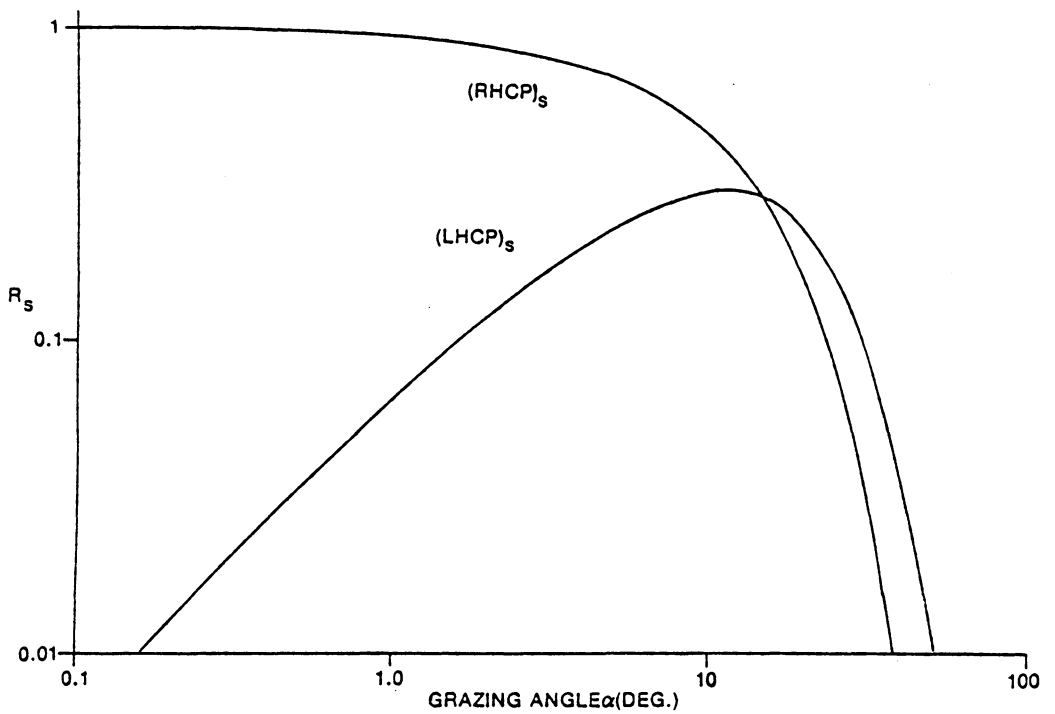

Figure 2.2-1 Components of the specular reflection coefficient as a function of the grazing angle for a RHCP incident wave at 870 MHz. From Butterworth [13]

incident RHCP wave. Medium dry soil, a frequency of 870 MHz, and a surface irregularity standard deviation of 0.1 m are assumed. Note that the opposite polarization, LHCP, dominates above the Brewster angle at 15°.

In order to determine the overall effect of the specular component, the effects of the mobile antenna pattern must also be considered. First, the specular component arrives at angles below the horizon where the antenna gain is several dB below the main beam gain, depending upon the antenna design. Second, the polarization discrimination of the antenna will attenuate the major component of the reflected wave for angles above the Brewster angle. Jamnejad's analysis [40] has shown the specular component to be 10 dB or more below a line of sight component for elevation angles above 20°; he assumed a frequency of 400 MHz and used a variety of terrain constants. A practical example, given in reference [21] and using typical parameters for LMSS, showed the specular component to be 23.5 dB below the LOS component and caused peak fluctuations in the signal level of only 0.22 dB. Finally, Butterworth's [13] analysis, which also included vehicle antenna effects, showed fade depths from specular interference to be less than 1 dB for elevation angles above 20°. Consequently, the influence of the specular component is expected to be negligible on LMSS links with elevation angles greater than 20°.

2.2.3 DIFFUSE COMPONENT

The diffuse component represents the sum of all of the waves scattered from the terrain around the mobile but outside the first Fresnel zone. The principal contribution is expected to come from the strip of area along the projection of the LOS component on the ground. Its interference with the direct component causes rapid fluctuations in the received signal level. Again, one of the most complete, practical treatments of the diffuse component is by Beckmann and Spizzichino [5]. The phase of this component is incoherent (uniformly distributed), and its amplitude is taken to be Rayleigh distributed. A simple relationship to determine the average magnitude of the diffuse component is given as:

$$R_d = \rho_d R_o \qquad (2.2\text{-}2)$$

where R_d is the diffuse reflection coefficient, ρ_d is the diffuse scattering coefficient, and R_o is the plane earth reflection coefficient. This equation is similar to (2.2-1) for the specular component. ρ_d is, in a way, inversely related to ρ_s, and it approaches unity for rougher surfaces. For non-directional antennas and very rough surfaces, values for ρ_d have been reported to range from 0.2 to 0.4 with R_d having an average value of 0.35. If the scattering surface is absorptive (i.e., it is covered with vegetation) then R_d will be on the order of 0.1 [5].

Again, the antenna pattern will affect the influence of the diffuse multipath on the received signal. Most of the diffuse waves are expected

to arrive at the horizon or 0° point of the antenna elevation gain pattern; another approximation would consider them to be distributed ± 10° about the horizon [76]. Consequently, the contribution of the diffuse component will require integration over the relevant portion of the antenna gain pattern. A steep gain rolloff at the horizon will discriminate against low angle multipath. Additionally, the polarization state of the diffuse component is not known so the effect of antenna cross-polar discrimination cannot be exactly determined. If the average R_d is assumed to range from 0.2 to 0.4, the diffuse component contribution will be 8 to 14 dB below the direct component. Analysis by Jamnejad [40], which included antenna effects, predicted a diffuse to direct component ratio of -18 dB or less for elevation angles above 20°. However, even though the average diffuse component is very small with respect to the direct component, one must keep in mind that it is Rayleigh distributed so fades as large as 5 dB can be expected for small percentages of time. Consequently, the effect of the diffuse component on the signal fading statistics cannot be ignored.

2.2.4 COMBINATION OF THE COMPONENTS

The received signal at the mobile antenna output, R_{total}, is found from the vector sum of the direct, R_{dir}, the specular, R_{spec}, and the diffuse, R_{dif}, components. Using the notation of Smith et al. [69]:

$$R_{total} = R_{dir} + R_{spec} + R_{dif} \qquad (2.2\text{-}3)$$

The direct and specular components combine coherently. The magnitude of their sum is:

$$|R_{dir} + R_{spec}| = |R_{dir}| \ (1 + g_x \ |R_s|) \approx |R_{dir}| \qquad (2.2\text{-}4)$$

where g_x is the cross polar antenna gain and $|R_s|$ is the magnitude of the specular reflection coefficient; their product is assumed to be very small. The magnitude of the total is given as:

$$|R_{total}| \approx |R_{dir} + R_{dif}| = |R_{dir}| \ (1 + |R_d|) \qquad (2.2\text{-}5)$$

where $|R_d|$ is the magnitude of the diffuse reflection coefficient. $|R_d|$ is Rayleigh distributed so $|R_{total}|$ will be Rice distributed.

If the direct component is shadowed by a factor, F, then the total signal magnitude is given as:

$$|R_{total}| = |R_{dir}| \ (F + |R_d|) \qquad (2.2\text{-}6)$$

Further discussion of the signal fading statistics is treated in later sections.

2.3 APPROACHES TO THE MODELING OF DIFFUSE SCATTER

The diffuse component reflected from the terrain causes a significant portion of the fading on LMSS links. Consequently, being able to describe

the characteristics of this component is highly desirable. So far, two basic approaches have been taken to describe diffuse scattering; they are not independent. The first is a full analytical model that tends to view diffuse scattering from a microscopic level. The second approach is a statistical model which views diffuse scattering from a macroscopic level. The following two sections discuss each approach and concludes that a statistical model will provide more immediate results to the LMSS problem.

2.3.1 ANALYTICAL APPROACH

The full analytical approach starts with basic electromagnetic theory to describe the amplitude, phase, and depolarization of waves scattered from rough surfaces. This issue has been studied for the past several decades and is still an area of active research. (A list of many of the literature reports has been assembled by A. B. Salmasi at JPL [63].) Recent work by Bahar [4] was reviewed in order to determine the applicability of current analytical models. In his papers, an "exact" solution for the scattered field from a rough surface is developed. His rigorously derived solution requires knowledge of the height and slope of the surface irregularities. Since a wide variety of terrain conditions are expected for LMSS, extracting a useful model to describe the diffuse component from Bahar's work would not be a trivial exercise, especially for surfaces covered with absorptive material such as grass or shrubs. A recent lecture by Gary Brown [10] on his rough surface scattering work also

showed that analytical models have a way to go before they can be expected to provide a practical solution to the LMSS diffuse scatter problem.

2.3.2 STATISTICAL APPROACH

This approach to describe scattering takes a macroscopic view because it assumes that the resultant amplitude and phase of the diffuse waves can be described by their statistical properties without regard to the actual surface variations and electromagnetic theory that are essential to an analytical approach. However, the two approaches are not unrelated; the statistical model approximates the "exact" solution from the analytical approach, and an analytical approach can be useful in determining the parameters of the statistical model. Thus, changes in the physical characteristics of the scattering surface can be modeled by changing statistical parameters such as mean or standard deviation. Also, statistical models can be easily justified by experiment. The theoretical reasoning behind choosing a Rayleigh distribution to describe the diffuse component has been treated by Flock [28], Beckmann and Spizzichino [5], and others in [6], [39], [47], and [54]. A brief summary of their arguments is given here.

The diffuse component may be considered to be the sum of many phasors with amplitude A_i and phase ϕ_i. In equation form:

$$Re^{j\theta} = \sum_{i=1}^{n} A_i \, e^{j\phi_i} \qquad (2.3\text{-}1)$$

If the following conditions are satisfied: the mean square value of each A_i is much smaller than the mean square value of R, each ϕ_i is uniformly distributed, and n is sufficiently large; then R can easily be proven to be Rayleigh distributed and θ uniformly distributed. (The A_i's may be arbitrarily distributed.) The given conditions are reasonable assumptions for scattering from a rough surface so the Rayleigh model seems to be theoretically well justified.

2.4 FADING SIGNAL CHARACTERISTICS

The statistical behavior of fields and signals for terrestrial mobile communications has been extensively developed. Two good texts by Lee [47] and Jakes [56] are available on the subject in addition to many papers like those by Clarke [22], Gans [30], and Lin [48]. Much of the theory can be applied to the LMSS problem or at least serve as a guide in the analysis.

2.4.1 ENVELOPE LEVEL STATISTICS

As the vehicle moves, it travels through a standing wave field set up by the sum of the direct component and the multipath components; the multipath component will cause rapid fluctuations in the received signal, while shadowing will cause slower, deeper fading. If the direct component were ignored, then the received signal would just be the resultant of the multipath components, and the received signal envelope would be Rayleigh

distributed by the argument presented earlier. The expression for a Rayleigh probability density function is given as:

$$p(r) = \frac{2r}{\alpha^2} \exp(-r^2/\alpha^2), \quad r \geq 0 \qquad (2.4\text{-}1)$$

$$= 0 \quad , \quad r < 0$$

where r is the envelope (voltage) of the received signal and α^2 is the mean square value or the average power of r.

Usually though a direct component is present on satellite links so the received signal, $re^{j\theta}$, in the absence of shadowing may be expressed as:

$$re^{j\theta} = Ae^{j\phi_o} + we^{j\phi} \qquad (2.4\text{-}2)$$

where A is the constant, direct component (ϕ_o is the reference phase) and w is the Rayleigh distributed multipath interference (ϕ is uniformly distributed). Norton et al. [54] and Beckmann [6] have shown that r, in (2.4-2), will have a Rice (or Rice-Nakagami) distribution. Following their notation, the Rice probability density function is expressed as:

$$p(r) = \frac{2r}{k^2} \exp[-(A^2+r^2)/k^2] \, I_o(2Ar/k^2), \quad r \geq 0 \qquad (2.4\text{-}3)$$

$$= 0 \quad , \quad r < 0$$

$$\text{where } k^2 = \alpha^2/A^2 \qquad (2.4\text{-}4)$$

I_o is the modified Bessel function of zero order and α^2 is the average power in the Rayleigh component. For a unit amplitude constant component, (2.4-3) and (2.4-4) reduce to

$$p(r) = \frac{2r}{k^2} \exp[-(1+r^2)/k^2]\ I_o(2r/k^2),\ r \geq 0 \qquad (2.4\text{-}5)$$

$$= 0 \qquad , r < 0$$

$$\text{and} \quad k^2 = \alpha^2 \qquad (2.4\text{-}6)$$

(2.4-5) shows that a Rice distribution can be completely specified by the parameter k or by its decibel equivalent, K, which is more commonly used in the literature; K is defined as $20 \log_{10} k$. K may be interpreted as the power in the Rayleigh component relative to the power in the constant component.

The lognormal distribution is also referred to in later chapters to describe shadowing effects. For future reference, its probability density function may be written as (from Lee [47]):

$$p(r) = \frac{1}{\sqrt{2\pi}\ \sigma\ r} \exp\ [-(\ln r-\mu)^2/2\sigma^2],\ r \geq 0 \qquad (2.4\text{-}7)$$

$$= 0 \qquad , r \leq 0$$

where μ and σ are the mean and standard deviation of lnr. If r is converted to its dB form, R, with R defined as 20 $\log_{10}$r, then it will be normally distributed.

$$p(R) = \frac{1}{\sqrt{2\pi}\ \sigma_R} \exp[-(R-\mu_R)^2/2\sigma_R^2] \qquad (2.4\text{-}8)$$

where μ_R and σ_R are the mean and standard deviation of R. μ_R and σ_R are related to μ and σ of (2.4-7) by the following equations:

$$\mu_R = 20\mu \log_{10}e \quad \text{dB} \qquad (2.4\text{-}9)$$

$$\sigma_R = 20\sigma \log_{10}e \quad \text{dB} \qquad (2.4\text{-}10)$$

where e is the base of the natural logarithm, 2.7183.

The established method of displaying signal level or fade depth information is with a cumulative distribution function (or simply, distribution function) typically plotted on normal probability paper. A cumulative distribution function (CDF) can refer to the function for which the signal exceeds a level R, G(R), or to the function for which the signal is below a level R, F(R). G(R) and F(R) are defined as:

$$G(R) = P\{r > R\} = \int_R^\infty p(r)dr \qquad (2.4\text{-}11)$$

$$F(R) = P\{r \leq R\} = \int_0^R p(r)dr \qquad (2.4\text{-}12)$$

where p(r) is the probability density function (pdf) of the received signal level. From probability theory (Papoulis [56]), the following properties apply to G(R) and F(R):

$$0 \leq F(R) \leq 1 \tag{2.4-13}$$

$$F(-\infty) = 0,\ F(+\infty) = 1 \tag{2.4-14}$$

$$F(M) = 0.5 \quad \text{when } M = \text{median value} \tag{2.4-15}$$

$$F(R_1) \geq F(R_2) \quad ,\quad R_1 > R_2 \tag{2.4-16}$$

$$G(R) = 1 - F(R) \tag{2.4-17}$$

A specially designed paper (called probability paper) is available for the display of CDF's. The abscissa has a nonlinear probability scale for G(R) or F(R) in percent and the ordinate is usually a linear scale for R. On normal probability paper, normally distributed random variables will plot as a straight line. Since the normal distribution is a symmetric function, the mean value of a normally distributed random variable, R, can be found at the 50% point. The standard deviation of R can be found from the difference in R between the 50% and 84% points or between the 16% and 50% points. Normal probability paper is used to display all the signal level CDF's henceforth.

Examples of CDF's for Rice distributed signals are given in Figure 2.4-1 for various values of K. The ordinate values represent the signal power relative to the direct, LOS component and is calculated as 20 $\log_{10} r$ for the r in (2.4-5). Examples of CDF's for a lognormally distributed signal

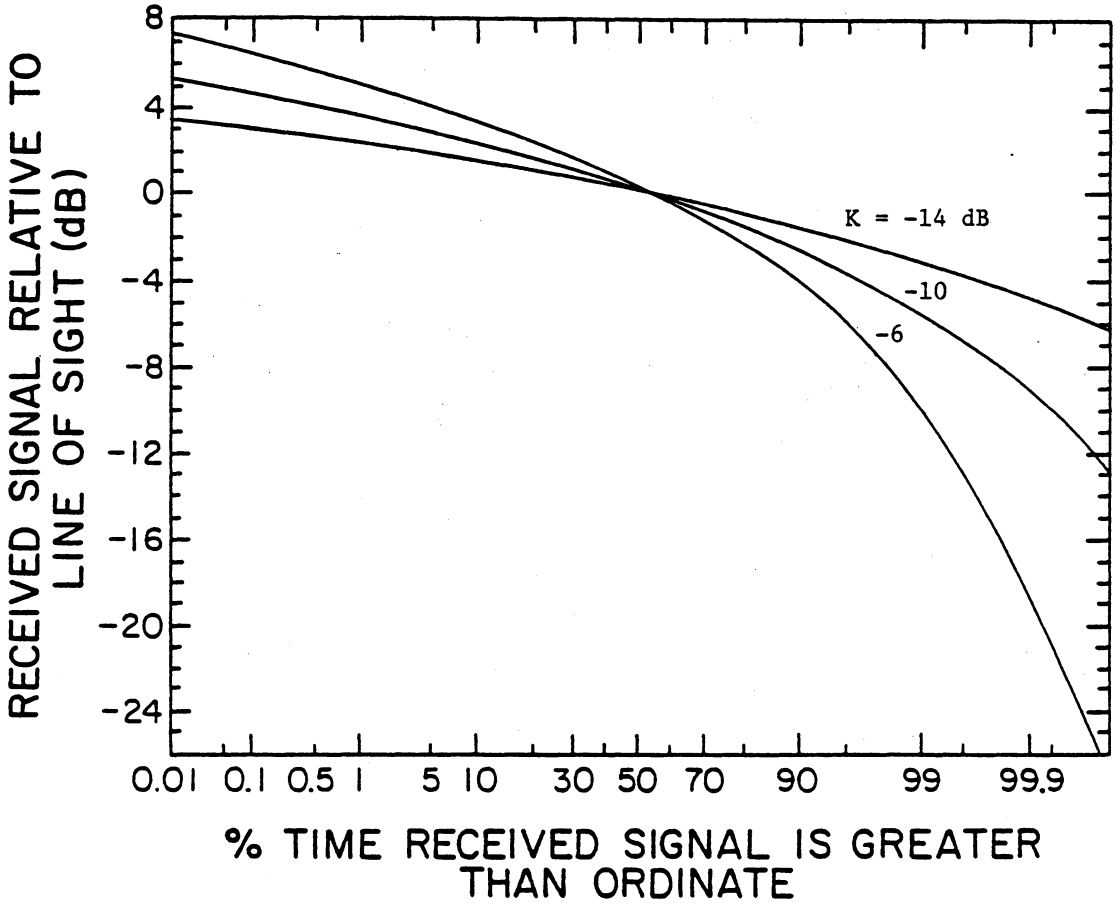

Figure 2.4-1 Cumulative distribution functions for Rice distributed signals.

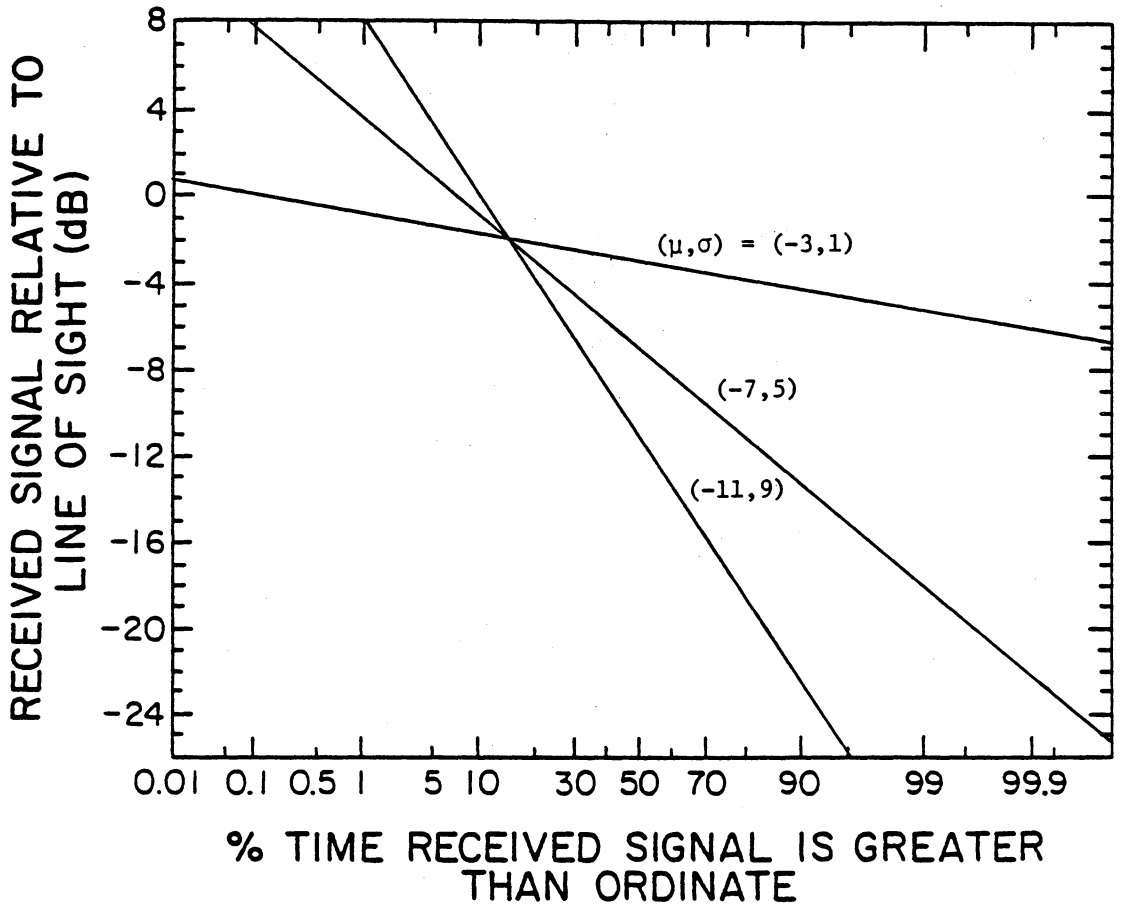

Figure 2.4-2 Cumulative distribution function for lognormally distributed signal.

are given in Figure 2.4-2 for various means and standard deviations. Note that a lognormal distribution, when expressed in dB, plots as a straight line on normal probability paper.

2.4.2 FADE RATE STATISTICS

So far the discussion has centered on the fade depth statistics and the dynamic characteristics have been ignored. For accurate channel modeling, one would also like to know about the dynamic characteristics of LMSS signals,such as at what rate fades occur and how long they last. The solution depends on the presence of shadowing, the speed of the mobile, the relative direction of the source, and the antenna pattern.

The two measures typically used in the LMSS program to describe the fading rate characteristics are the level crossing rate (LCR) and the average fade duration (AFD). These statistics are sometimes referred to as secondary statistics. They are time dependent because they are a function of the speed of the mobile.

The LCR is defined as the number of times that the signal envelope crosses a threshold level with positive slope in a given period of time. The AFD is defined as the average amount of time that the signal envelope spends below a threshold level. These two statistics are illustrated using Figure 2.4-3 which shows the signal envelope over a time period of T seconds. There are three positive level crossings marked as "1" through

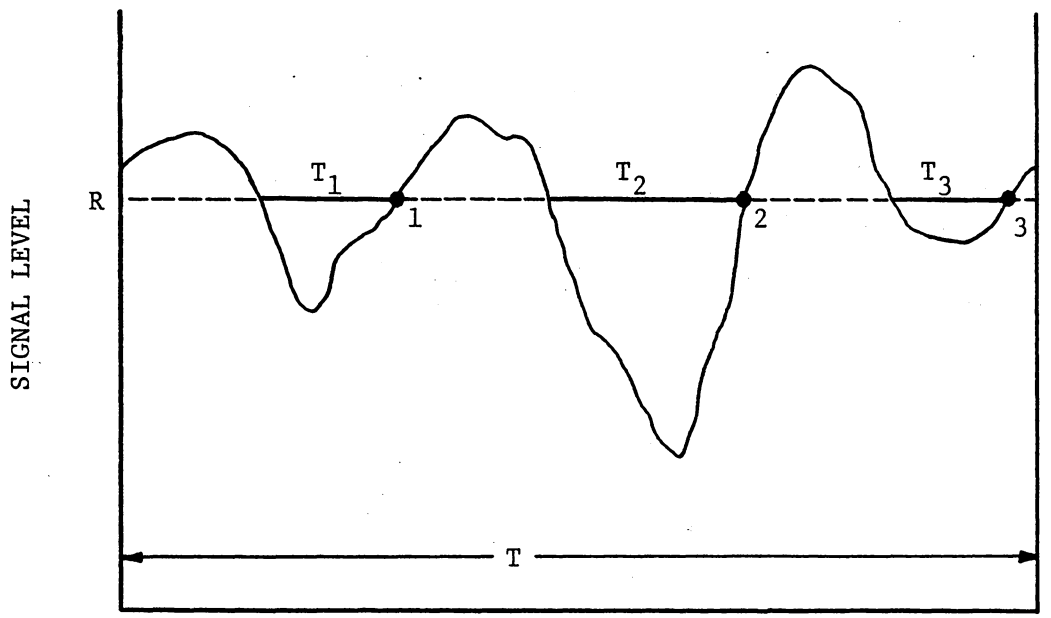

Figure 2.4-3 Signal level plot to illustrate level crossing rate and average fade duration.

"3" at threshold level R. There are also three fades below threshold level R; these are marked "T_1" through "T_3".

Consequently, the LCR, denoted as N(R), may be computed as:

$$N(R) = \frac{3}{T} \text{ crossings/sec.} \qquad (2.4\text{-}18)$$

and the AFD, denoted as T(R), may be computed as:

$$T(R) = \frac{T_1 + T_2 + T_3}{T} \text{ sec.} \qquad (2.4\text{-}19)$$

To eliminate the time parameter and the influence of vehicle speed, the LCR and AFD can be normalized by converting seconds to wavelengths of travel. The normalized LCR and AFD, denoted as N'(R) and T'(R), may then be computed from the following equations:

$$N'(R) = N(R)/N_o \text{ crossings/wavelength} \qquad (2.4\text{-}20)$$

$$T'(R) = T(R)\ N_o \text{ wavelengths} \qquad (2.4\text{-}21)$$

$$\text{where } N_o = \frac{V}{\lambda} \text{ wavelengths of travel/sec} \qquad (2.4\text{-}22)$$

V is the vehicle speed and λ is the wavelength of the transmitted signal. All subsequent plots of LCR and AFD in this report will be presented using normalized units. Normalized LCR will be given in crossings per

wavelengths of travel (denoted as $1/\lambda$), and normalized AFD will be given in wavelengths of travel (denoted as λ).

Lee [47] also presents analytical formulas for the LCR and AFD as a function of the statistical properties of the signal envelope. For the LCR:

$$N(R) = \int_0^\infty \dot{r}\, p(R, \dot{r})\, d\dot{r} \qquad (2.4\text{-}23)$$

where r is the signal envelope, $\dot{r}$ is dr/dt, and $p(R, \dot{r})$ is the joint probability density $p(r, \dot{r})$ at r=R. For the AFD:

$$T(R) = F(R)/N(R) \qquad (2.4\text{-}24)$$

where F(R) is the cumulative distribution function defined in (2.4.12). Normalization of (2.4-23) and (2.4-24) with (2.4-20) and (2.4-21) is still applicable.

From the work of Lin [48] and Loo [49] the normalized LCR of a Rice distributed signal can be found to be:

$$N'(R) = \sqrt{\pi}\, k\, p(R) \qquad (2.4\text{-}25)$$

where p(R) and k are those defined in (2.4-5) and (2.4-6). The corresponding normalized AFD using (2.4-5), (2.4-24), and (2.4-25) is

$$T'(R) = \frac{\int_0^R p(r)dr}{\sqrt{\pi}\ k\ p(r)} \qquad (2.4\text{-}26)$$

The curves for these LCR and AFD functions are given in Figures 2.4-4 and 2.4-5 for various values of K.

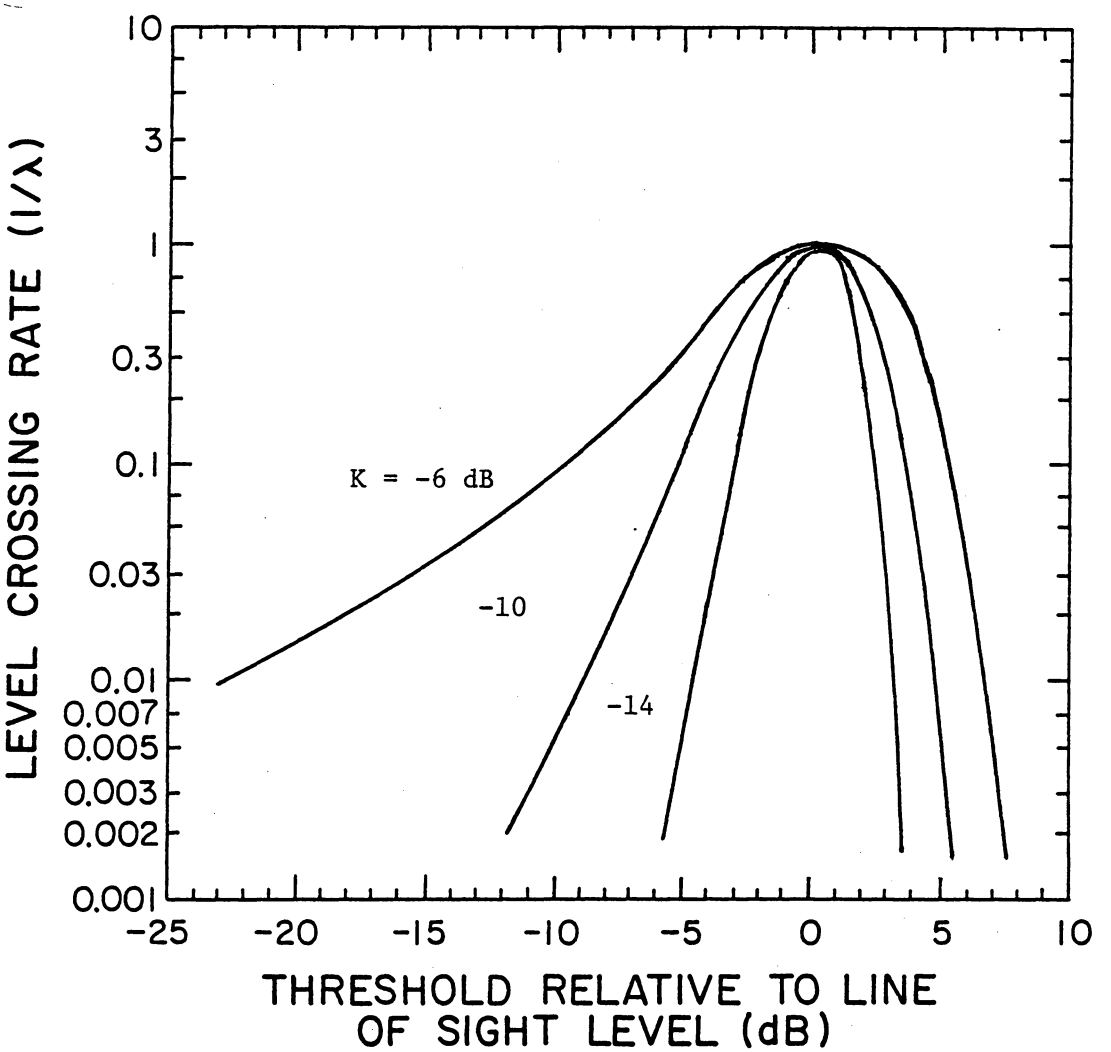

Figure 2.4-4 Normalized level crossing rate curves for Rice distributed signals.

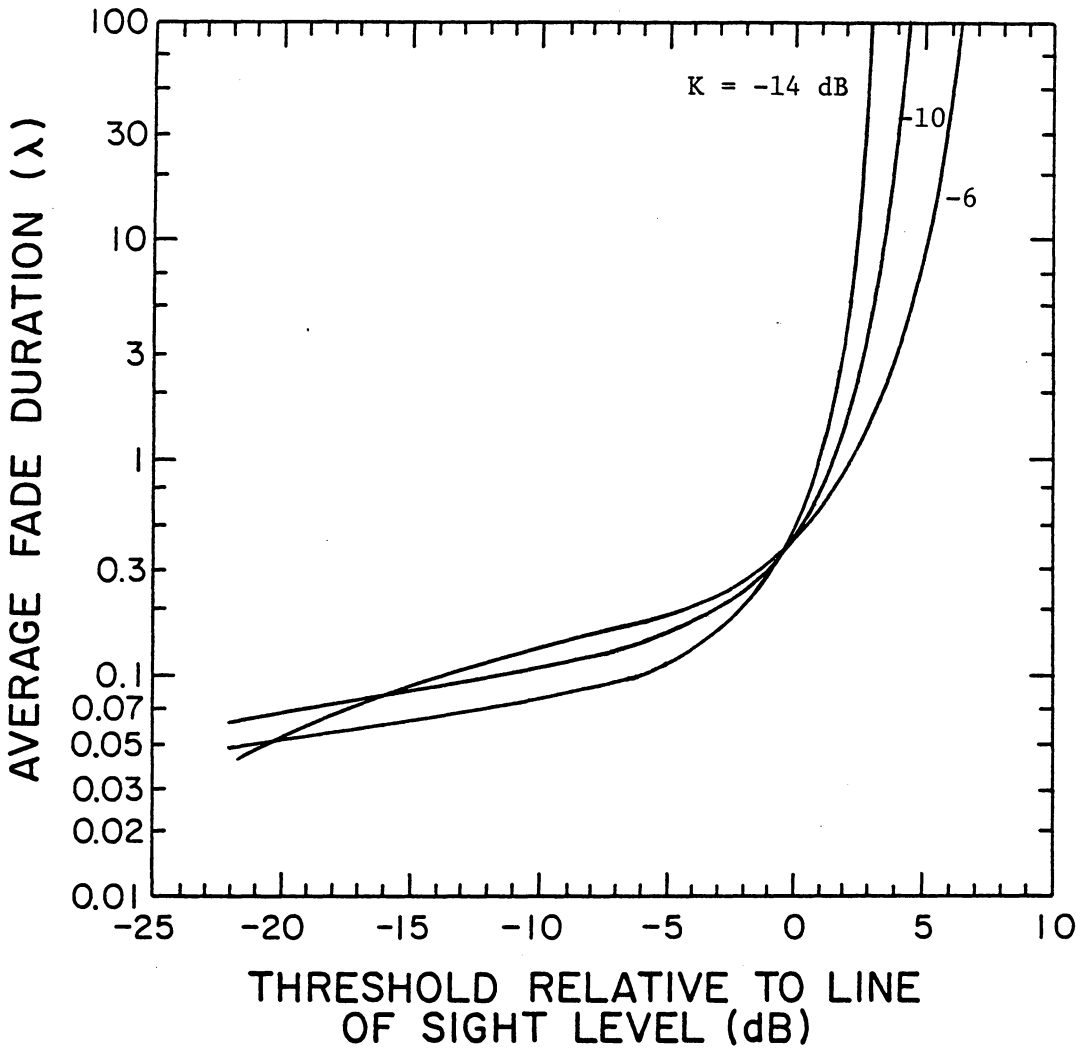

Figure 2.4-5 Normalized average fade duration curves for Rice distributed signals.

III. PROPAGATION EXPERIMENTS

3.1 INTRODUCTION

There have been only a limited number of experimental studies performed with the intent of characterizing earth-space propagation related to land mobile operations. Several studies have been performed though, both experimental and theoretical, to characterize terrestrial mobile radio performance in urban centers [7], [39], [47]. However, this information is of limited value because proposed land mobile satellite systems are expected to operate in much less severe and much different conditions. The CCIR [20] has already recognized this need for further study. This chapter discusses all of the known experimental measurements and available data to characterize satellite-to-land-mobile propagation.

Four different investigators have made measurements related to this effort. The pioneering work was performed by Garry Hess of Motorola using the ATS-6 satellite. He was followed by Roy Anderson of General Electric also using the ATS-6 satellite. More recent measurements have been made by Wolf Vogel at the University of Texas and the Communications Research Centre (CRC) of Canada. The lack of satellites operating at the frequencies of interest led Vogel to use stratospheric balloons and the CRC to use a tethered balloon and a helicopter to carry transmitters for simulating a distant satellite source. The latest phase of the CRC program has used the L-band transponder on the MARECS-A satellite.

The following four sections are a fairly detailed summary of the experiments just mentioned. Each section begins with a description of the experiment characteristics and data collection procedure. This is followed by the results of data analysis and general observations about the data. The final section concludes this lengthy discussion with a summary of the experimental results.

3.2 COMMUNICATIONS RESEARCH CENTRE MEASUREMENT PROGRAM

The Communications Research Centre (CRC) of Canada has conducted a rather large propagation measurement program to characterize the land mobile satellite channel. This section summarizes their work as published in IEEE [37] and IEE [12] papers and from more detailed internal reports [13], [14]. Initially a meteorological balloon and a helicopter were used to simulate an 870 MHz satellite source. More recent measurements have used the MARECS-A satellite as an L-band (1550 MHz) source. In each experiment a van specially equipped with receiving and data collection equipment was used as the mobile receiving station.

3.2.1 EQUIPMENT CONFIGURATION AND DATA ANALYSIS

The mobile laboratory equipment consisted of specially designed mobile vehicle antennas, a narrowband receiver, and a computer controlled data collection system. The vehicle antenna was designed to receive right hand circularly polarized (RHCP) signals with an omnidirectional azimuth pattern; the balloon and helicopter experiments used a conical log spiral

design while the MARECS-A experiment used a crossed drooping dipole design. Antenna effects will be discussed later. The receiving system consisted of a low noise amplifier and an envelope detection receiver. A field strength meter was initially used as the receiver for the balloon experiment, but all subsequent measurements used a microprocessor controlled spectrum analyzer. The receiver output was digitized by a high speed digital voltmeter and stored on disk with the entire system operated under computer control. Also a separate receiver system quadrature demodulated the signal and continuously recorded it on tape for later reconstruction in laboratory simulations.

Data samples of signal strength were taken as a function of the distance travelled and often enough to resolve the rapid fluctuations. For an 870 MHz system, samples were taken every 5 cm or about seven times per wavelength of travel. For the L-band measurements, samples were taken at 2.5 cm intervals. The general terrain features and routes taken were noted for each file in order to later combine data from similar regions or to contrast the results for varying conditions. The first step in the data analysis was to convert the data points to a dB level relative to the LOS signal level. The principal result derived from this data was the cumulative probability distribution curve of the relative received signal level. Secondary statistics curves, the level crossing rate and average fade duration, were also found from the data and normalized as discussed in Section 2.4. The average fade duration curves were computed directly from the level crossing rate and cumulative distribution of signal strength curves.

3.2.2 BALLOON EXPERIMENT

The first phase of the CRC mobile measurement program used a meteorological balloon to simulate a satellite source. The balloon carried an 840 MHz transmitter which provided an EIRP of a few milliwatts. The transmitter and receiver both used a conical log spiral antenna ; its gain pattern will not discriminate out low angle multipath.

The balloon was tethered at an altitude of about 300 m in a location to give an elevation angle of 15 to 20° from measurement routes. Measurements were only made on short runs to keep the elevation angle nearly constant. Also driving speed was limited to 6 km/hr in order to keep the received signal within the field strength meter's bandwidth.

Measurements were made over a variety of sites which included both clear line of sight and shadowed conditions. A typical cumulative distribution function for data taken under open terrain and clear line of sight conditions is shown in Figure 3.2-1. Note that a curve for a Rice distribution for a K of -14 dB has been overlayed.
Other data sets taken at different sites and at varying elevation angles also took a Rician shape with the diffuse multipath component in the range 10 to 14 dB below the LOS component; the average K was about -11 dB. The results of data taken in shadowed regions are shown in Figure 3.2-2. The shape of the curves indicate that shadowing effects tend to follow a lognormal distribution. Mean attenuations as high as 9 dB were observed with a standard deviation of 6 dB, depending on the foliage density. This

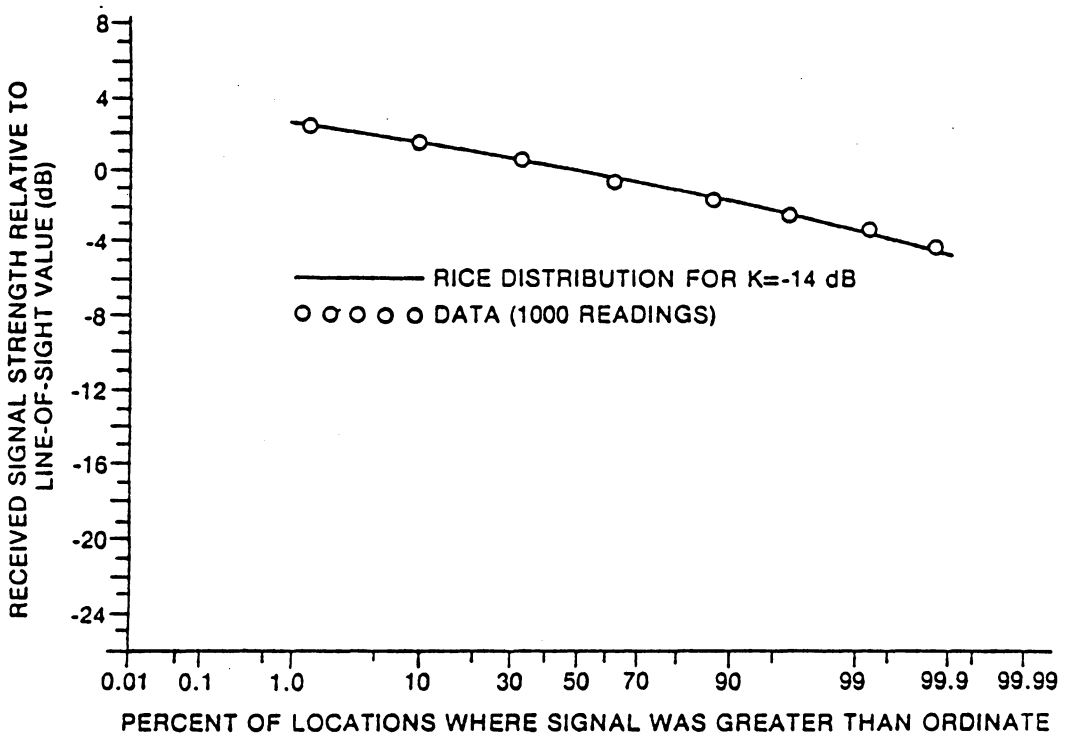

Figure 3.2-1 Comparison of the cumulative distribution function of an unshadowed data set with a Rice distribution. From Butterworth [13]

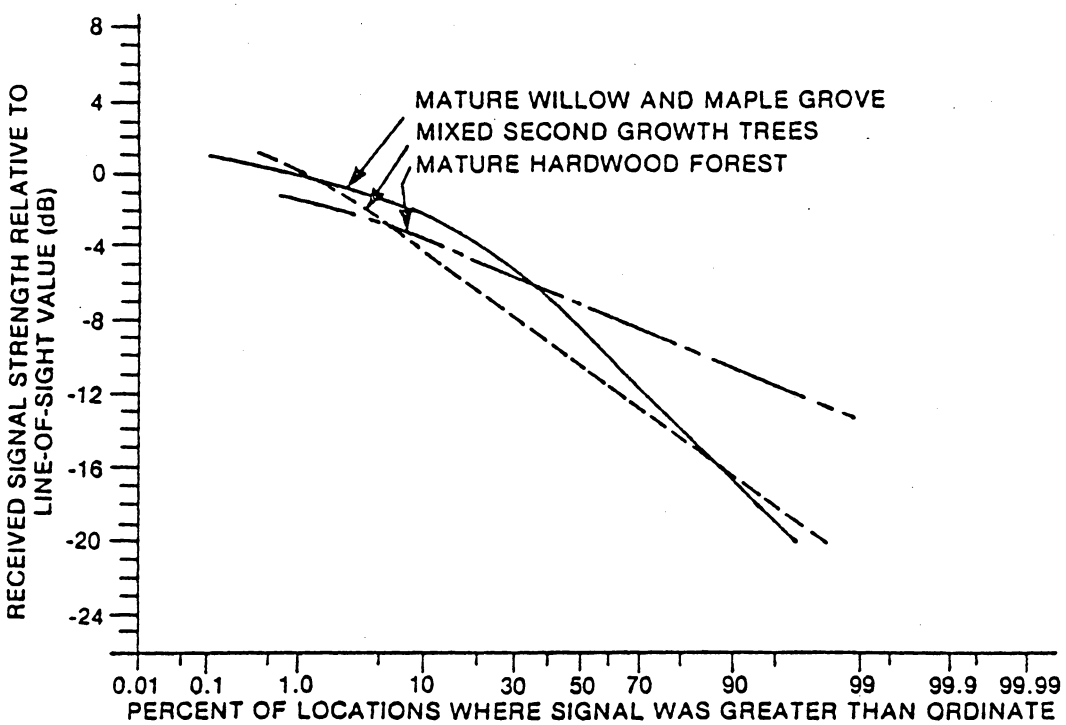

Figure 3.2-2 Distribution functions of data sets from balloon measurements for various shadowed regions. From Butterworth [13]

initial experiment gave an indication of the range of statistical parameters for a variety of sites. However, since the measurements were made only on short routes, no exact quantitative conclusions were made.

3.2.3 HELICOPTER EXPERIMENTS

The next phase of the CRC mobile propagation measurement program used a helicopter to carry the transmitter. The 870 MHz transmitter was similar to the one previously carried by the balloon and used the same antenna. However, the antenna had to be mounted on the side of the helicopter so spurious reflections may have been present. Also the field strength meter was replaced by a spectrum analyzer, which removed the previous limitation on driving speed. The improvements in equipment and procedure allowed for a more extensive set of measurements.

The area chosen for the measurement routes was located just northwest of Ottawa. About 35% of the area was covered by immature timber of mixed species with the rest being cleared land. About 40% of the area was farmland. One third of the length of the test routes was through wooded regions. Also roadside powerline poles ran along most of the length of the routes. However, there were no areas of significant build-up along the routes.

Four parallel routes totaling 90 km in length were chosen in the previously described region. Each roadway had one lane in each direction. One route was an unpaved, gravel road with no shoulders and very little

setback of trees. The other two routes were paved county roads with gravel shoulders and a "reasonable" setback.

The procedure for collecting data was relatively simple. At the beginning of a data collection run, the helicopter and mobile would position themselves in a region with a clear line of sight. The helicopter would hover while the elevation angle was checked with a clinometer. A LOS reference was established and then, both the mobile lab and helicopter travelled parallel routes at the same speed in order to maintain a constant bearing and thus simulate the fixed look angle of a distant satellite. The direction of travel and LOS azimuth were roughly perpendicular.

The first set of measurements was made in September 1982 while the trees were still in leaf. The data taken represented a distance of 50 km (about one million readings). All the data were recorded for an elevation angle of 15° because this was considered to be a worst case condition. The resulting cumulative distribution functions for the entire data set as well as for light and heavy shadowing conditions are all shown in Figure 3.2-3. There are several things to note in these curves. First, the signal enhancement seen in the overall and light shadowing curves (portion of curves above 0 dB level) indicates the presence of multipath since this is the only phenomenon which would produce signal enhancement [12]. Secondly, note that the median signal level in the heavy shadowing curve is 10.5 dB below the line of sight. This signal loss can be primarily attributed to fading due to vegetation blockage. The experimenters stated

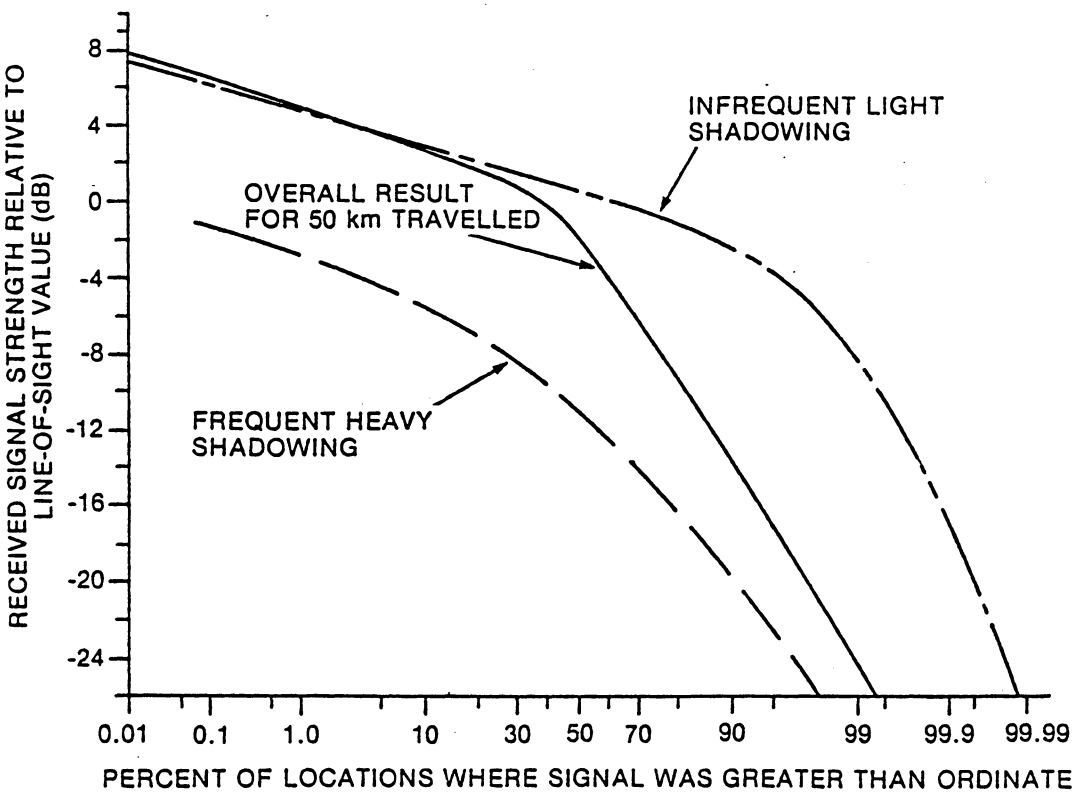

Figure 3.2-3 Distribution functions for September 1982 helicopter measurements. From Butterworth [13]

that the excess path loss from the overall statistics was 12.5 dB for 90% coverage and 22.3 dB for 99% coverage *[13]. Finally note from the infrequent lightly shadowing curve that about 97% of the data points were within ± 5 dB of the line of sight signal level.

The corresponding curves for level crossing rate are shown in Figure 3.2-4. Both curves peak at about 0.2 positive crossings per wavelength. However, the crossing rate was fairly uniform over range of thresholds for the frequent heavy shadowing case while most crossings occurred at the 0 dB threshold for the infrequent light shadowing case.

The curves for average fade duration are shown in Figure 3.2-5. Both curves were similar below the -15 dB threshold after which they diverged. The heavy shadowing case showed longer duration fades at lower thresholds than the light shadowing case.

A second set of measurements was made in June 1983 using the same procedure as before. For these measurements data were taken at elevation angles of 5, 15, 20, and 30°.

The cumulative distribution functions of the June data for the varying elevation angles are shown in Figure 3.2-6. Note that lowering the elevation angle seemed to have the effect of increasing the shadowing as

---

*Author's note: These results differ slightly from the corresponding curve, Figure 3.2-3. Also see Figure 3.2-9.

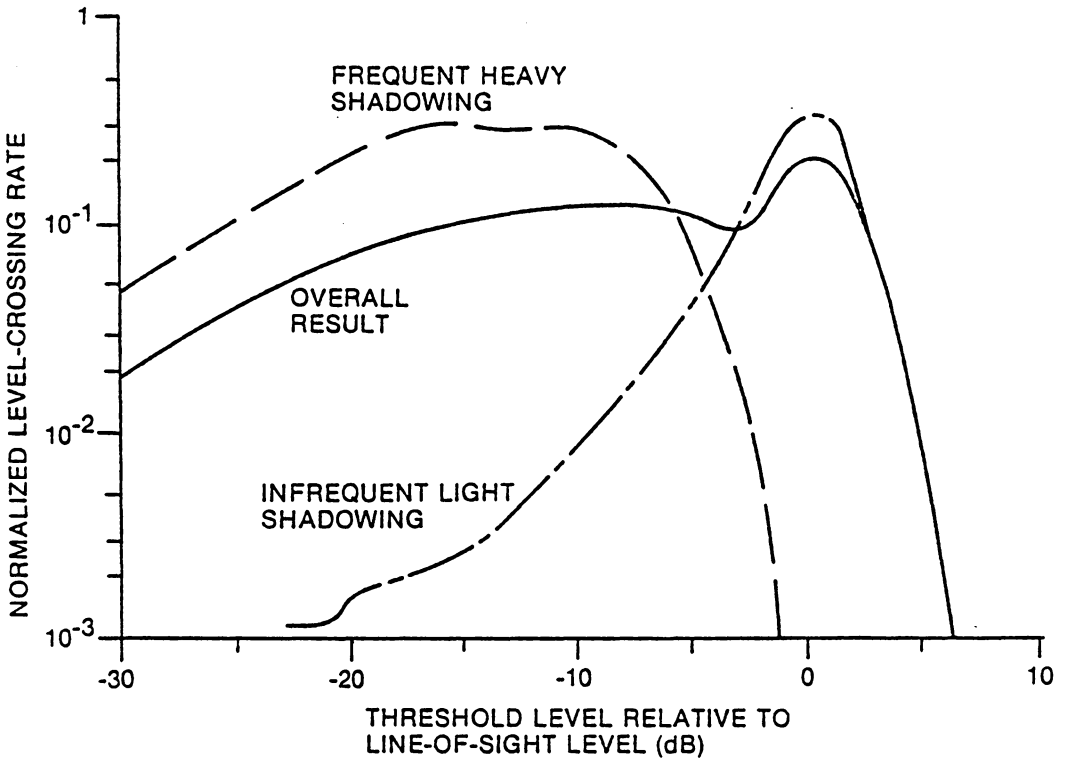

Figure 3.2-4 Normalized level crossing rate for September 1982 helicopter measurements. From Butterworth [13]

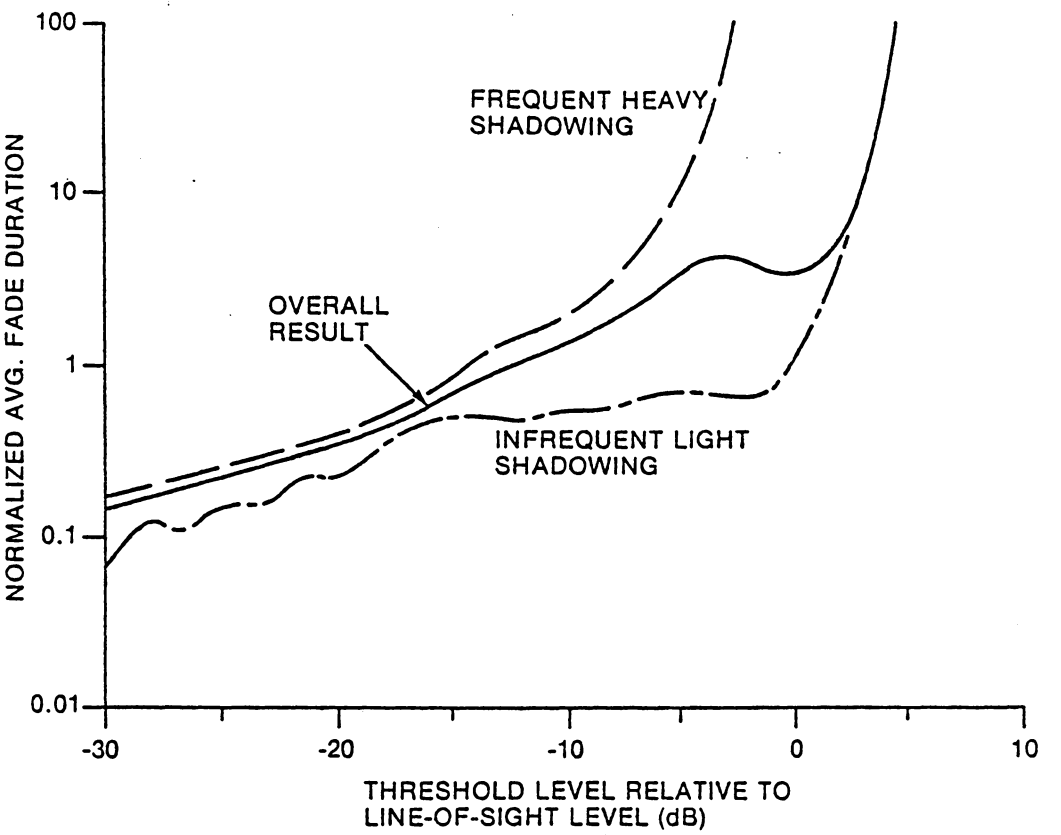

Figure 3.2-5 Normalized average fade duration for September 1982 helicopter measurements. From Butterworth [13]

observed in the earlier September data. The corresponding level crossing rate and average fade duration curves are shown in Figures 3.2-7 and 3.2-8 respectively. These curves also show that lowering the elevation produced the same effect as increased shadowing as observed earlier. Of special interest were the slowly varying fades of 7 to 8 dB observed while travelling through open terrain during data collection at 5° elevation angle. This fading was superimposed on the rapid variations due to diffuse multipath effects and was assumed to be due to specular reflection [13].

Note that the June, 15° elevation angle data indicated an excess path loss of 8 dB for 90% coverage and 18.3 dB for 99% coverage. These numbers show a 4 dB variation from the September overall results as is shown in Figure 3.2-9. The experimenters estimated errors of plus or minus 2 dB above the 90% coverage level due to variations in the helicopter heading and from the non-constant azimuth pattern of the transmitting antenna. Consequently, for 99% coverage in the northwest Ottawa area, estimated path loss was concluded to be about 20 dB at 15° and 14 to 16 dB at 20° [13].

3.2.4 MARECS-A SATELLITE EXPERIMENTS

The most recent phase of the CRC mobile propagation measurement program used INMARSAT's MARECS-A satellite. The satellite generated an L-band (1542 MHz) CW signal with an EIRP of 28 dBW. The receiving and data collection equipment were basically unchanged from the previous

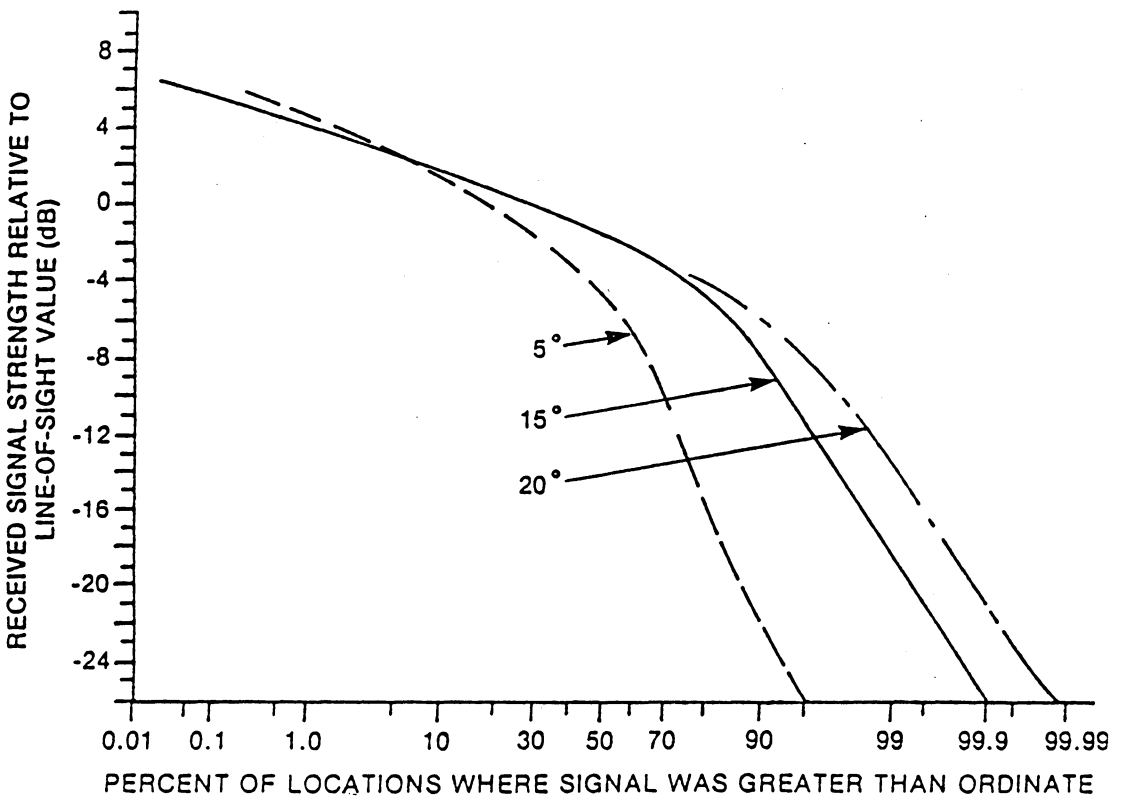

Figure 3.2-6 Distribution functions for June 1983 helicopter measurements. From Butterworth [13]

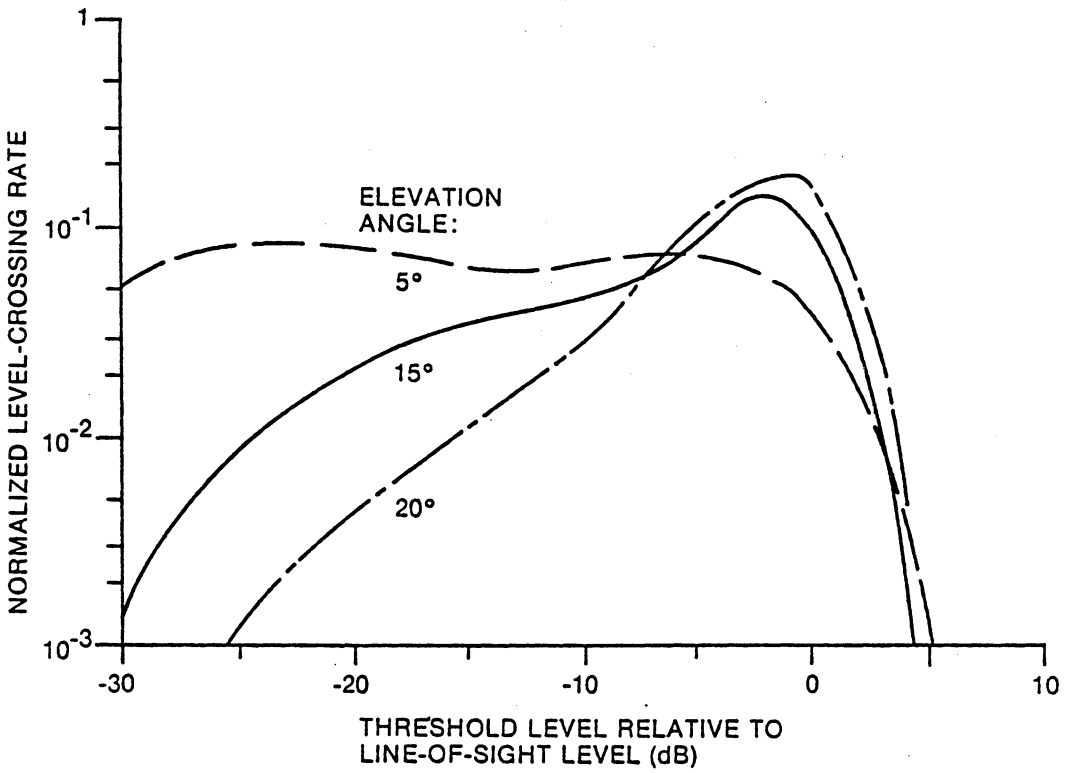

Figure 3.2-7 Normalized level crossing rate for June 1983 helicopter measurements. From Butterworth [13]

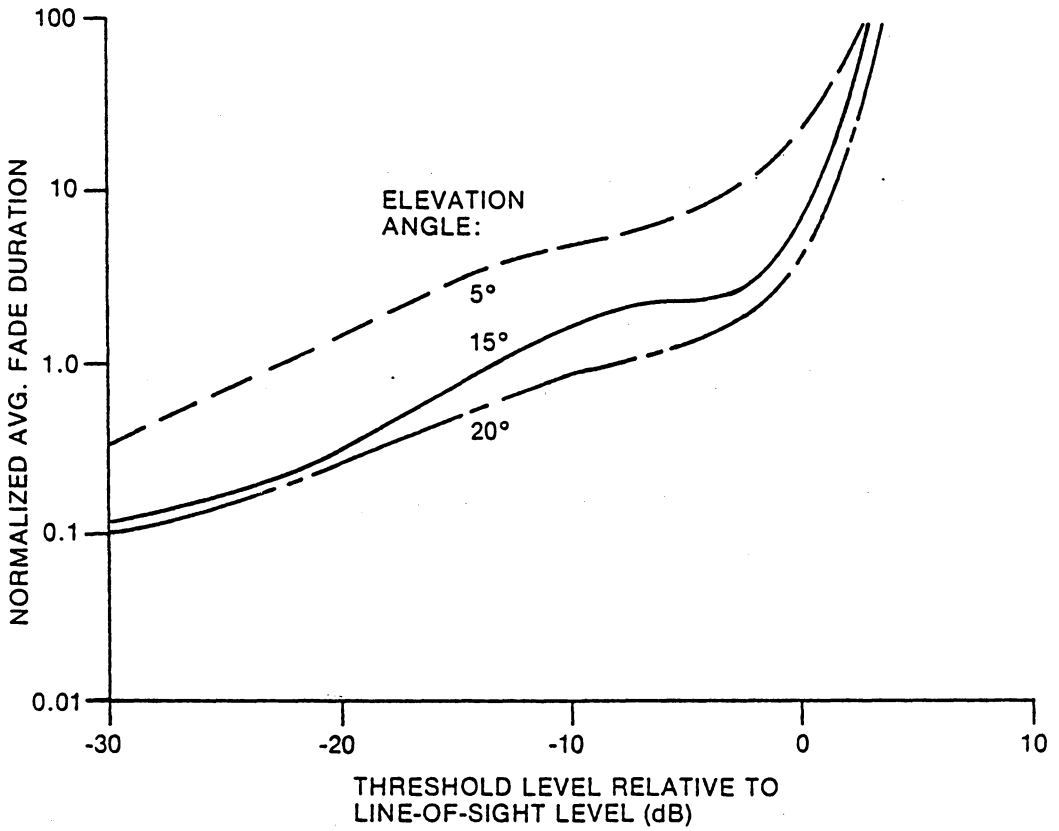

Figure 3.2-8 Normalized average fade duration for June 1983 helicopter measurements. From Butterworth [13]

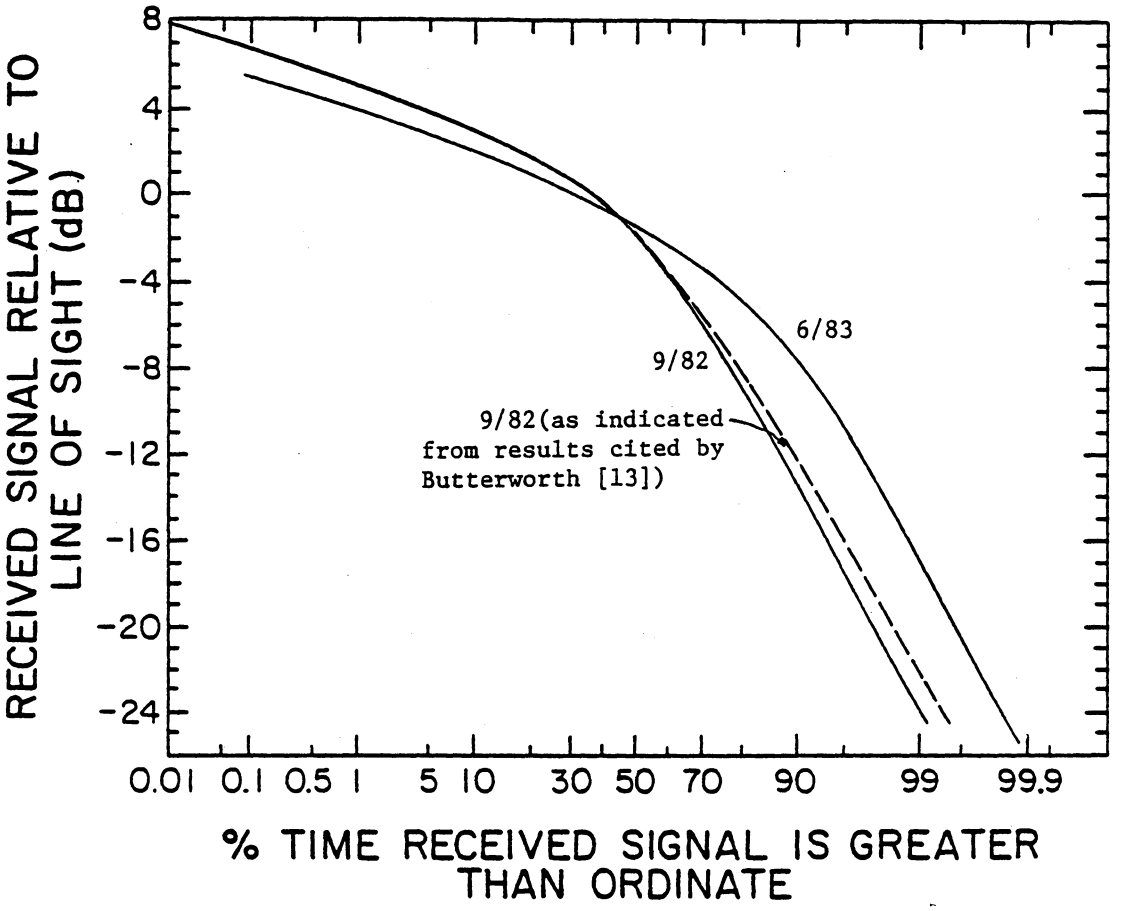

Figure 3.2-9 Comparison of distribution functions at 15° elevation angle for the September 1982 and June 1983 helicopter measurements.

experiment except for the retuning of the spectrum analyzer and the use of a different antenna. As mentioned previously, a crossed drooping dipole design was used. The gain for this design drops more sharply for small angles than did the conical log spiral design and provided some rejection of low angle multipath [37]. Also an additional L-band and a C-band ground station were used in a sophisticated scheme to control the signal frequency and to monitor the amplitude. Frequency control was required because satellite drift and oscillator instability would push the signal outside the narrow bandwidth of the receiver. The scheme used maintained the frequency within ± 20 Hz of nominal. Amplitude monitoring was required due to fluctuations in the output power of the MARECS transponder. These variations turned out to be less than 1 dB.

Three measurement routes representative of different classes of terrain were selected in the Ottawa area. The first route was in an older suburban residential area. The streets were bordered by one and two story single family homes. The second route was characterized as rural/forested. The terrain was hilly and about 35% was covered by a mixture of immature deciduous and coniferous trees. Occasionally there was a cleared area. The roadway itself was a paved provincial highway with one lane in each direction and gravel shoulders. The third route was classified as rural/farmland. The area was almost entirely flat, open fields with the only obstructions being power line poles and occasional trees. About 5% of this route was through wooded areas. The roadway itself was a paved country road with one lane in each direction and gravel shoulders.

The data collection procedure was basically the same as before although driving speed had to be reduced to maintain a large enough dynamic range. The satellite's elevation angle averaged 19° over the measurement routes.

The first series of measurements were made in November 1982 when the deciduous trees were without leaves. The cumulative distribution of signal strength for all three routes is shown in Figure 3.2-10. The corresponding curves for level crossing rate and average fade duration are shown in Figures 3.2-11 and 3.2-12 respectively.

A second series of measurements were made over the same routes in June 1983. The cumulative distribution functions for these measurements are shown in Figure 3.2-13. The level crossing rate and fade duration curves were not included in the report. A sample time plot of the signal level showing the effects of shadowing is given in Figure 3.2-14. Note that the row of trees causes rapid variations in signal level while the dense vegetation causes a more steady, deep fade.

The experimenters made a few important general observations about the results. First they compared the November and June results. As expected the suburban and rural farmland curves were essentially the same in both measurement periods. Deviations were typically less than 1 dB. However, the rural forested curve showed larger attenuation values for the June data. This phenomena was explained as extra foliage attenuation due to the leaves on the deciduous trees, which were not present in November. This seasonal variation in the distribution curve is shown more

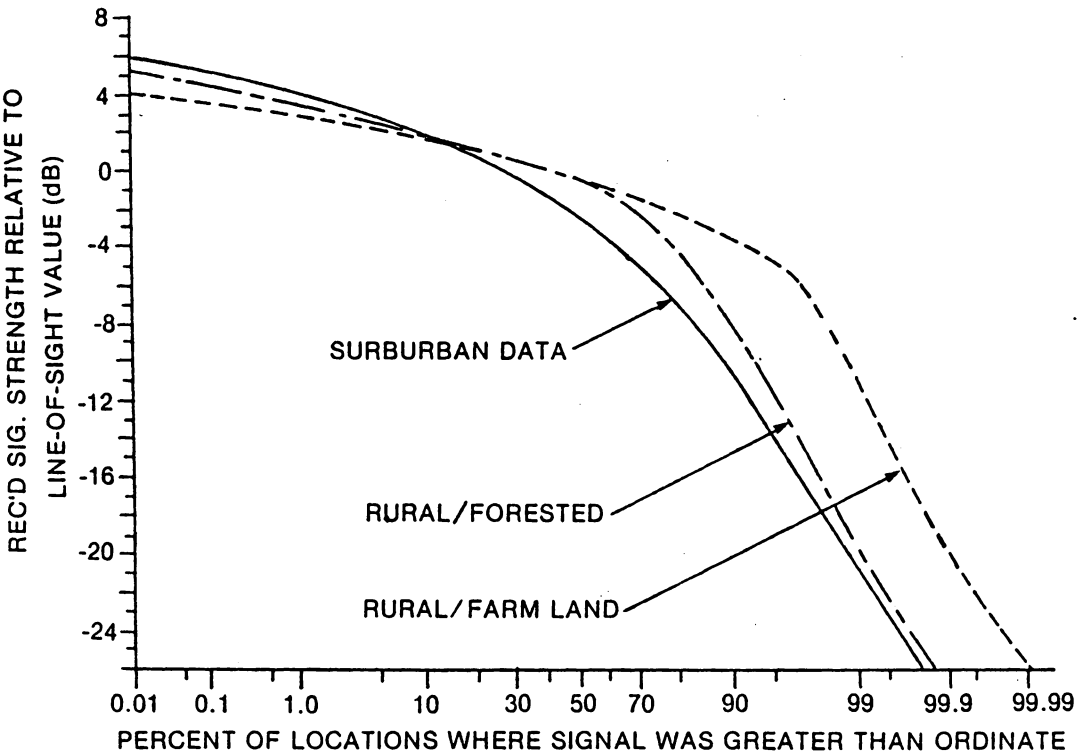

Figure 3.2-10 Distribution functions for November 1982, MARECS-A measurements. From Butterworth [14]

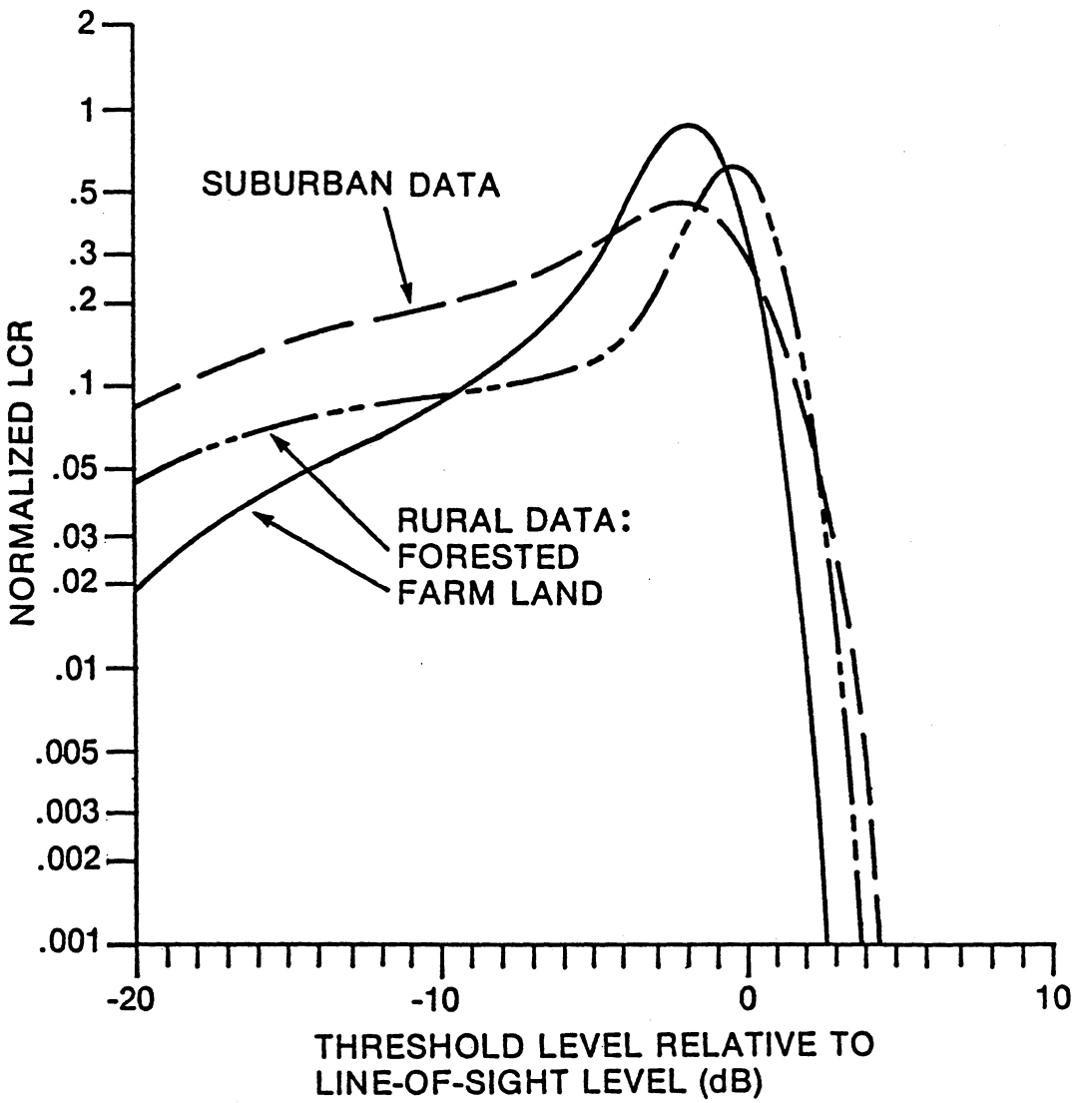

Figure 3.2-11 Normalized level crossing rate for November 1982 MARECS-A measurements. From Butterworth [14]

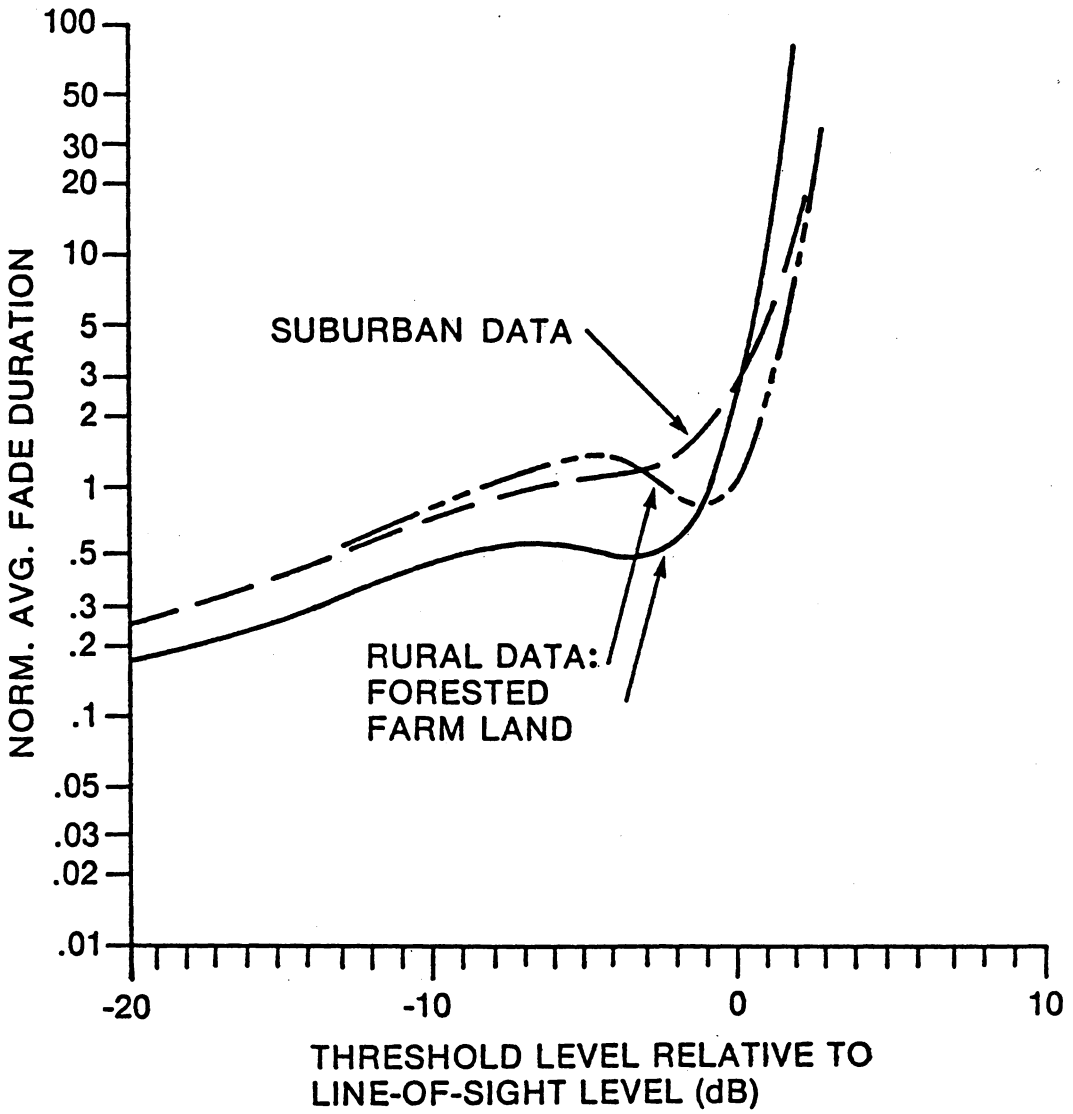

Figure 3.2-12 Normalized average fade duration for November 1982, MARECS-A measurements. From Butterworth [14]

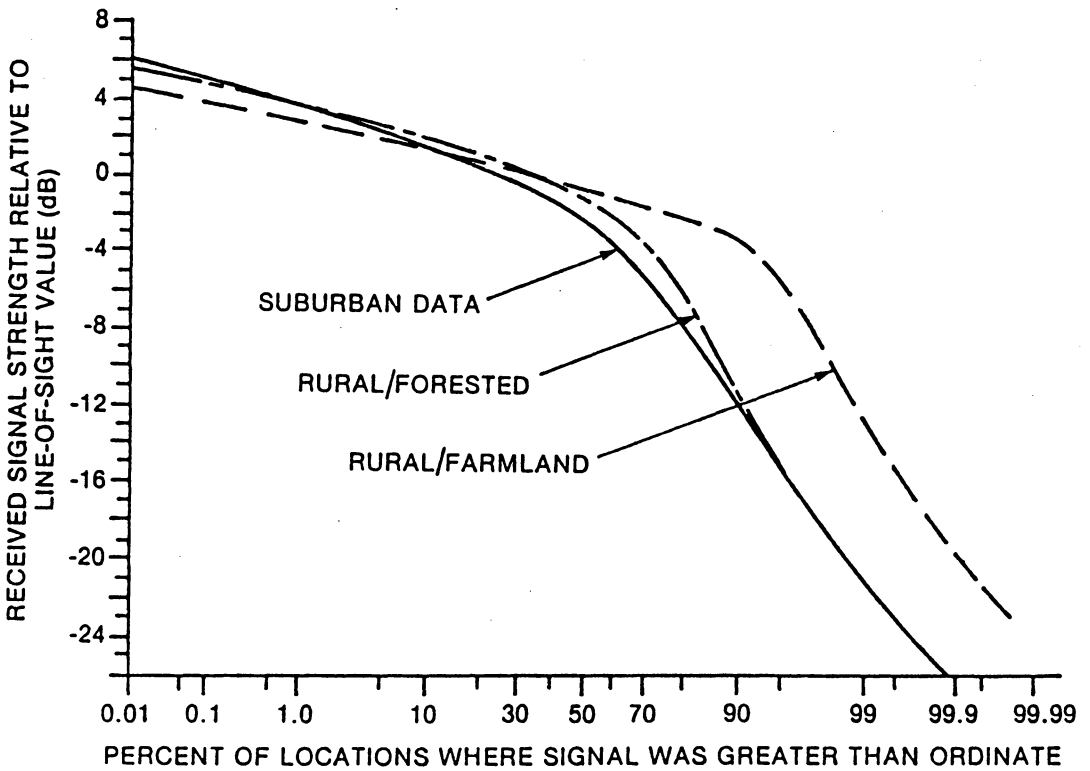

Figure 3.2-13 Distribution functions for June 1983, MARECS-A measurements. From Butterworth [14]

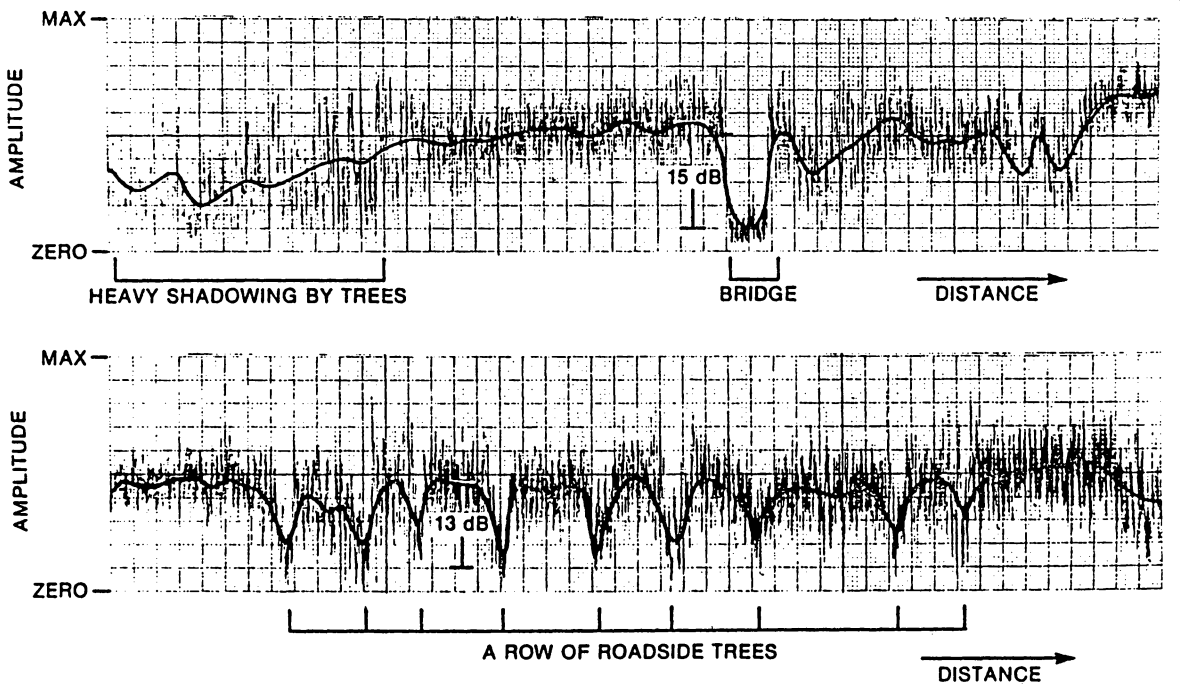

Figure 3.2-14 Time plots of the signal level showing the effects of shadowing obstacles. From Butterworth [15]

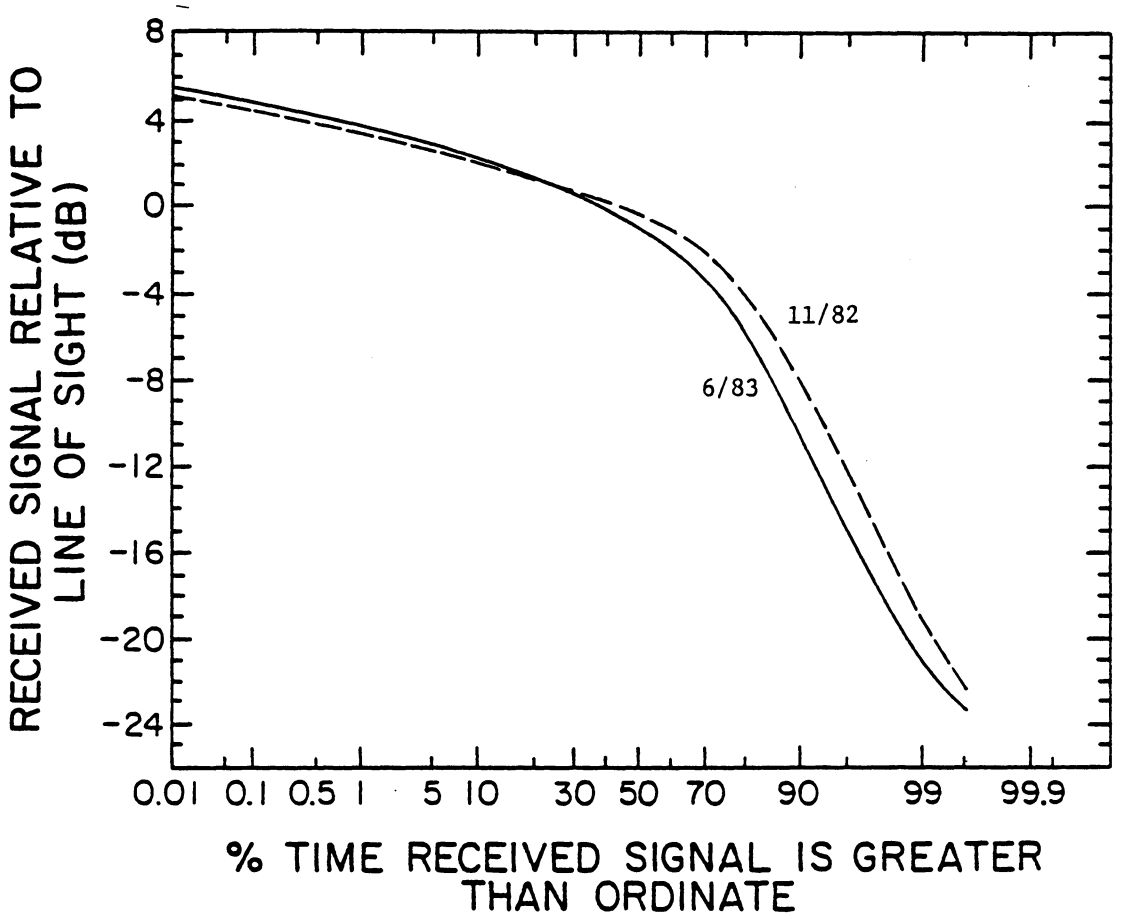

Figure 3.2-15 Comparison of rural/forested distribution functions from November and June MARECS-A measurements showing seasonal variation.

graphically in Figure 3.2-15. Secondly they made some observations about the shape of the cumulative distribution first. The portion of the curve to the left of the knee followed a Rician shape and was relatively insensitive to the amount of shadowing. The portion to the right of the knee tended to be a straight line, indicating a lognormal distribution, and its intersection point with the Rician portion, the knee, moved to the left as the amount of shadowed data increased. Also, the rural data curves had deviated from a straight line at the highest percentages. This effect was attributed to the limited dynamic range of the receivers. Finally, the observed excess path loss ranged from 4 to 12 dB for 90% coverage and from 12 to 21 dB for 99% coverage.

3.3 VOGEL BALLOON EXPERIMENTS

Another experimental program to measure propagation characteristics in a simulated land mobile satellite environment has been performed under NASA sponsorship at the University of Texas by W. J. Vogel. Two experiments were conducted. The first concentrated on elevation angles in the 10 to 35° range and the second in the 30 to 80° range. The objectives were to measure an 869 or 1501 MHz CW signal from a simulated satellite transmitter (in each case a stratospheric balloon) with a receiver on a moving vehicle and then analyze the statistical properties of the received signal. This work was similar to that done by the Canadian CRC as previously described. The following summary comes from a status report [75], a final report [75] submitted to JPL, and a presentation at the recent JPL MSAT-X propagation workshop [77].

3.3.1 FIRST EXPERIMENT

The balloon used to carry the transmitter was flown at an altitude of 40 km and was tracked by the National Scientific Balloon Facility (NSBF). The transmitter itself could generate a CW signal or a narrowband FM (NBFM) signal for use in transmitting telemetry messages and recorded voice messages. The receiving equipment and data collection system were mounted in a modified passenger van. The receiving antenna was mounted on the roof of the van and was a crossed drooping dipole design, the same as the transmitter antenna. The receiver consisted of a low noise amplifier and mixer section followed by an amateur radio communications receiver. The receiver output was digitized and stored by the computer controlled data collection system at a sampling rate of 1/8 wavelength intervals of vehicle travel. This system also measured the signal frequency, controlled the receiver's rf gain, and stored other information that helped to describe the data.

Data were collected during two flights, one on October 10, 1983 and the other on January 11, 1984. For each flight, the mobile receiver was driven within a line of sight path from the transmitter. The van was able to follow the balloon from the position, heading, and speed information provided by the NSBF.

The flight of October 11 provided 8 hours worth of data over 600 km of roads. The path taken was typically on two lane roads through rolling country with a few small cities and towns along the way. The terrain

bordering the roadside consisted of tall pine trees, mixed forest, and occasional grazing land. The vegetation during the last hour of data collection changed from trees to shrubs. Some problems were experienced in following the balloon so all of the data were taken at elevation angles below 30°.

The flight of January 11th was only about 1 ½ hours long. Data collection was delayed due to mechanical problems and transmitter failure halted data collection early. The path taken was typically on two lane roads through pine forests.

The data were collected in one second bursts and then grouped into five minute blocks for storage. Examples of plots for the one second data bursts are shown in Figures 3.3-1, 3.3-2 and 3.3-3. The first example, Figure 3.3-1, was taken while crossing a reservoir causeway. The second two examples, Figure 3.3-2 and 3.3-3, were taken nearly consecutively on a two lane road through a pine forest. The elevation angle was 28° and the balloon was observed to graze the tree tops. The first plot shows large signal variation probably due to shadowing while the second shows signal variation largely due to diffuse multipath effects. The plot of Figure 3.3-4 and 3.3-5 show five minute signal plots for light and heavy shadowing, respectively. Data taken over the same paths during the two separate flights looked comparable.

The overall signal level distribution taken from 7.66 million samples, at van speeds greater than 10 mph and elevation angles from 10 to 35°,

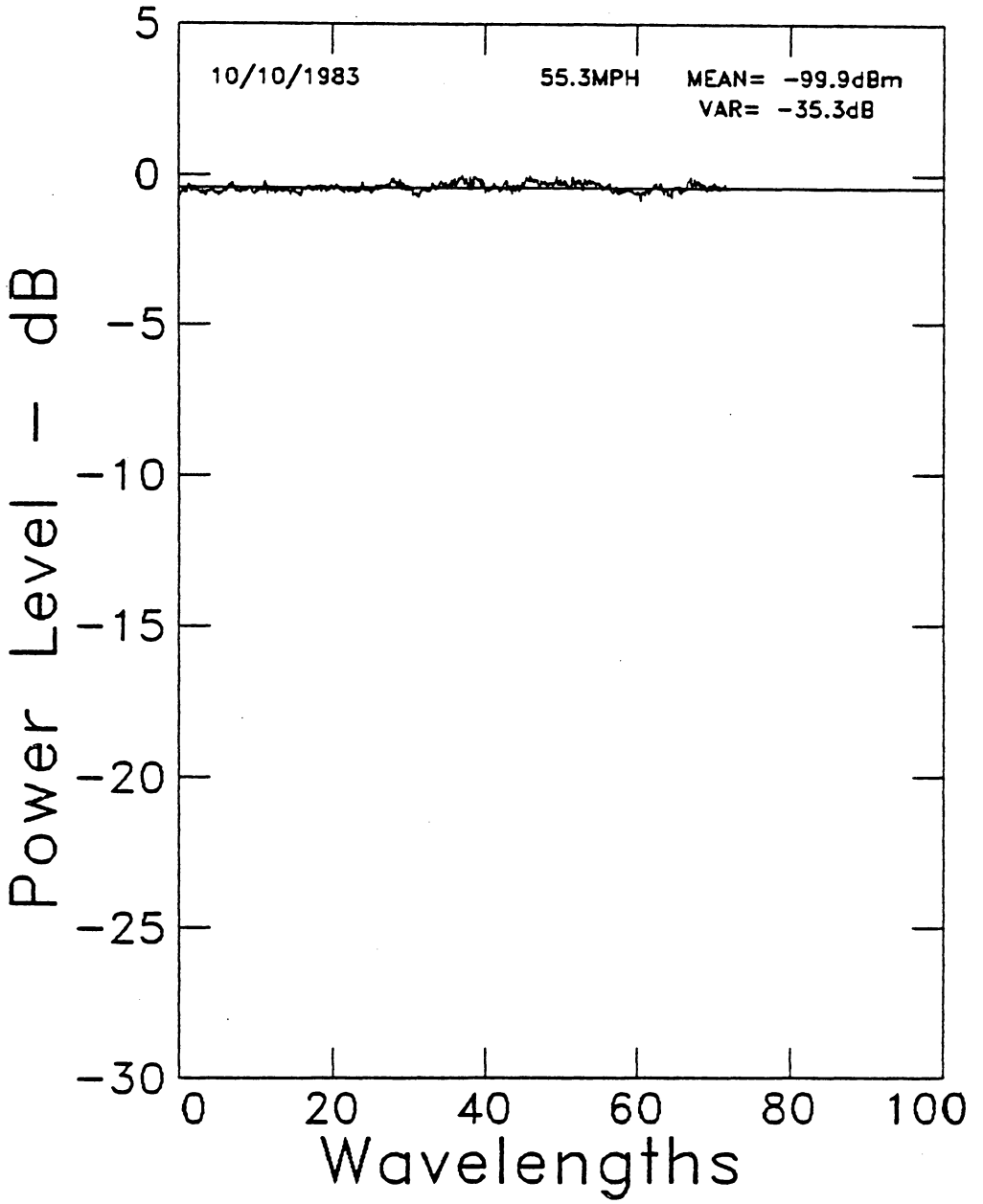

Figure 3.3-1 A time plot of received signal level for one second, taken while crossing a reservoir causeway. From Vogel [75]

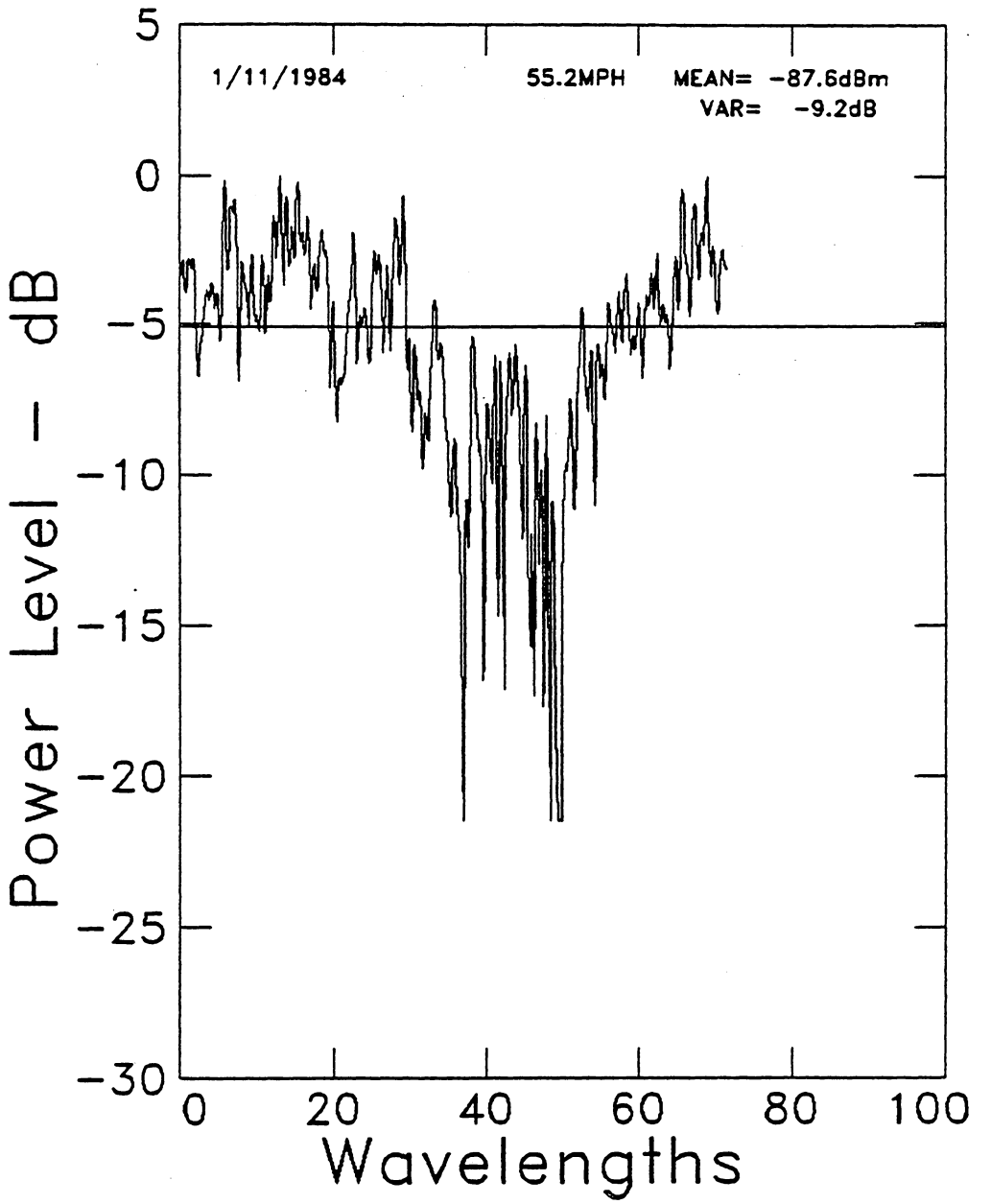

Figure 3.3-2 A time plot of received signal power for one second taken in a pine forest. From Vogel [75]

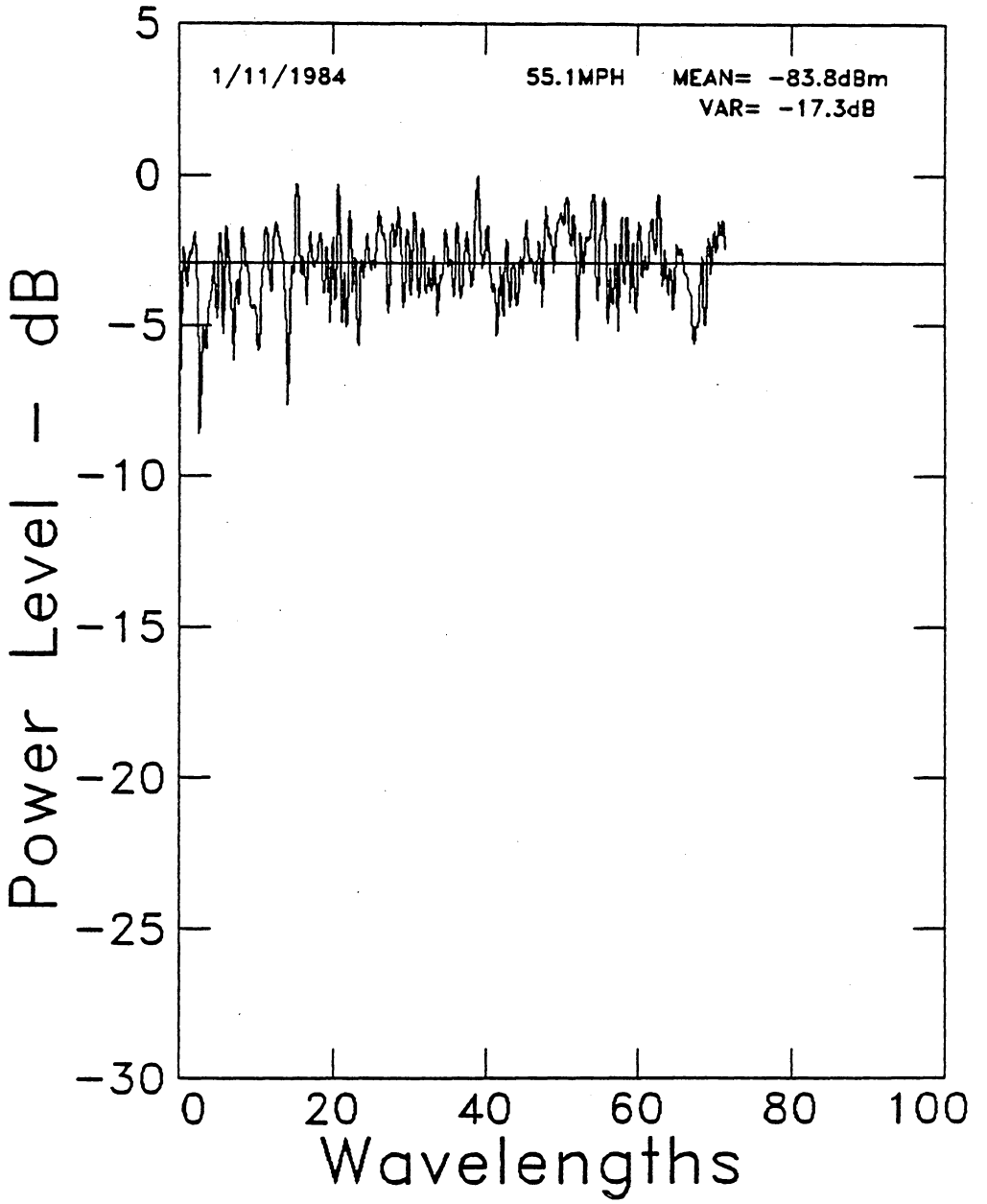

Figure 3.3-3 A time plot of received signal power for one second, taken in a pine forest two seconds after Figure 3.3-2. From Vogel [75]

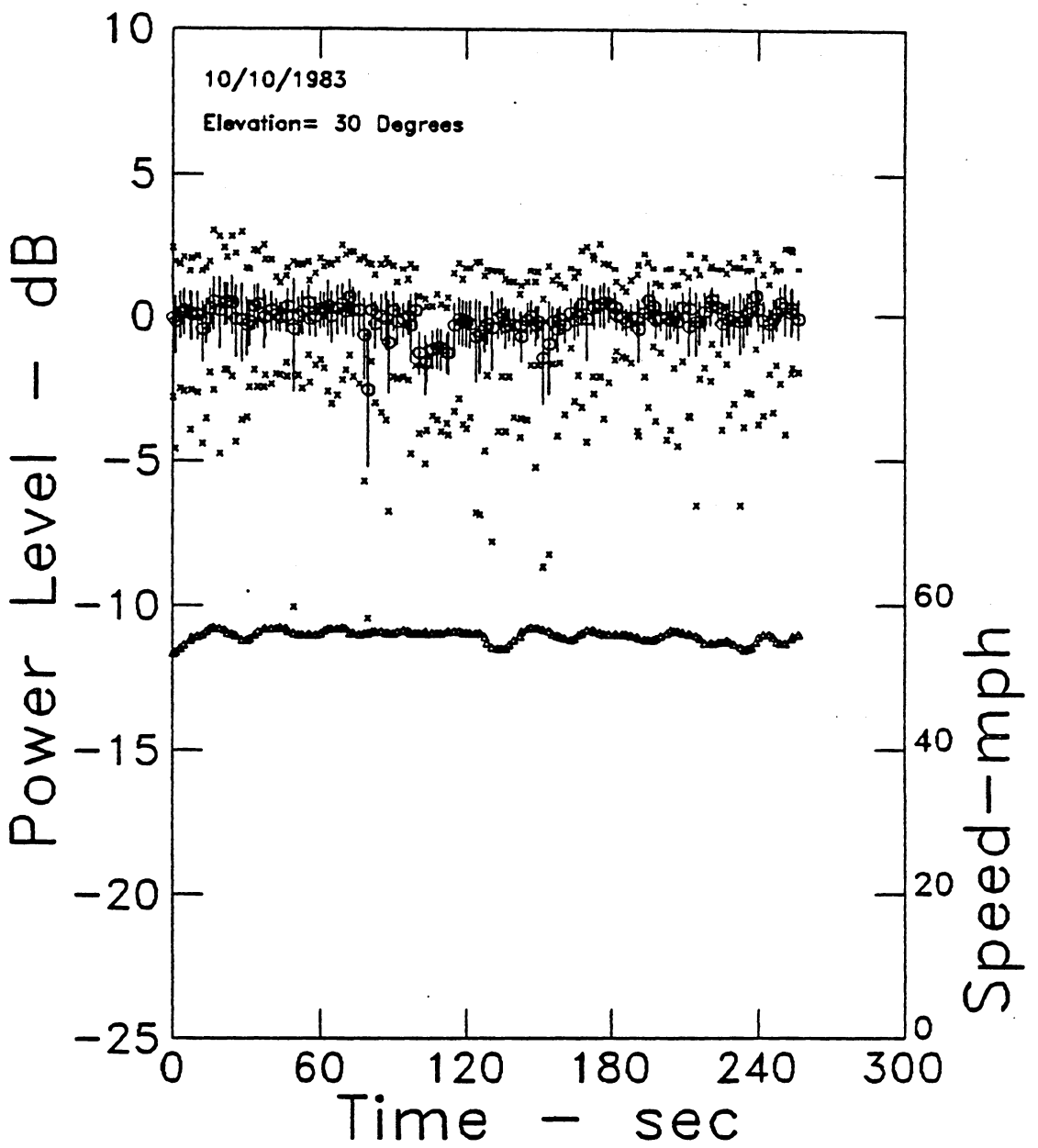

Figure 3.3-4 Five minute signal plot for lightly shadowed route. Each symbol is for a one second interval: speed of the van (triangles), mean signal level (circles), ± one standard deviation limits (vertical lines), and extreme values (x). From Vogel [75]

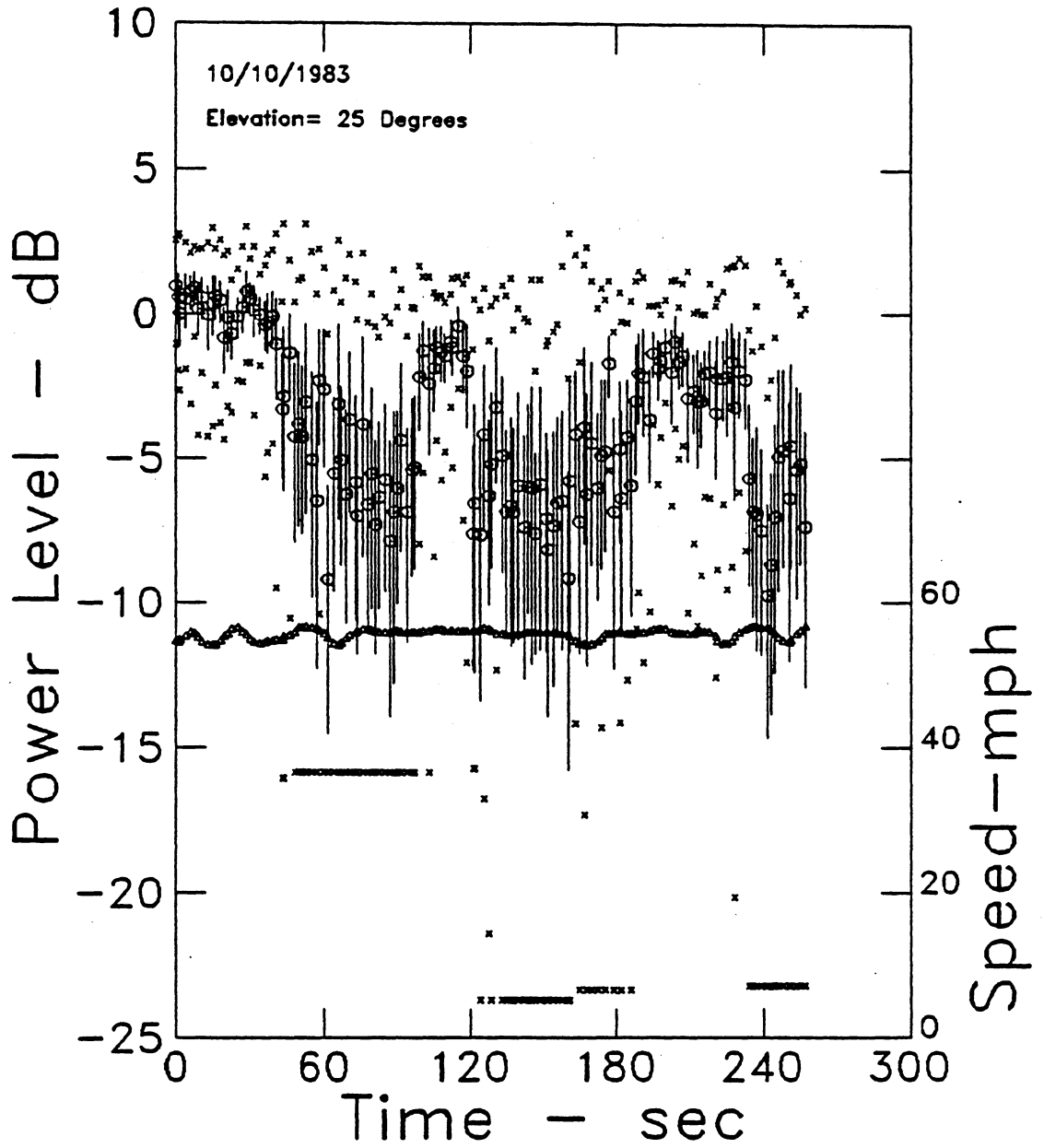

Figure 3.3-5 Five minute signal plot for heavily shadowed route. Each symbol is for a one second interval: speed of the van (triangles), mean signal level (circles), ± one standard deviation limits (vertical lines), and extreme values (x). From Vogel [75]

is shown in Figure 3.3-6. A distribution function for the 15 to 20° range is shown in Figure 3.3-7. For comparison, a set of Rice distributions is shown in Figure 3.3-8 for various values of the Rice parameter K (note the different definition for K). The measured data follows the Rice distribution except for the sharper drop at probability levels of 90%-85% and above.

Vogel's data also showed some elevation angle dependence in the signal level distribution. Table 3.3-1 shows signal level for three probabilities from data grouped by elevation angle. The figures show shallower fading for higher elevation angles except for the 20 to 25° data. However, the elevation angle dependence of the statistics needs to be regarded with uncertainty. To analyze the data, a free space correction was required to obtain the received signal power relative to a pure line of sight signal. This correction proved to be difficult to calculate for several reasons: uncertainty in the balloon's range and elevation, an antenna pattern that varied from the ideal, and the variability of transmitter power with temperature. A best guess was made to correct the errors and consequently there was some uncertainty in the elevation angle dependence of the results [75].

The other fading statistics, level crossing rate and average fade duration, are shown in Figure 3.3-9 and Figure 3.3-10, respectively, from the combined data sets. The results were normalized, but were presented on a conditional probability scale. Absolute probabilities for each fading statistic can be obtained by multiplying the conditional

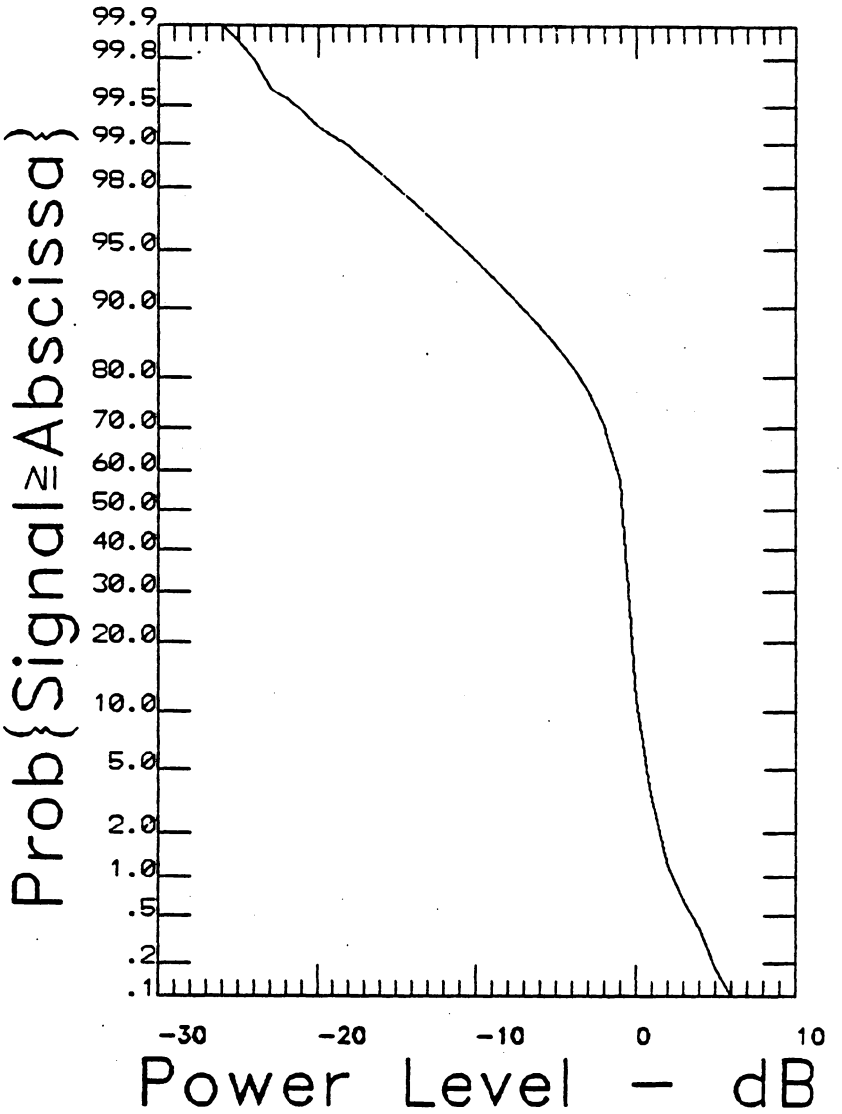

Figure 3.3-6 The overall signal level distribution function for elevation angles from 10 to 35°. From Vogel [75]

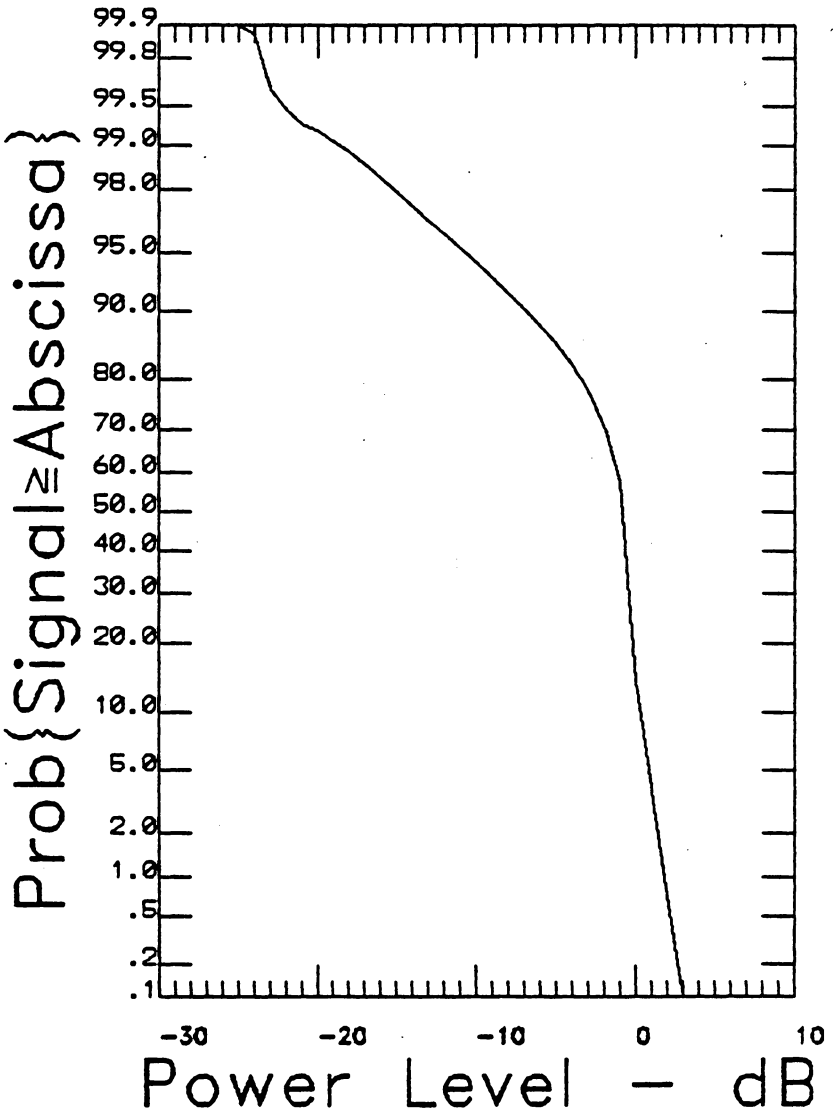

Figure 3.3-7 The signal level distribution function for elevation angles from 15 to 20°. From Vogel [75]

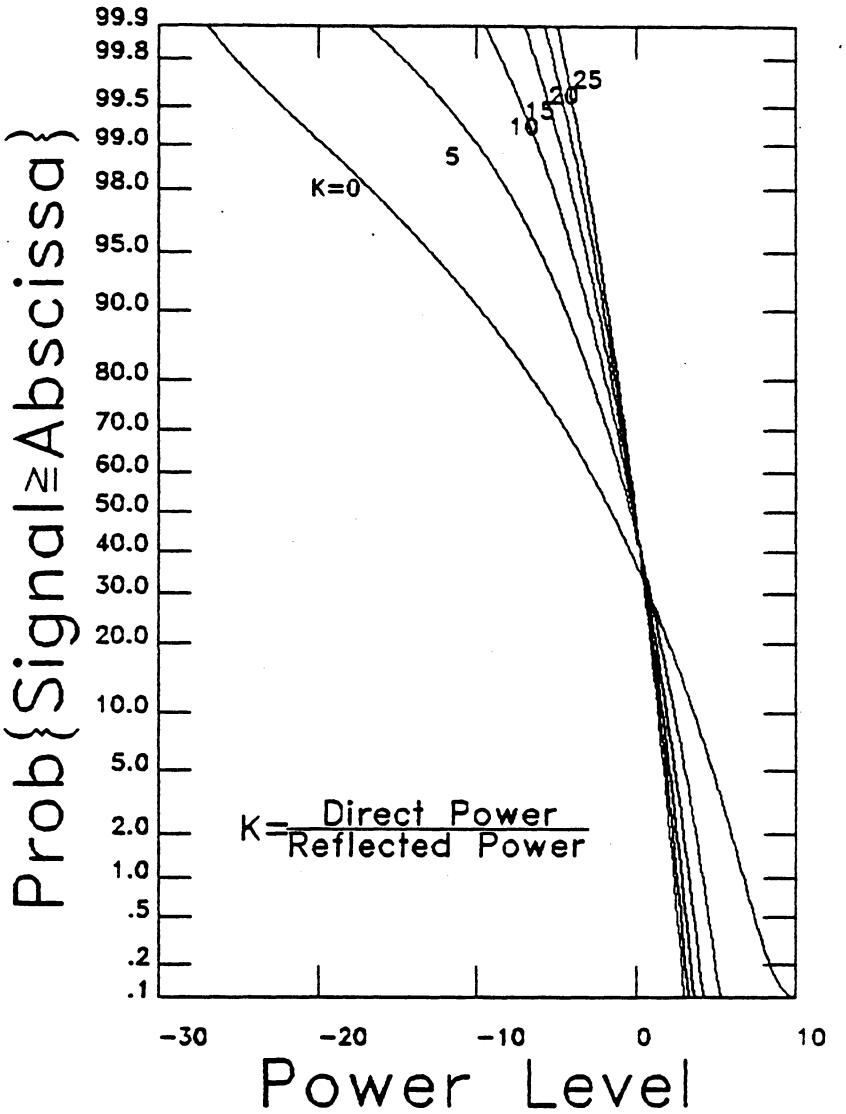

Figure 3.3-8 A set of Rice distribution curves for varying levels of diffuse reflected power for comparison to Figures 3.3-6 and 3.3-7. From Vogel [75]

Table 3.3-1
Power distribution vs elevation angle. From Vogel [75]

Elevation Angle (degrees)	Signal level in dB relative to mean for probability of		
	50%	90%	99%
10 ≤ elev. < 35	-1	-7	-18
10 ≤ elev. < 15	-1	-9	-20.5
15 ≤ elev. < 20	-1	-8	-18.5
20 ≤ elev. < 25	-1.5	-9.8	-20.3
25 ≤ elev. < 30	-0.8	-2.2	-8.2
30 ≤ elev. < 35	-0.5	-1.2	-4.5

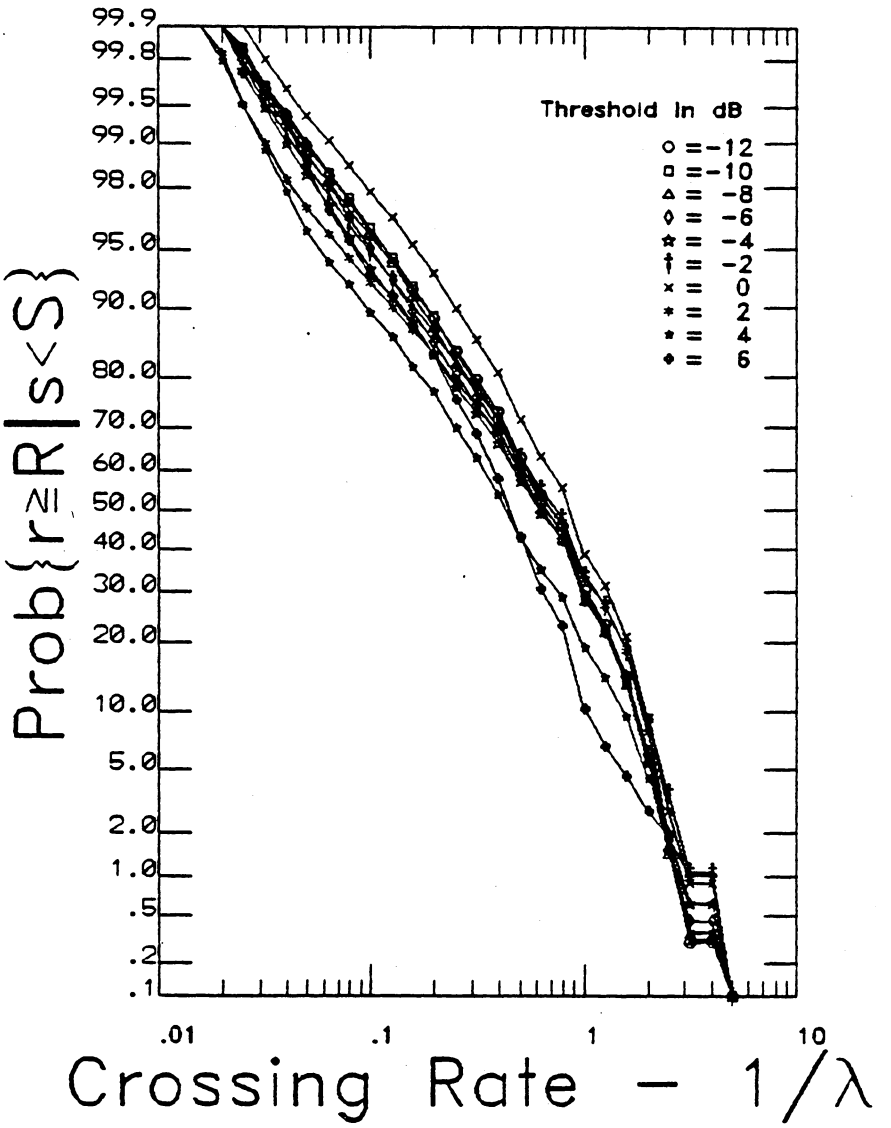

Figure 3.3-9 The conditional level crossing rate distribution function for all the data between 10 and 35° elevation angle. From Vogel [75]

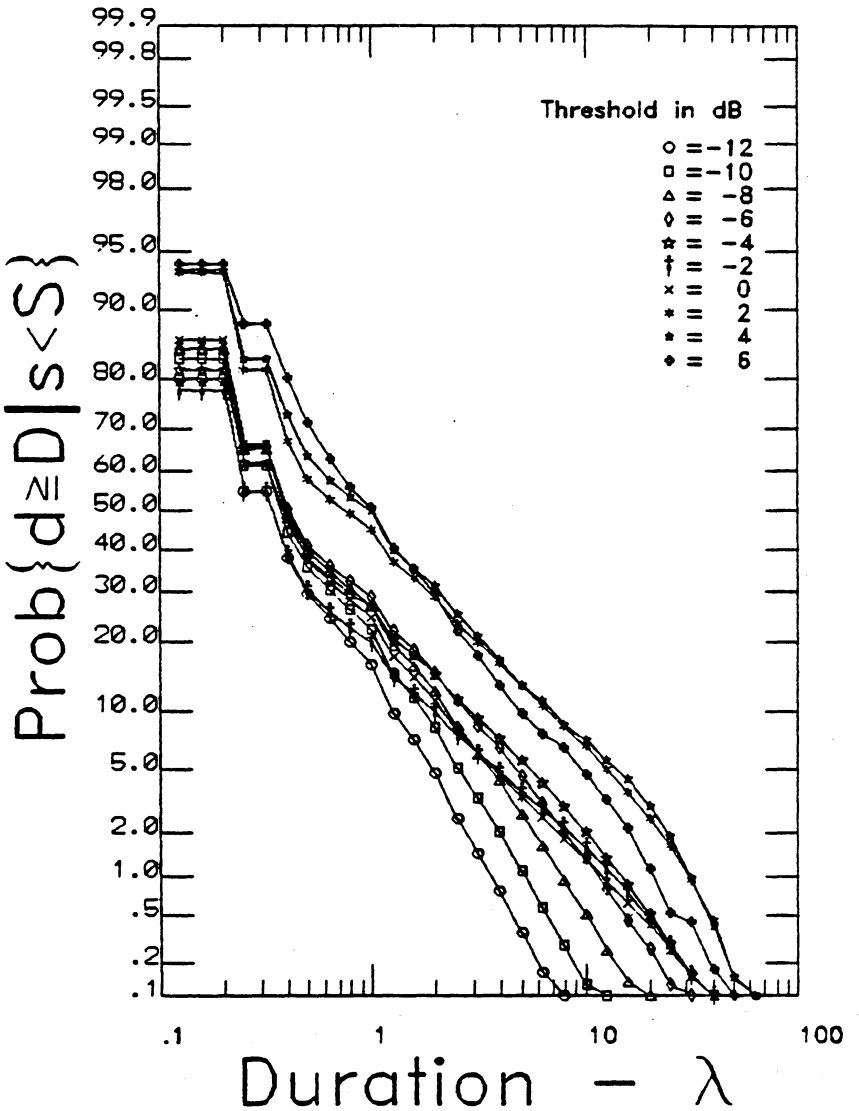

Figure 3.3-10 The conditional fade duration probability distribution function for all the data from 10 to 35° elevation angle. From Vogel [75]

probabilities by the signal level probability density. This form of presentation is different from that discussed by Lee [47] and used by other experimenters. Vogel's data can be translated to the other form by taking the mean level crossing rate and fade duration (50% level) at each threshold. Vogel noted that both the fade duration and crossing rate curves were insensitive to changes in elevation angle. He also observed that the spread of the data with signal level threshold was small but that the highest crossing rate for a given probability usually occured for a threshold of 0 dB. Crossing rates for a 0 dB threshold at 50% and 1% probability levels were 0.6 and 3 to 5 positive crossings per wavelength, respectively. Fade duration at the 50% probability level varied from 0.4 to 1 wavelength and at the 1% level varied from 3 to 30 wavelengths, depending upon the threshold.

3.3.2 SECOND EXPERIMENT

A second recent balloon experiment was conducted in November of 1984. The experiment objectives were the same as before. For this experiment a 1501 MHz transmitter was added to the existing one at 869 MHz. Also, a microstrip array antenna and a heli-bowl antenna were added to the mobile receiver. Both of these antennas were azimuth pointed to the balloon. The signals were quadrature demodulated and stored on analog tape for processing and analysis to be done off-line. Twenty-two hours of data were collected. At the time of this writing, the data had not been reduced so no results are yet available.

3.4 HESS ATS-6 MEASUREMENTS

Some pioneering work in determining excess path loss statistics for a land mobile satellite link was performed by Dr. Garry Hess of Motorola. The NASA ATS-6 satellite was used as the transmitting source during a three week data collection period in March 1978. Data were taken on routes primarily in urban regions between Chicago and San Francisco at both UHF (860 MHz) and L-band (1550 MHz). The collected data were analyzed to obtain signal behavior statistics, and these results were used to develop a simple five parameter equation to predict excess path loss. The following summary comes from Hess' IEEE paper [35], an internal report [34], and a phone conversation with Dr. Hess [36].

The experiment was implemented by using a mobile test van to receive and store the satellite signals. The ATS-6 satellite transmitted right hand circularly polarized (RHCP) carriers at both 860 MHz and 1550 MHz. These signals were received with conventional quarter-wave whip antennas mounted on the van roof. Note that this type of antenna did not discriminate low angle multipath components. The receiving equipment consisted of a bandpass filter and a low noise amplifier followed by a spectrum analyzer to serve as a selectable bandwidth receiver. The spectrum analyzer output was both digitized for real time analysis and stored on magnetic tape for off-line analysis. Also, odometer information and a voice commentary were tape recorded.

Five measurement parameters were recorded during data collection in order to characterize the received signal. The first parameter was local environment. Hess used four broad categories: urban, semi-urban, suburban, and rural. Data were collected mostly in and around large cities so conditions varied from urban to suburban type regions. Very little data were collected in rural areas except for routes through Estes Park, Colorado and while crossing Nevada [36]. The second parameter was link frequency, either 860 MHz or 1550 MHz. The third parameter was elevation angle. Data were collected at locations between Chicago and San Francisco where the elevation angle varied from 19 to 43°, respectively. The fourth parameter was the vehicle heading. This parameter became important because blockage of the line of sight component by buildings changed according to the test van heading relative to the satellite azimuth. The fifth parameter was the side of the street where the satellite appeared to be. Some locations showed a dependence on this parameter because the LOS component was not shadowed as often when the satellite appeared to be on the opposite side of the street.

The results of the data analysis were displayed using a special cumulative distribution function (CDF) which shows both the small-scale (temporal) and large-scale (spatial) behavior of the signal. Hess credited the idea for this form of presentation to a paper by Haakinson and Jennings [32]. The small scale coverage statistics were derived from individual data files that described signal variations over short runs of a few hundred wavelengths. First probability density functions and cumulative distribution functions were formed for each short run file. Then the

signal powers above which the signal stayed 50, 70, 90, and 95% of the time were noted. These numbers described the small scale or temporal variability of the signal. Then the set of signal powers for one probability level from files considered similar were used to generate another cumulative distribution function [34]. This second CDF described the large scale or spatial variation in the signal. Consequently, large-scale coverage information would be shown for a specified level of small-scale coverage.

An example of this cumulative distribution function for urban Denver at 860 MHz with all vehicle headings shown in Figure 3.4-1.
Note that the vertical axis corresponds to received signal power in dBm with the free-space reference level marked as "L-O-S". The horizontal axis corresponds to percent spatial coverage with individual curves for the differing temporal coverage percentages. The lower dashed lines indicate the excess path loss for what Hess refers to as 90/90 coverage, which is 25 dB in this case. This means that 25 dB or less excess path loss would be observed for 90% of the locations in urban areas 90% of the time. The "ledge effect" in Figure 3.4-1 was explained as being a result of using data for all vehicle headings. Significant differences in the curves were observed though when the CDF was segregated with respect to vehicle heading as shown in Figure 3.4-2. Note that only a 6 dB path loss was observed for 90/90 coverage on paths parallel to the satellite azimuth (SW/NE) whereas a 29 dB path loss was observed on routes perpendicular to the satellite azimuth (NW/SE). This was explained by the presence of a LOS component generally available for the parallel routes but heavy

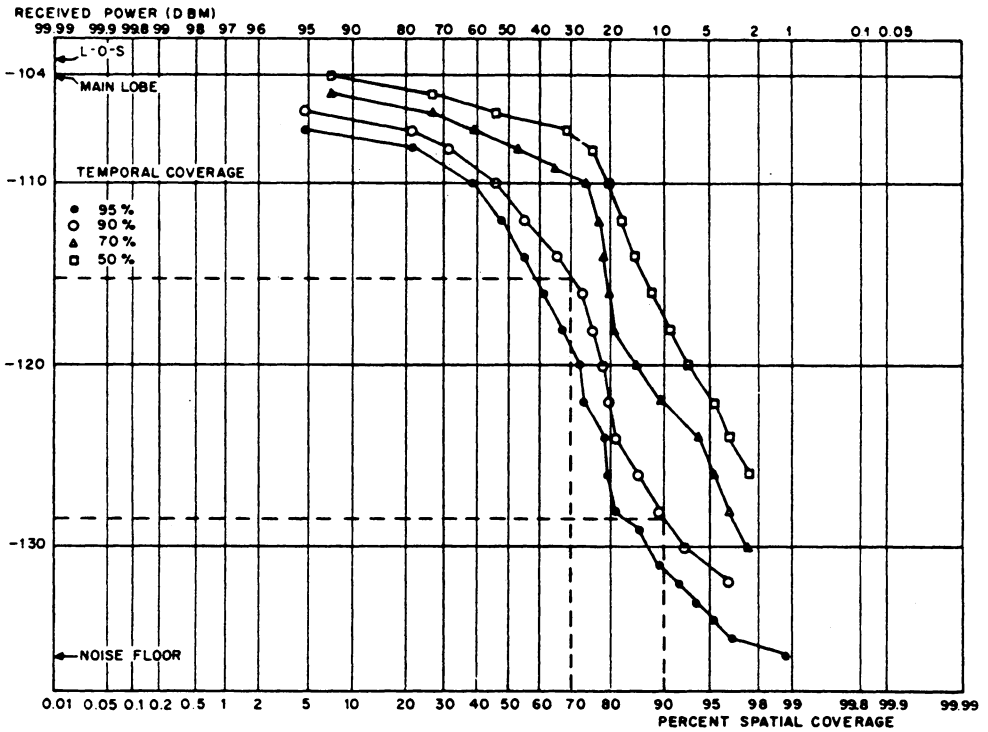

Figure 3.4-1 Signal level distribution function for urban Denver at 860 MHz. Data is for all azimuths. From Hess [35]

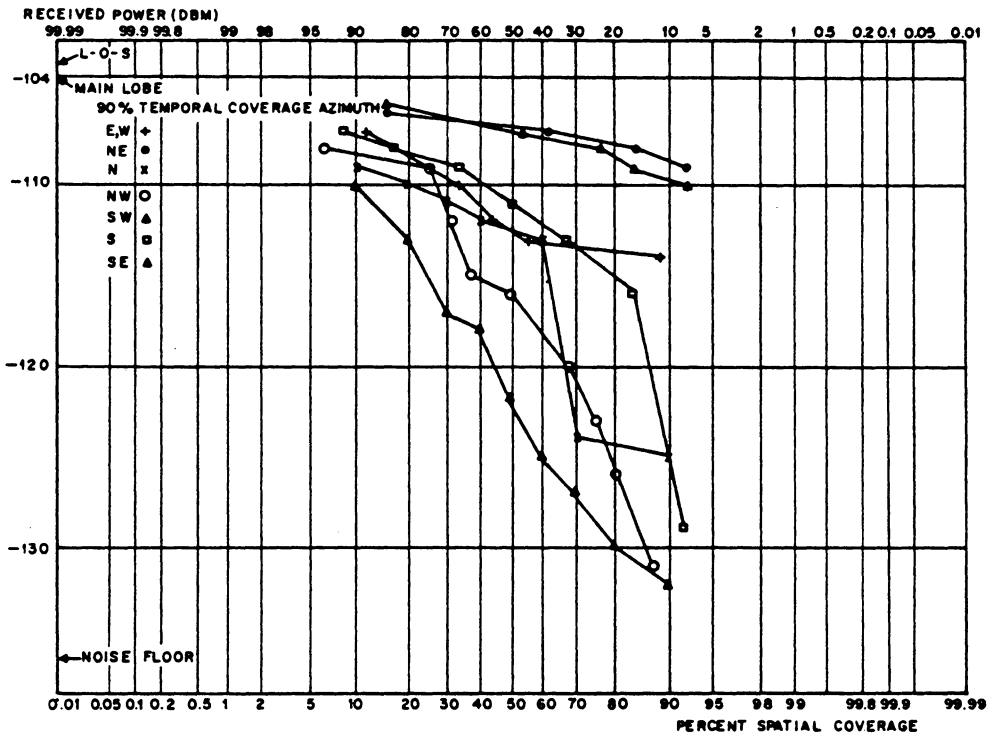

Figure 3.4-2 Signal level distribution function of data from Figure 3.4-1 with azimuths segregated. From Hess [35]

shadowing of the LOS component by buildings on the perpendicular routes [35].

Only a limited amount of data were collected in rural regions. The signal behavior here was similar to behavior in suburban locations probably because there was little shadowing in both regions. The bulk of the rural data was collected in deep canyons at Estes Park, Colorado. A path loss of 15 dB was observed for 90/90 coverage with most of the fading attributed to evergreen foliage. For comparison, suburban data showed path losses for 90/90 coverage to vary from 4 to 16 dB [34]. Hess also collected rural region data while crossing Nevada but noticed a severe fade only when he went under a railroad overpass [36].

The signal strength distribution functions were then used to generate a model to predict excess path loss associated with 90% temporal coverage and any percentage value for spatial coverage. The model was based on polynomial fits using the five measurement parameters previously mentioned. Further details of the model are discussed in Section 4.1. The model showed that local environment and vehicle heading were the most significant parameters. Surprisingly the other parameters, frequency, street side, and elevation angle, were only marginally significant. Hess gave an example of frequency insensitivity by showing that a change in link frequency from L-band to UHF resulted in only a 1.4 dB change in the excess path loss prediction [35].

The secondary fading statistic, level crossing rate, corresponding to the signal strength CDF of Figure 3.4-1 is shown in Figure 3.4-3. These curves were segregated according to vehicle heading relative to the satellite azimuth. Note that the curves took different shapes for vehicle headings either parallel and perpendicular to the satellite azimuth, but that in both cases, the LCR was insensitive to frequency for heading differences of 180°. Also note that in both graphs the LCR is significantly depressed relative to the LCR for a Rayleigh fading signal, marked by the solid line connecting the circles.

The other fading statistic, average fade duration, is shown in Figure 3.4-4 with the same circumstances as for Figure 3.4-3. Similar to the LCR graphs, the fade duration was generally insensitive to frequency and vehicle headings 180° apart. However, the graphs show the average fade duration to be longer than for a Rayleigh fading signal again marked by the solid line connecting the circles.

The fading statistics thus show a satellite signal to fade at a slower rate but for a longer period than a terrestrial signal with Rayleigh behavior. Hess concluded from his results that shadowing loss was more important than multipath cancellation loss [34].

3.5 ANDERSON ET AL. ATS-6 EXPERIMENT

Anderson et al. of General Electric also performed a land mobile satellite experiment using the ATS-6 satellite. Their overall goal was to

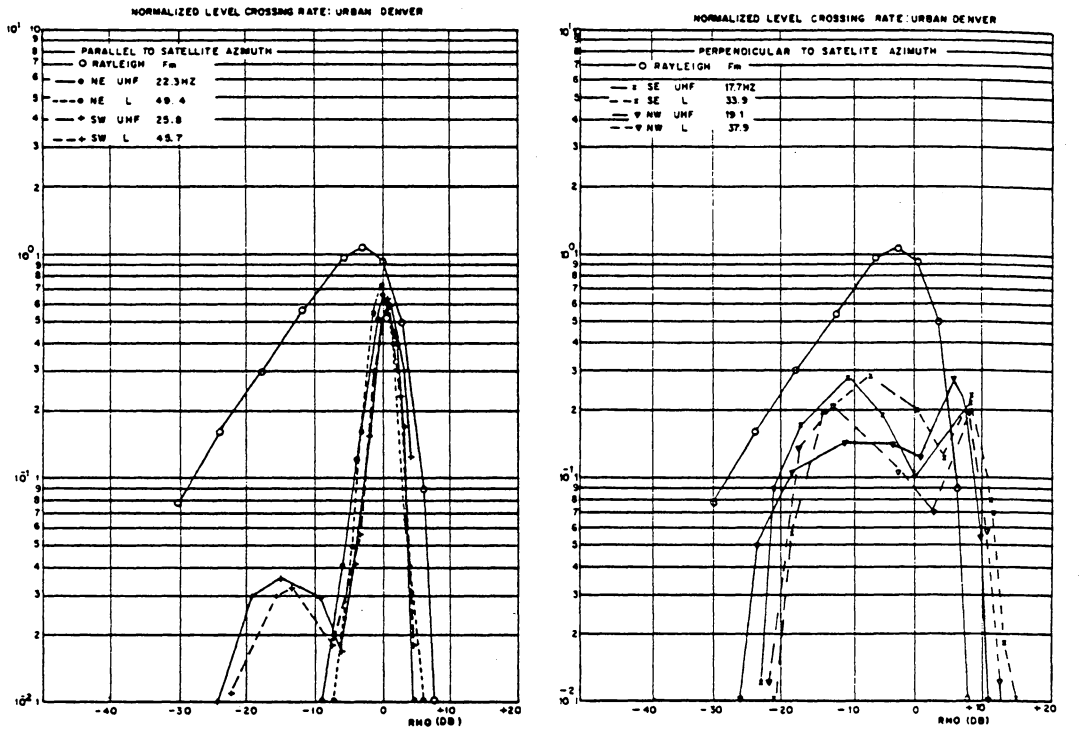

Figure 3.4-3 Normalized level crossing rate for urban Denver data. Azimuths are segregated. From Hess [34]

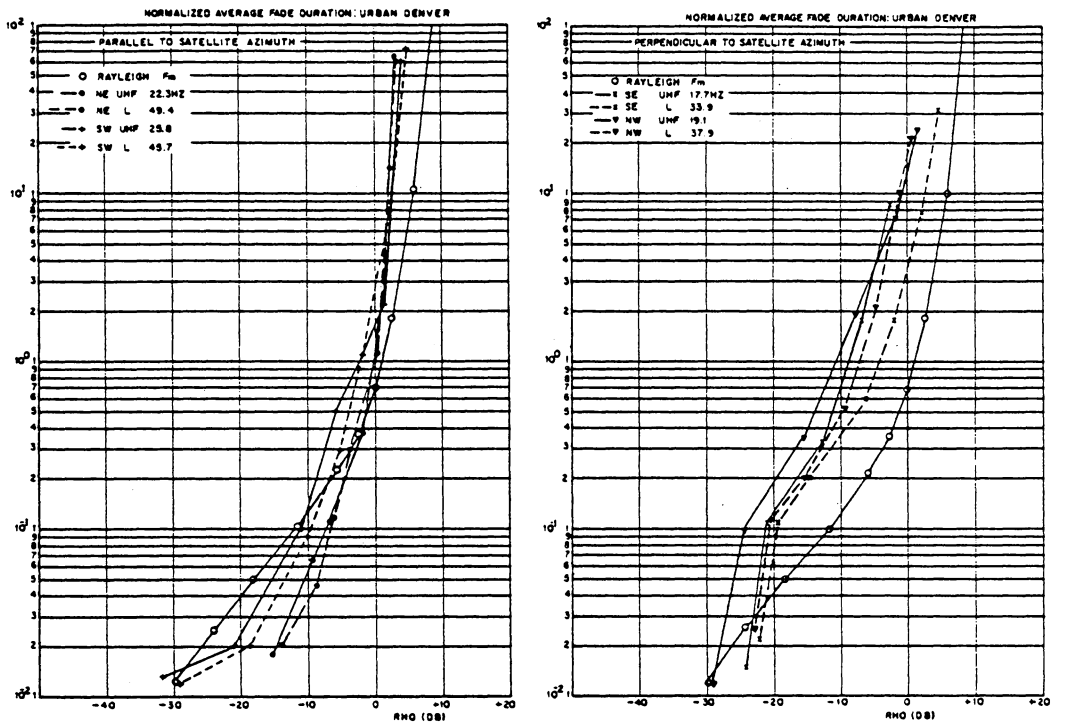

Figure 3.4-4 Normalized average fade duration for urban Denver data. Azimuths are segregated. From Hess [34]

demonstrate the feasibility of new applications of satellite-aided mobile communications with a series of communications and position fixing experiments using automotive vehicles, ships, and aircraft. Consequently, the characterization of propagation effects was limited and more qualitative than in previously discussed experiments. One experiment of particular relevance to this effort was the field test of a mobile communications system (using ATS-6) to dispatch freight trucks. The following summary comes from the final report describing operational testing in the trucking industry [2] and from the IEEE paper describing GE's experiment program [3].

Five tractor-trailer trucks were equipped with radios that were modified to operate at L-band (1651 MHz transmit and 1551 MHz receive). The system used narrowband FM to transmit the analog voice signals. Communications between the trucks and a base station were relayed through GE's research lab so that all signals could be stored for later analysis. The right hand circularly polarized (RHCP) signal from ATS-6 was received by the trucks using a specially designed antenna mounted on the cab. This antenna was a linearly (vertically) polarized array of the Wheeler type designed to be omnidirectional in azimuth.

The trucks travelled through several different types of terrain including regions with foothills, open plains, mountains, and forested, rolling hills. Elevation angles to the satellite over the routes varied from 9 to 23°. All of the voice communications were recorded and subjectively judged for signal quality. Overall, communication was found to be

reliable 93% of the time with reliable meaning "clearly understood" messages.

As expected, communication reliability varied with the terrain. The highest reliability , 97%, was found in the midwestern open plains region where the elevation angle was 26°. In the western Appalachian foothills region of Ohio and Tennessee with a 22° elevation angle, data showed signal blockage occurred 9% of the time and blockage was caused by the surrounding mountains and foothills. Data taken through routes in the Appalachian mountains gave similar results. Also in that region Anderson estimated an additional 6% of the time attenuation or blockage was due to trees. However, trees only seemed to cause brief fades or just slightly decrease the signal level. Data taken in the Piedmont region of Virginia and North Carolina with an elevation angle of 11° also showed hills and trees to be the main blocking factors. The percentages of blockage time broke down as follows: hills, 4.2%; trees, 3.2%; structure blockage, 1.1%; and overpasses, 0.7% [2]. Anderson's report also included a strip chart recording of the received signal power from typical communication with a truck. The graph showed peak fluctuations of 2 to 3 dB with a deep fade (more than 20 dB) due to an underpass [2].

One separate test showed that the ATS-6 L-band signal passing through the center of a tree at 9° elevation angle was attenuated in excess of 20 dB [2].

Anderson concluded that satellite communications worked well with mobiles in non-urban areas and predicted even better performance using a satellite positioned at higher elevation angles. Anderson also made some general conclusions concerning propagation. First, he noted that vegetation is a serious screen to L-band signals. Trees would cast a sharply defined shadow and cause brief dropouts. Furthermore, complete blockage of the signal would occur for buildings, overpasses, and mountains. Generally, he found that blockage effects were sharply defined and attenuated the signal below any reasonable margin. Finally, Anderson noted that multipath reflection effects were significantly smaller than for a terrestrial link. Consequently, a clear line of sight would mean good communications [2].

3.6 COMPARISON OF THE DATA

In spite of the variety of experimental characteristics, a comparison of the different data sets showed that the signal fading statistics behaved in a fairly uniform manner. A comparison of signal distribution functions from two CRC measurements and Vogel's first experiment is given in Figure 3.6-1. Both experimenters observed Rice distribution characteristics at high signal levels, lognormal characteristics at low signal levels, and a pronounced "knee" in between. Both the CRC and Vogel results showed the Rician portion to be insensitive to elevation angle and shadowing.

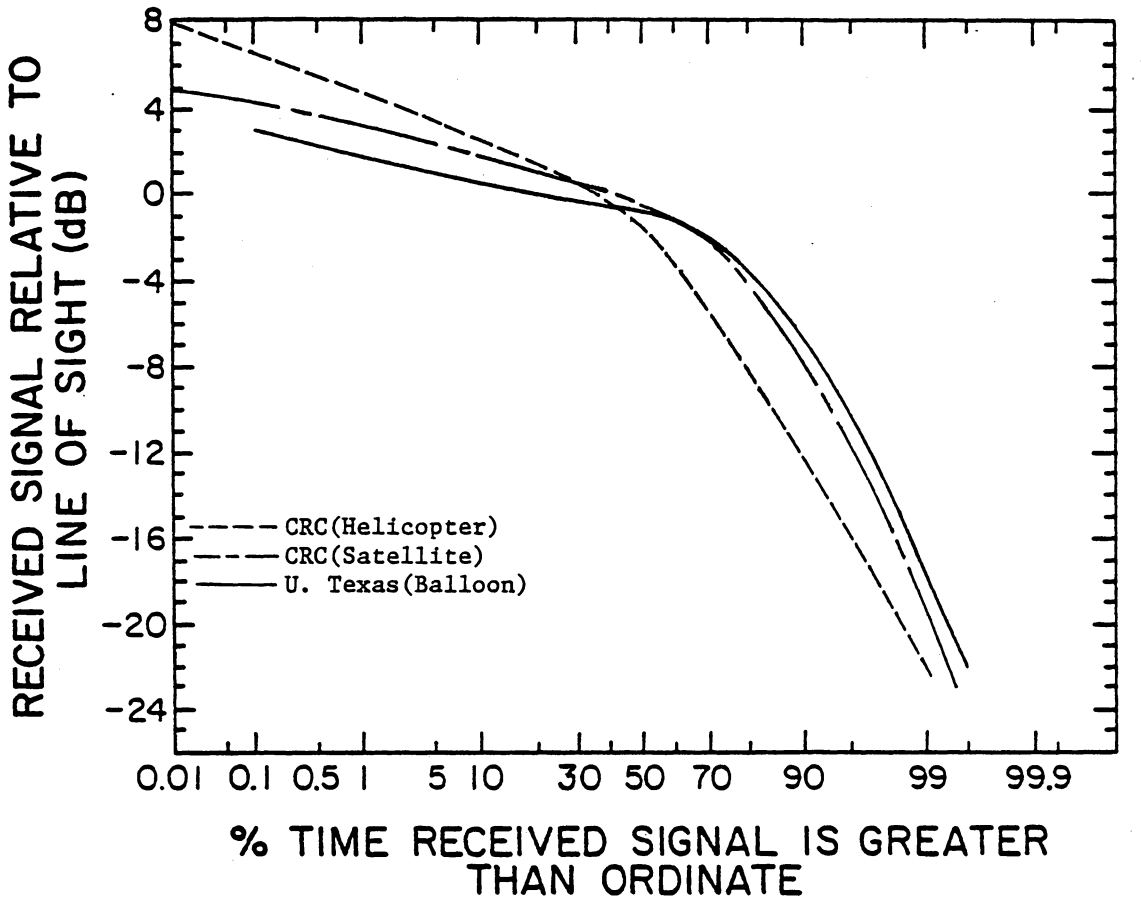

Figure 3.6-1 A comparison of the distribution functions for two CRC experiments and Vogel's first experiment.

Vogel also reanalyzed his data in the same way as Hess, and a comparison of these results is given in Figure 3.6-2. Note that Hess' data is for urban regions, but it still exhibits the same general properties as Vogel's rural data with a lower overall signal power.

A comparison of the level crossing rate and average fade duration results corresponding to the distribution functions of Figure 3.6-1 is given in Figure 3.6-3 and 3.6-4. Again, there is some agreement at least to an order of magnitude. Vogel's results were not reported in the same way as the CRC and were obtained by taking the mean value of the threshold curves of Figures 3.3-9 and 3.3-10. The threshold curves were close together and thus the flattened appearance for Vogel's data.

3.7 SUMMARY OF EXPERIMENTAL RESULTS

In this chapter all reported experimental results known to us on the topic of earth-space propagation related to land mobile operations were examined. Since the treatment was rather lengthy, the following summary is included.

1. A comprehensive (and useful) set of experiments were conducted by the CRC of Canada at 870 and 1542 MHz. They found the following:

    a. Mobile measurements made with a balloon-borne transmitter in wide open regions showed signal statistics due to multipath

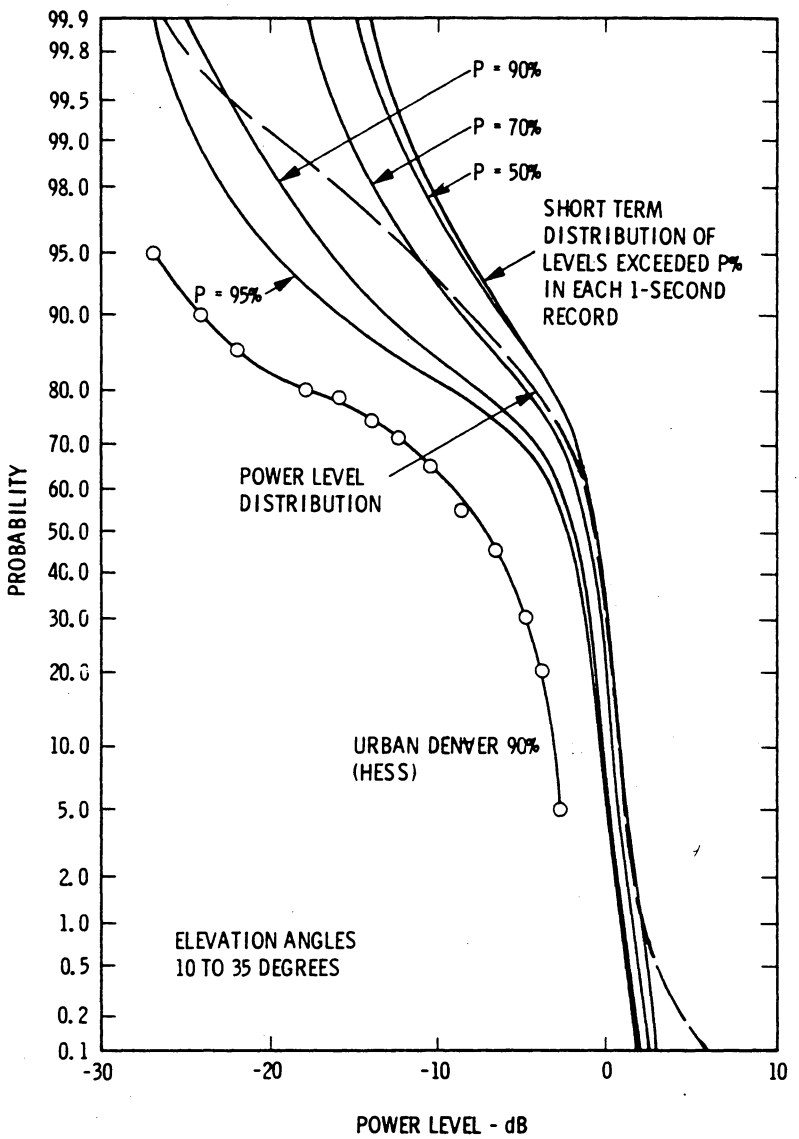

Figure 3.6-2 A comparison of the distribution functions from Vogel's first experiment and Hess' urban Denver data. From Vogel [77]

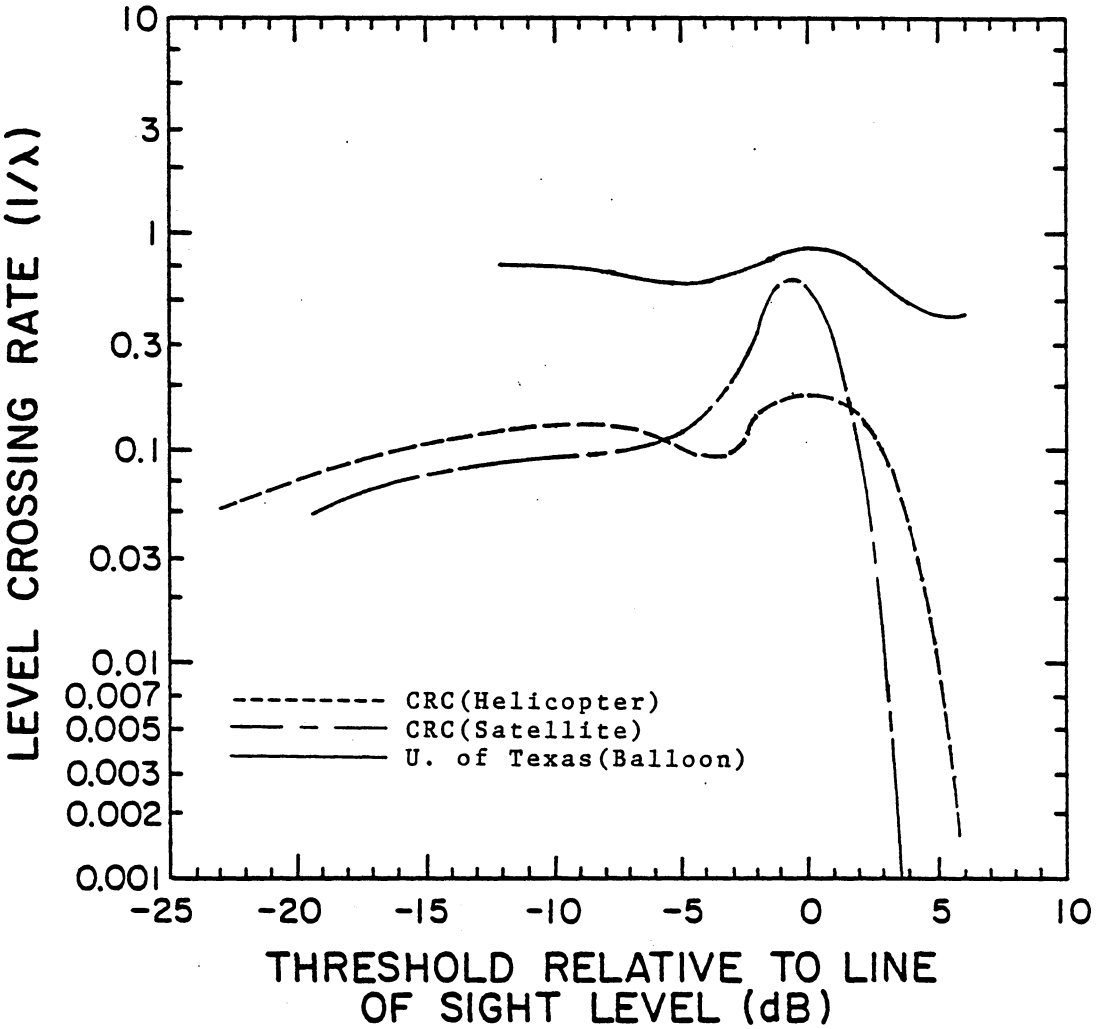

Figure 3.6-3 A comparison of the level crossing rates corresponding to the distribution functions of Figure 3.6-1.

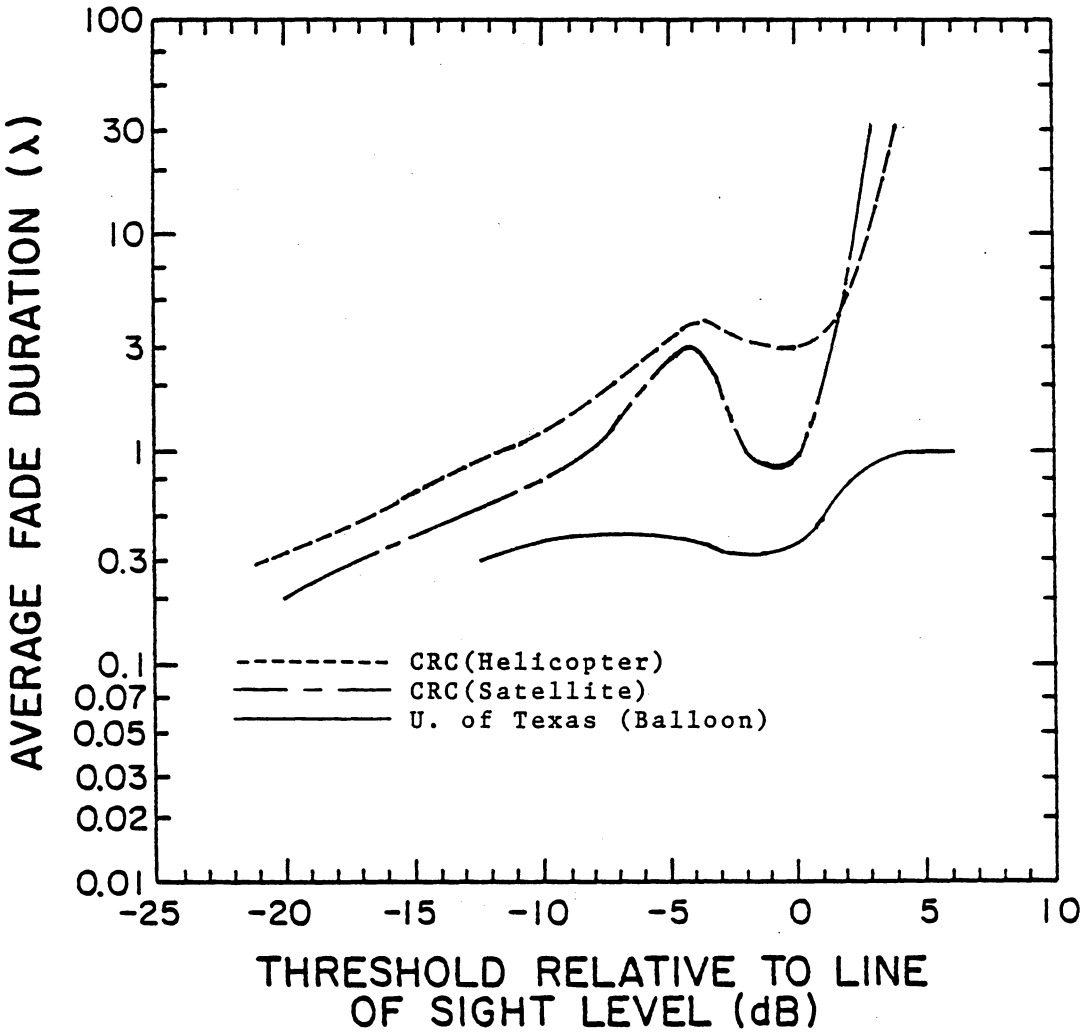

Figure 3.6-4 A comparison of the average fade durations corresponding to the distribution functions of Figure 3.6-1.

interference to follow a Rice distribution. The mean value for the diffuse to line of sight component ratio was -11 dB.

b. More extensive mobile measurements using a helicopter-borne transmitter on a variety of test routes showed that signal statistics were heavily dependent on the vegetation present. For a source at 15°, mean attenuation due to multipath fading and vegetation shadowing was as high as 10 dB in some areas. Another set of measurements using the helicopter was made for elevation angles of 5, 15, and 20°. The signal statistics showed that lowering the elevation angle had the same effect as increasing shadowing. For 99% coverage in the measurement area, margins of 20 dB would be needed at 15° elevation angle and about 14 to 16 dB at 20° elevation angle.

c. Specular reflection was observed in open terrain at 5° elevation angle and caused slow fading with fade depths of 7 to 8 dB.

d. Measurements made at L-band (1542 MHz) with the MARECS-A satellite at 20° elevation angle showed the same vegetation dependent characteristics as found for lower signal levels. The Rice portion of the curves changed little with the amount of shadowing. Data taken in the spring and fall showed changes in signal statistics due to seasonal variation in foliage attenuation. Margins to provide 99% coverage to the test area

varied from 12 dB in a rural farmland region to 21 dB in a suburban region.

2. Similar experiments using balloon flights at the University of Texas were also conducted. The signal power distribution tended to follow a Rice distribution for higher signal levels and was relatively insensitive to elevation angle. Time plots of received signal strength show only small variations in open terrain but deeper fades occuring in the presence of vegetation and man-made blockage. Fade depth decreased with higher elevation angles, but problems in computing a free space correction lead to uncertainty in the dependence of the results on elevation angle.

3. Garry Hess conducted excess path loss measurements using the ATS-6 satellite at both 860 MHz and 1550 MHz. Most of the measurements were made in urban regions with very little data taken for rural regions. Hess noticed no significant fluctuations in signal strength while crossing open terrain in Nevada. Measurements made in Estes Park, Colorado showed a 15 dB margin required for 90/90 coverage with the signal loss attributed to foliage blockage. Suburban data showed required margins for 90/90 coverage to vary from 4 to 16 dB. Significant differences were observed in the fading statistics with respect to direction of travel relative to satellite azimuth. Worst and best performance was observed for travel perpendicular and parallel to satellite azimuth, respectively. Link frequency showed little effect (on the order of 1 dB) on excess path loss. Satellite

elevation angle also showed little effect. Level crossing rate and average fade duration were observed to be independent of frequency. Compared to terrestrial sources, satellite signals faded at a lower rate but fades tended to last longer.

4. Anderson made qualitative observation about propagation based on an experiment to communicate with trucks at L-band using the ATS-6 satellite. He observed that multipath fading only caused a 2 to 3 dB variation in signal strength. Vegetation proved to be a serious screen to L-band signals. Fades due to blockage by trees, hills, and man-made structures were often brief but severe and well defined. Usually a clear line of sight meant "good" communications.

IV. MODELING AND SIMULATION EFFORTS

This chapter briefly discusses the reported efforts to model or simulate the fading and shadowing effects for LMSS links. The purposes of this information are: 1) to observe what modeling approaches have and have not been successful, and 2) to guide future work and minimize duplicated effort by the Virginia Tech Satellite Communications Group in developing their own simulation studies of LMSS signal statistics.

Section 4.1 summarizes the Hess empirical model for predicting fade margins from five measurement parameters. Section 4.2 summarizes the CRC analytical modeling and simulation efforts to describe the fading statistics from field measurements. Section 4.3 mentions the capabilities of the simulators at JPL for evaluating LMSS communication links.

4.1 HESS MODEL

Hess [34], [35] developed an empirical model from his measurement data to predict the margins required for 90% temporal coverage and any specified large scale coverage. Thus the model is not a pure statistical model, but it does make margin predictions based upon the statistical properties of the data. A summary of the model equations is given in Table 4.1-1; the model coefficients are given in Table 4.1-2.

Table 4.1-1
Hess model for predicting fade margins assuming
90% temporal coverage. From Hess [34]

MARGIN EXCESS PATH LOSS + K * SLOPE

EXCESS PATH LOSS A0 + A1*ENVIR + A2*ADJAZ + A3*FREQ
+ A4*SIDE + A5*ELEV

SLOPE B0 + B1*ENVIR + B2*ADJAZ + B3*FREQ
+ B4*SIDE + B5*ELEV

K	Spatial Coverage
0	50%
1.3	90%
1.65	95%
2.33	99%

VARIABLE	RANGE OF VALUES
ENVIR	Urban=1, Semi-urban=0, Suburban=-1
ADJAZ	-COS (2*(Vehicle heading - Sat. Azimuth))
FREQ	UHF = 1 , L-band =1.8
SIDE	+1 away, -1 towards satellite
ELEV	19° to 43°

Table 4.1-2
Coefficients of the Hess model for suburban/rural data. From Hess [34]

EXCESS PATH LOSS	SLOPE
A0 = 11.3 dB	B0 = 5.47 dB
A1 = 0 dB	B1 = 0 dB
A2 = 0.801 dB	B2 = 0.854 dB
A3 = 0.150 dB	B3 = 1.02 dB
A4 = 0.351 dB	B4 = 0.081 dB
A5 = -0.168 dB	B5 = -0.046 dB

To generate the model, values for excess path loss and slope were found from the mean and standard deviation, respectively, of lognormal fits to the data. Then the excess path loss and slope values were independently fitted to polynomials of the five measurement parameters mentioned in Section 3.4: local environment, vehicle heading, frequency, street side, and elevation angle. The coefficients of Table 4.1-2 for these parameters are for Hess' suburban/rural data only (coefficients for the urban data can be found in [34] or [35]); consequently, the local environment parameter is dropped. Also note that elevation angle was the least significant parameter. For the overall data set, the coefficients for frequency, street side, and elevation angle were only marginally significant [34].

We compared the Hess model values to those from the CRC MARECS-A experiment. The following values for the model variables were used:

1. Difference between satellite azimuth and vehicle heading = 90°: ADJAZ = 1
2. Frequency was at L-band : FREQ = 1.8
3. Both sides of the street were used : SIDE = 0
4. Elevation angle was about 20° : ELEV = 20

The computed excess path loss and slope were:

EXCESS PATH LOSS = 9.0 dB

SLOPE = 3.6 dB

The corresponding margins were:

Spatial coverage (%)	Margin (dB)
50	9.0

90	13.7
95	14.9
99	17.4

These results are plotted in Figure 4.1-1 along with the CRC MARECS-A signal level distributions. In this case, the Hess model does not predict fade margins very well. However, the coefficients for the model were based on a small data set. Applying the Hess model in the future to a much larger data base with the inclusion of a few more parameters would probably produce much better results and may be a useful approach for predicting fading margins.

4.2 CRC MODELING AND SIMULATION

The CRC measurement program discussed in Section 3.2 is accompanied by analytical modeling and hardware simulation efforts. This section summarizes some of the useful results from each.

4.2.1 STATISTICAL MODELING

Early in the CRC measurement program, multipath fading and vegetative shadowing were observed to have Rician and lognormal behavior, respectively. A first attempt at modeling the overall density function was to numerically convolve the Rice and lognormal density functions.

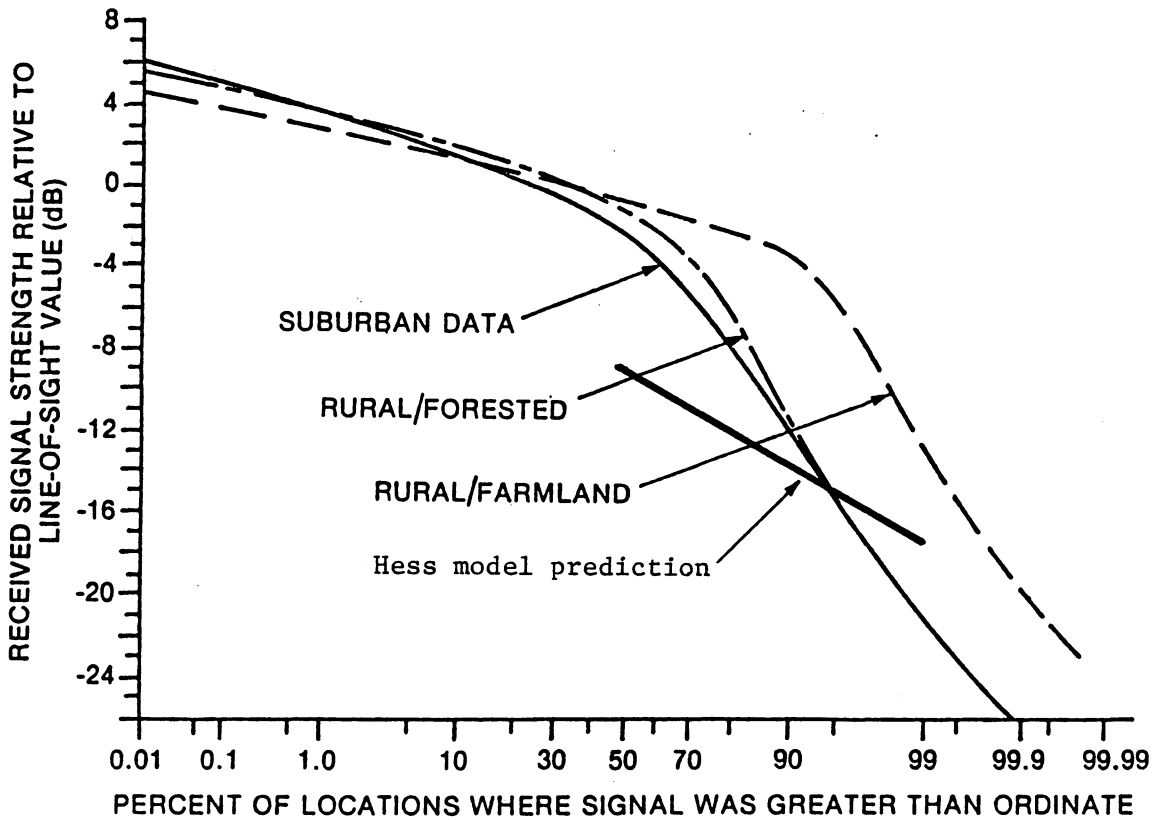

Figure 4.1-1 A comparison of the Hess model fade margin predictions to the CRC MARECS-A experiment and the measurement results.

Satisfactory fits of the resulting distribution function to the data were not obtained [12].

The next reported statistical modeling work was by Loo [49]. He proposes a statistical model that assumes the amplitude of the LOS component under vegetative shadowing is lognormally distributed and that the received diffuse multipath component is Rayleigh distributed. He first develops an equation for the probability density of the received signal amplitude which is given as:

$$p(r) = \frac{r}{b_o \sqrt{2\pi d_o}} \int_0^\infty \frac{1}{z} I_o(rz/b_o) \exp\left[- \frac{(\ln z-\mu)^2}{2d_o} - \frac{(r^2+z^2)}{2b_o} \right] dz \quad (4.2\text{-}1)$$

where b_o corresponds to the average Rayleigh multipath power; it corresponds to $\alpha^2/2$ defined earlier for the Rayleigh distribution and $k^2/2$ for the Rice distribution. μ and d_o are the mean and variance of $\ln z$ for describing the lognormal component. Loo numerically evaluated (4.2-1) and fit the resulting CDF's for the signal level to the CRC helicopter data using trial and error to determine b_o, μ, and d_o. Figure 4.2-1 shows the results of this work. The best fit is for the heavy shadowing case. For the light shadowing case, the fit in the median region is good, but there is some deviation at the tails of the distribution. For the overall results, the fit was rather poor in the median region but better at the tails.

Loo also derived equations for the normalized level crossing rate and average fade duration for his statistical model. He assumed that the rate

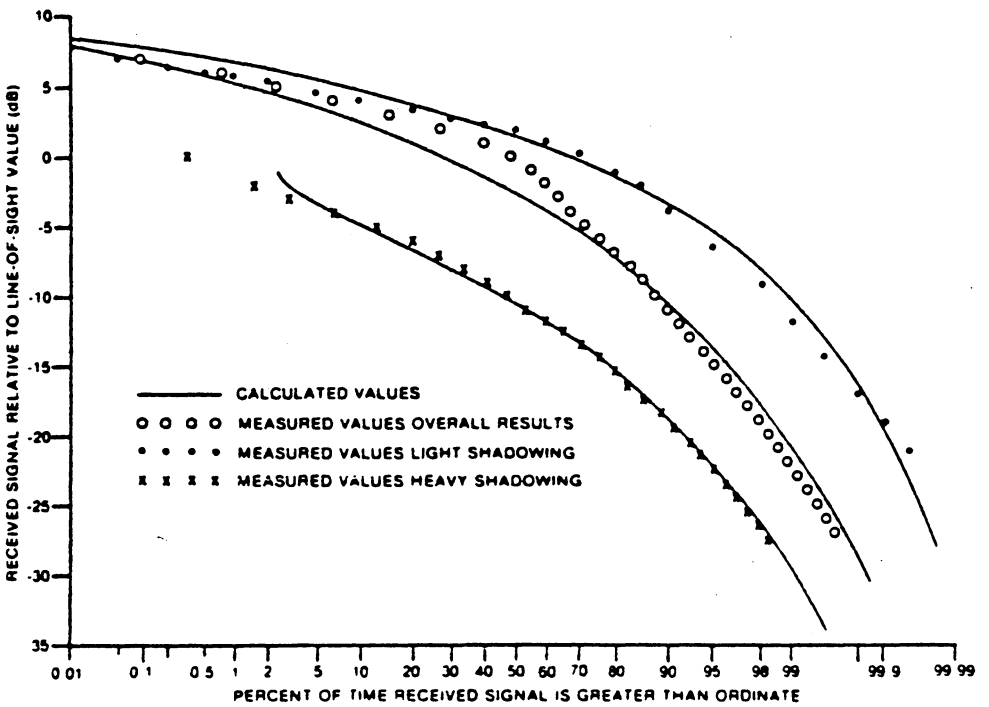

Figure 4.2-1 Comparison of distribution functions from the CRC helicopter data to the Loo model. From Loo [49]

of change of the received signal envelope from the lognormal and Rayleigh components could be correlated. Comparisons of calculated values from the model to the CRC helicopter measurements showed the best fit for the heavy shadowing case. These results are shown in Figure 4.2-2 and 4.2-3 with ρ denoting the correlation coefficient. Note that high correlations, ρ=0.7 to 0.8, gave the best fit. The same result was observed for the light shadowing case. Consequently, Loo concluded that the effects of foliage attenuation and multipath fading on the rate of change of the received signal envelope actually are correlated.

The planned future work with this model is the investigation of the phase distributions for the fading signal.

4.2.2 SIMULATION

A parallel effort at the CRC is the development of a hardware channel simulator reported by Butterworth in [14], and [15]. Their simulator was designed to reproduce the fading effects for land, sea, and air mobile applications. The input signal is split into two paths. On one path, the signal is amplitude and phase modulated by a Rayleigh fading generator to simulate additive Rayleigh distributed multipath. On the other path, the signal either passes through unaffected or is attenuated according to a lognormal distribution. This path simulates the direct component with the effects of vegetative shadowing. The signal outputs from the two paths are then added to simulate Rice or lognormal plus Rayleigh

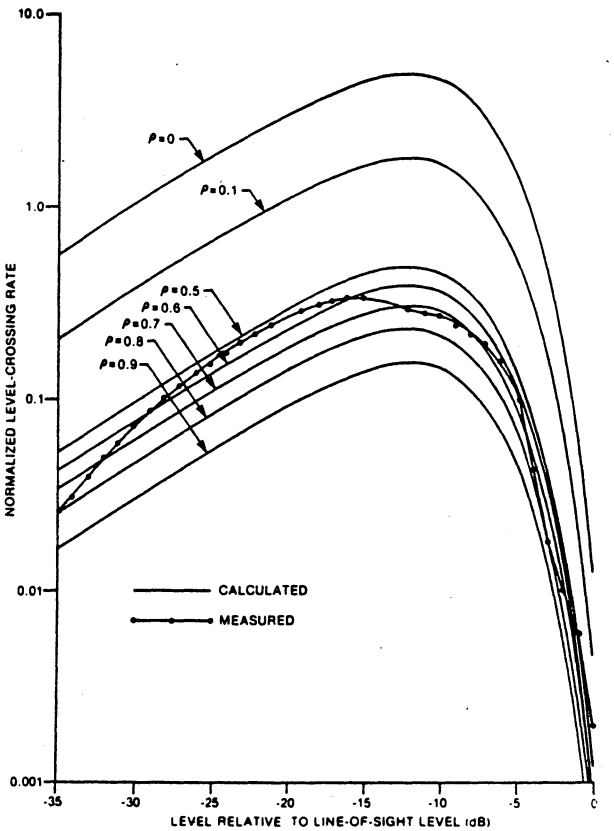

Figure 4.2-2 Comparison of the normalized level crossing rate from the Loo model and the CRC helicopter data (heavy shadowing case). From Loo [49]

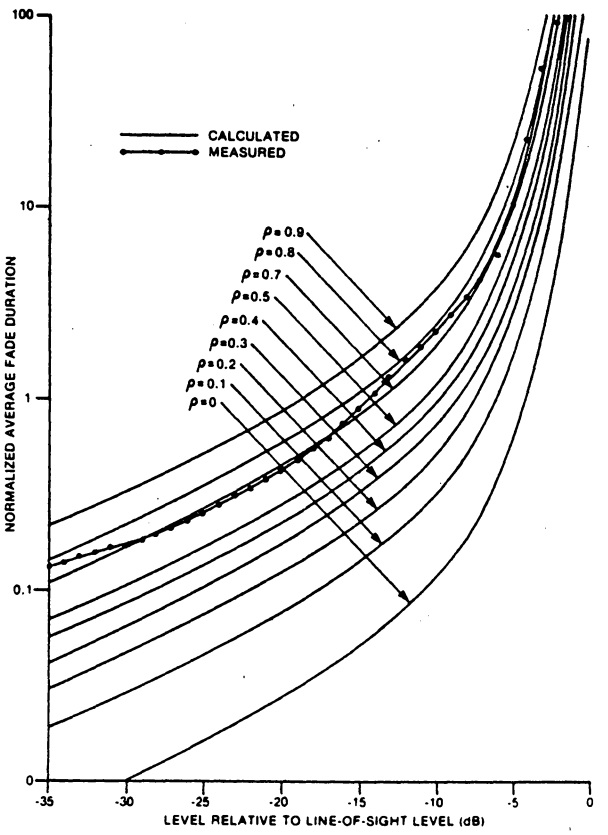

Figure 4.2-3 Comparison of the normalized average fade durations from the Loo model and the CRC helicopter data (heavy shadowing case). From Loo [49]

statistics. The multipath power and lognormal fading standard deviation are user selectable; the lognormal fading mean is automatically set to 2.5 times the standard deviation. The relative fading rate is preset so that the direct component fading varies one-hundredth as fast as the Rayleigh multipath fading. This rate was chosen from observations of data from the field measurements of Section 3.2. Vehicle speed is simulated by changing the cutoff frequency of Rayleigh multipath spectrum. The effects of a directional antenna are not included; an omnidirectional azimuth pattern is assumed.

To evaluate the simulator, the output signal was processed and analyzed with the same equipment as that used for field tests. Trial and error procedures showed that a multipath power 10 dB below the direct component, corresponding to a Rice K of -10 dB, best modeled measurement data for the unshadowed case. The mean and standard deviation chosen for the shadowing were -7.5 dB and 3 dB respectively. Shadowing effects were generated by concatenating files of shadowed and unshadowed data points in various proporations. Figures 4.2-4, 5, and 6 show the results from this mixing procedure on the signal statistics using 33% shadowed data points. Butterworth noted that these combined statistics matched the "suburban" curve of Figure 3.2-10, 11, and 12. The CDF's for other proportions of shadowed data is given in Figure 4.2-7. The 5% curve was noted to be a reasonable match to the rural/farmland curve of Figure 3.2-10 [15].

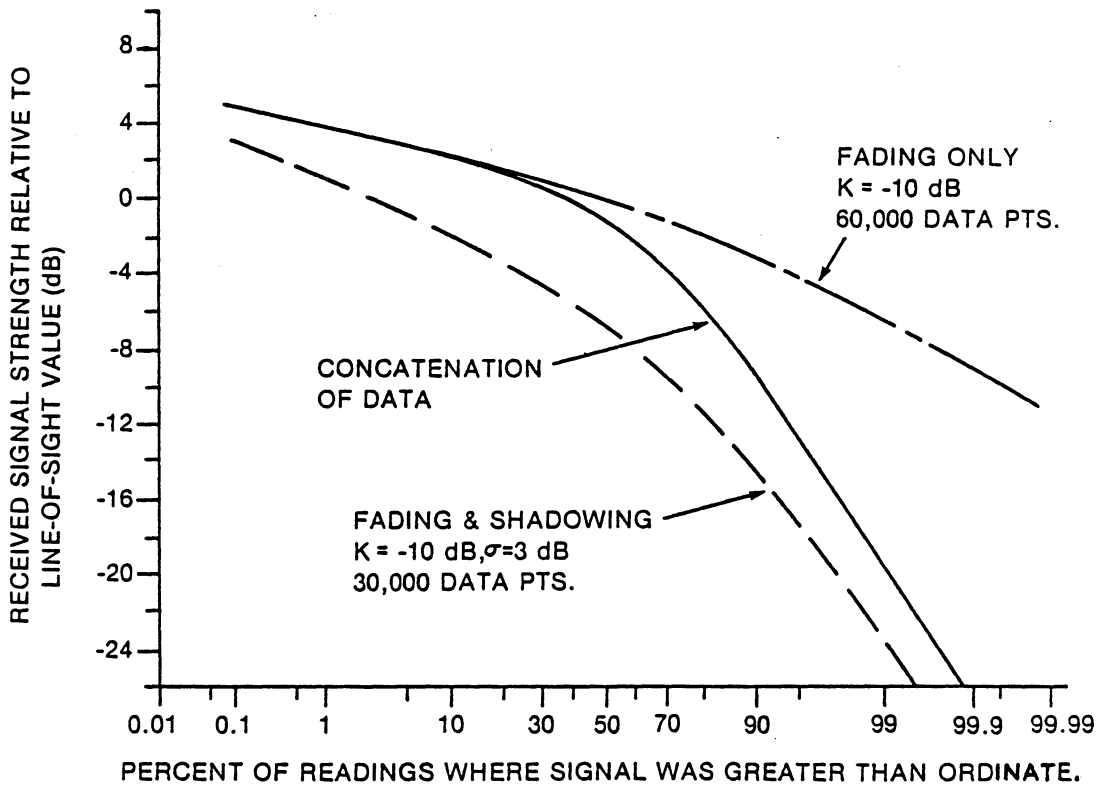

Figure 4.2-4 Distribution functions of simulator data with 33% shadowed data in the concatenated result. From Butterworth [14]

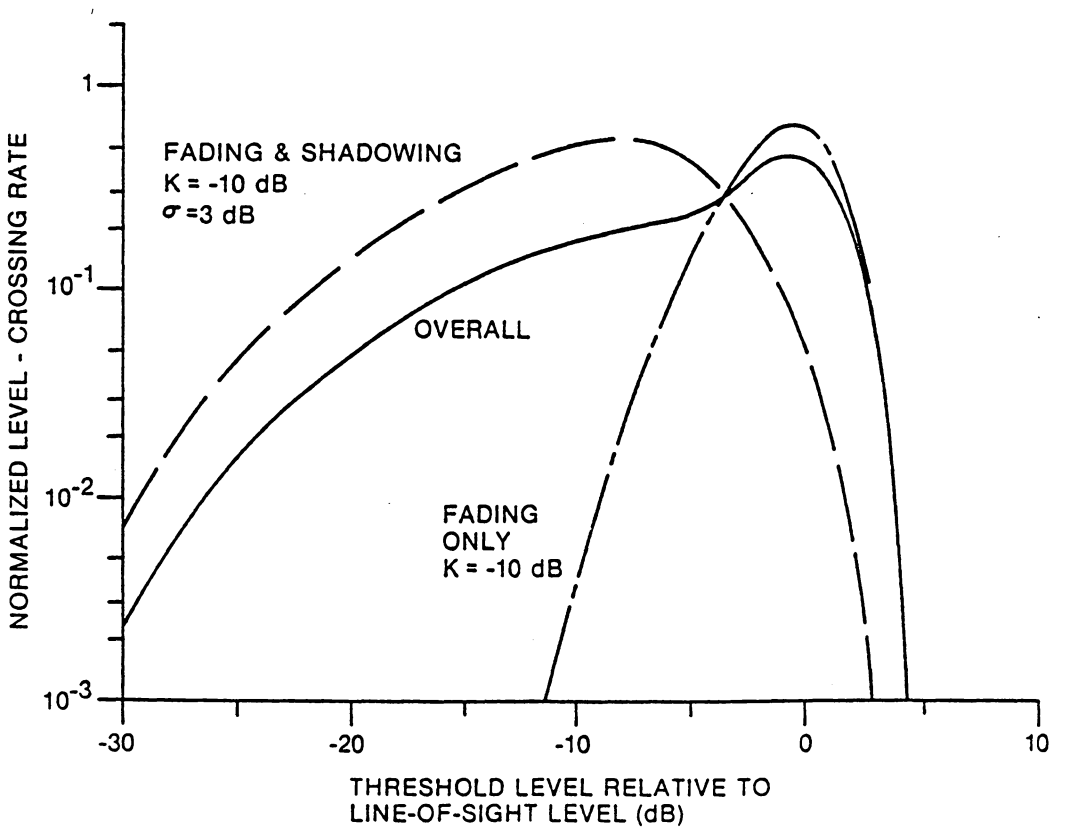

Figure 4.2-5 Normalized level crossing rate of the simulator data with 33% shadowing. From Butterworth [14]

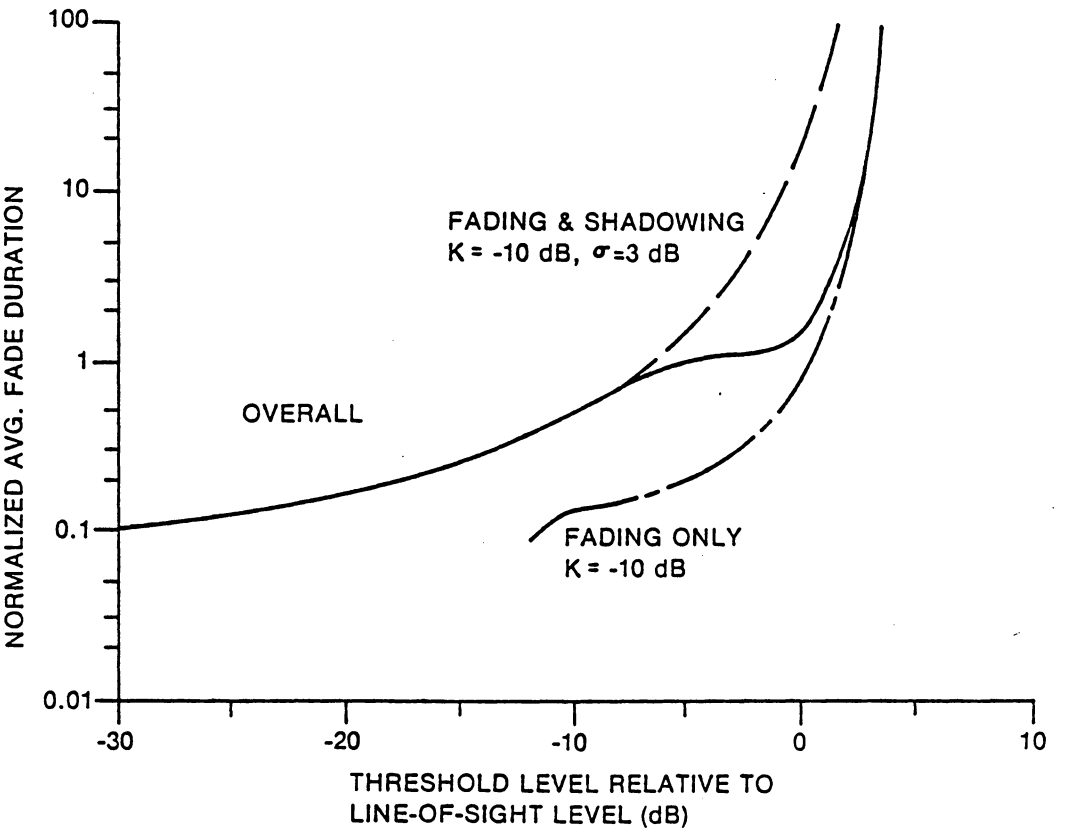

Figure 4.2-6 Normalized average fade duration of the simulator data with 33% shadowing. From Butterworth [14]

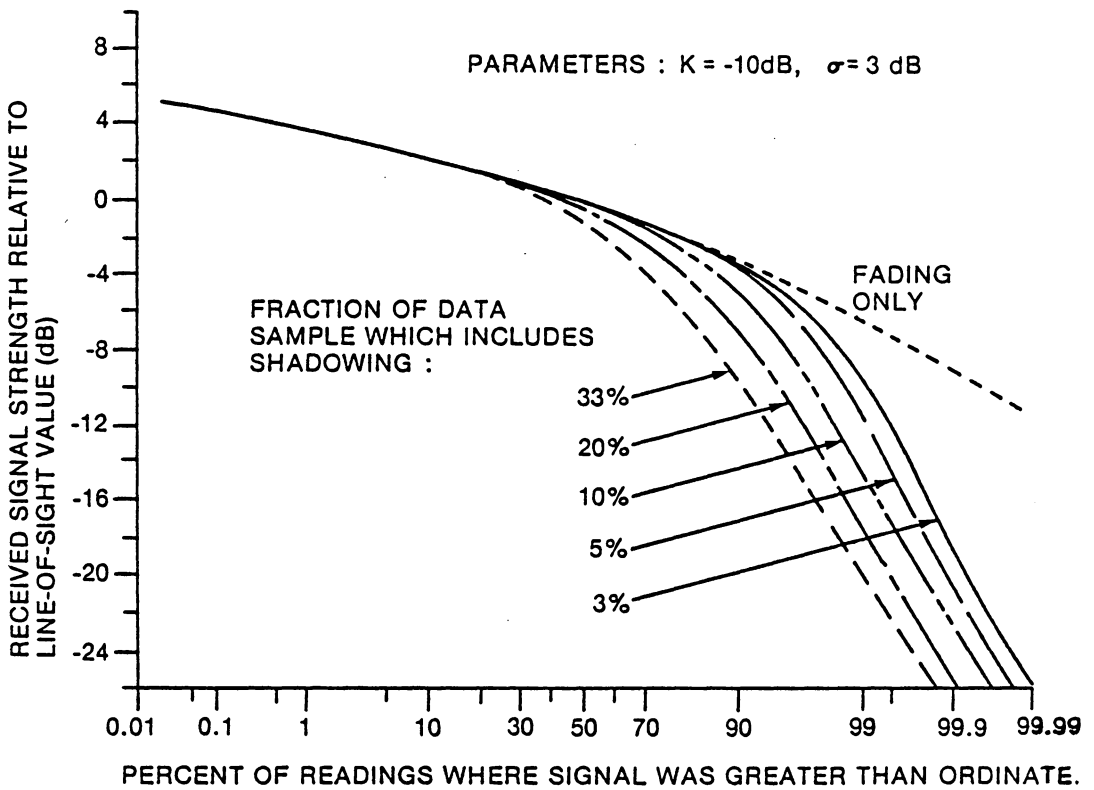

Figure 4.2-7 Distribution functions of the simulator data for various percentages of shadowing. From Butterworth [14]

4.3 JPL SIMULATORS

The Jet Propulsion Laboratory has developed two simulators for the LMSS channel: one is implemented in hardware [24], [25], [62], [64] and the other in software [26].

The hardware simulator was developed for end-to-end evaluation of LMSS communication links. It has the ability to simulate link impairments such as propagation effects, adjacent or co-channel interference, band limiting, nonlinearities, and thermal noise. To simulate propagation effects, the output of a Rayleigh multipath generator is added to the input signal; the resulting signal has Rician fading behavior. The technique is identical to that used for the CRC simulator of Section 4.2.2. Varying vehicle speeds are accounted for by changing the Doppler cut-off frequency of the multipath spectrum and by changing the Doppler shift of the direct component. The direct component may be attenuated (but not in a dynamic fashion) to simulate vegetative shadowing.

The reported results from the simulator are bit error rate evaluations of GMSK and 2-bit MSK modulation under various fading conditions [24], [25] and tests of NBFM modulation on voice systems [64]. No further analysis of the signal fading statistics have been reported other than verification that the output signal spectrum approximated theoretical predictions for a Rician fading signal.

The software simulator has been developed more recently and has slightly different capabilities. It simulates the Rayleigh distributed multipath in the same manner as the hardware simulator. The fading spectrum can be adjusted for the speed of the mobile, and Doppler shifts can be put into the direct component. Additionally, the effects of a specular component and the antenna gain pattern can be included.

A sample of the amplitude time plot from a simulation is shown in Figure 4.3-1. (The simulator produces 2400 samples for one second.) Note that this figure looks very similar to the Vogel timeplot of Figure 3.3-3. Analysis of the amplitude level statistics showed close agreement with a Rice distribution as expected. Histograms of the fade duration and non fade duration (probably better called interfade interval) for two different Rice K parameters, at a threshold of -5 dB, showed a trend to longer fades and longer interfade intervals for smaller K [26]. No further analyses were reported to correlate simulator output with the fading statistics observed from measurement. JPL also plans to include shadowing effects but no formal results have been reported yet.

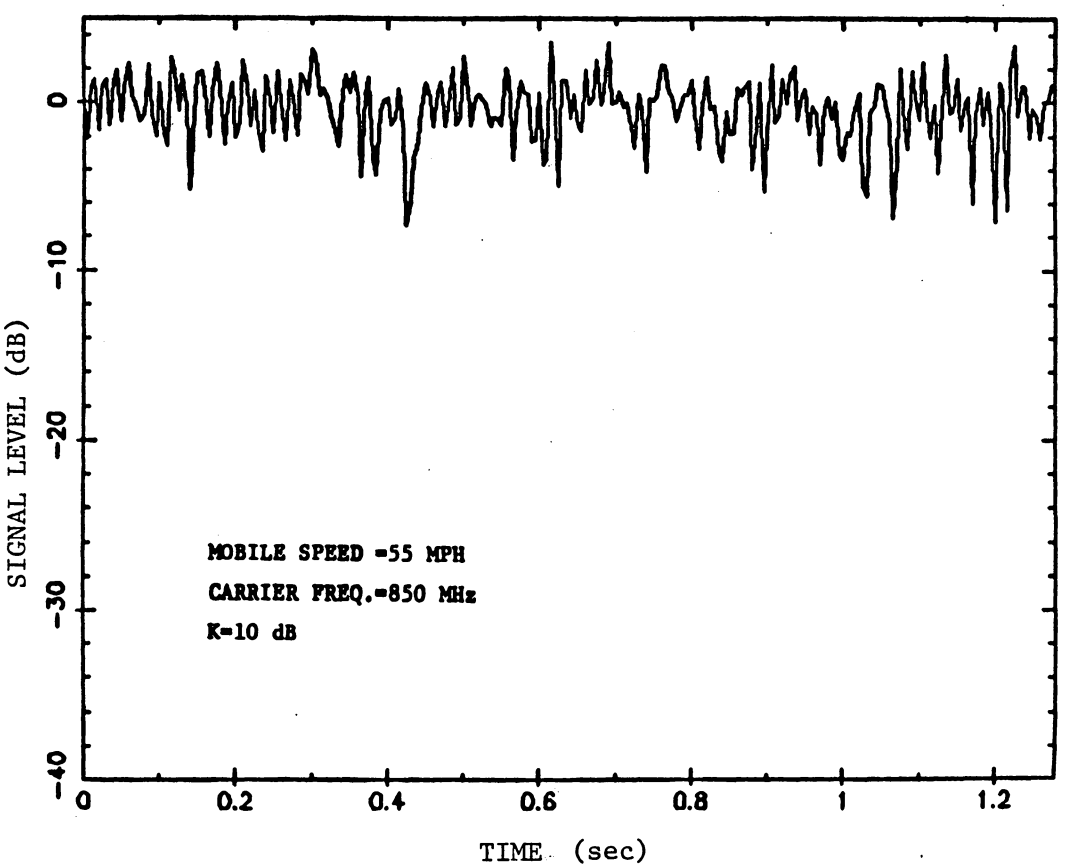

Figure 4.3-1 Sample time plot of the signal level from JPL's software channel simulator. From Divsalar [26]

V. PROPAGATION THROUGH VEGETATION

5.1 INTRODUCTION

Since vegetative shadowing is an important issue for LMSS operation, a literature study was conducted to answer some of the following questions:

1. How is vegetative loss predicted from the parameters of the medium and the path?

2. What are the individual effects of polarization, frequency, elevation angle, path length, and vegetation type and density on vegetative shadowing?

3. How does one describe the variations in signal level for a receiver moving in the presence of vegetation?

The problems are not trivial ones because of the complex nature of the medium. Much work has been done to describe propagation over and through vegetation on terrestrial communication links, but comparatively little has been done for satellite links. The following summary draws on both sets of information.

There are two aspects of vegetative shadowing that are of interest: mean path loss and spatial variation. Mean path loss is the average amount

of total loss expected from a given stand of vegetation; it may be determined from knowledge of the averaged properties of the medium and of the path. Quite often mean path loss is expressed in terms of specific attenuation, the rate of vegetative loss in dB/m. Mean path loss and specific attenuation have been the subject of many research efforts in this area and are addressed in Sections 5.2, 5.3, and 5.4. The spatial variation of total loss is of major interest when describing signal behavior for a mobile receiver. Here the total loss experiences random fluctuations due to multipath effects or to changes in the properties of the medium as the receiver is moved. Consequently, this behavior must be described by its statistical properties. Spatial variation is addressed in Section 5.5.

There have been two approaches to modeling vegetative path loss: analytical modeling and empirical modeling. Analytical modeling has produced few applicable results so far because of the lack of understanding of the parameters dominating propagation. Until recently, no useful analytical models other than diffraction models were available for describing propagation through vegetation at UHF frequencies [Nelson, 53]. Two of the latest analytical modeling efforts are discussed in Section 5.2.

Empirical modeling and experimental efforts, on the other hand, have a longer history. The first reported measurements were by Trevor [72] in 1940. Several sets of measurements have been made since then, primarily during the 60's, and around 1980. Four main empirical models followed

to characterize specific attenuation as a function of frequency [79]. These models have been referred to as exponential decay models because they assumed that signal power, in watts, decreases exponentially with vegetation depth. The most recent empirical modeling work has been done by Weissberger [78], [79] and is discussed in Section 5.3. Some of the most recent experimental efforts are also discussed in Section 5.3.

Section 5.4 contains a summary of the current knowledge on parameters affecting the magnitude and nature of mean path loss. Section 5.6 concludes with recommendations for the modeling assumptions that can be made based upon the information of the previous sections.

5.2 REVIEW OF ANALYTICAL MODELING EFFORTS

5.2.1 CYBERCOM STUDY

A recent effort is an Army sponsored program to assess the effects of foliage on wideband communication links in the 200 and 2000 MHz band for a ground mobile environment. Large theoretical and experimental efforts are involved. A good overview of the entire program has been given by Sass [66].

The theoretical portion of the program has been performed by the CyberCom Corporation [45], [46]. Their reports describe a stochastic model for radiowave propagation rigorously derived from discrete scattering theory. Tree trunks were modeled as infinitely long, circular dielectric

cylinders; branches as finitely long, circular dielectric cylinders; and leaves as flat circular dielectric disks. The end result is a set of equations to describe the effective dyadic susceptibility of the forest medium, the complex propagation constant of the mean field, and the space-frequency correlation function; all of these require knowledge of the scattering properties of the medium. These equations were also used to obtain mathematical expressions of specific attenuations for trunks, branches, and leaves based on knowledge of such forest parameters as trunk density, average trunk diameter, branch and leaf inclination angle distributions, fractional volume, and the permitivity of trunks, branches, or leaves. A graph of specific attenuation versus frequency for a forest of just trunks, with an exponential distribution of trunk diameters (mean diameter of 6.35 cm), is shown in Figure 5.2-1 for both vertical and horizontal polarizations. Similar curves were given for a forest path with a constant trunk size; these curves also approached an asymptotic level at higher frequencies and showed oscillatory behavior in the resonant region. Specific attenuation for a forest of leaves is shown in Figure 5.2-2. These curves show a distinct polarization dependence, but the magnitude of specific attenuation is smaller than that given for trunks. Unfortunately, a unified expression for specific attenuation including trunk, branch, and leaf effects was not studied.

The CyberCom report also discusses the applicability of their work to extending Tamir's [71] earlier slab model work to the 200 to 2000 MHz frequency range. Of interest is the derived expression for the reflection coefficient for the air-forest interface. The magnitude of the reflection

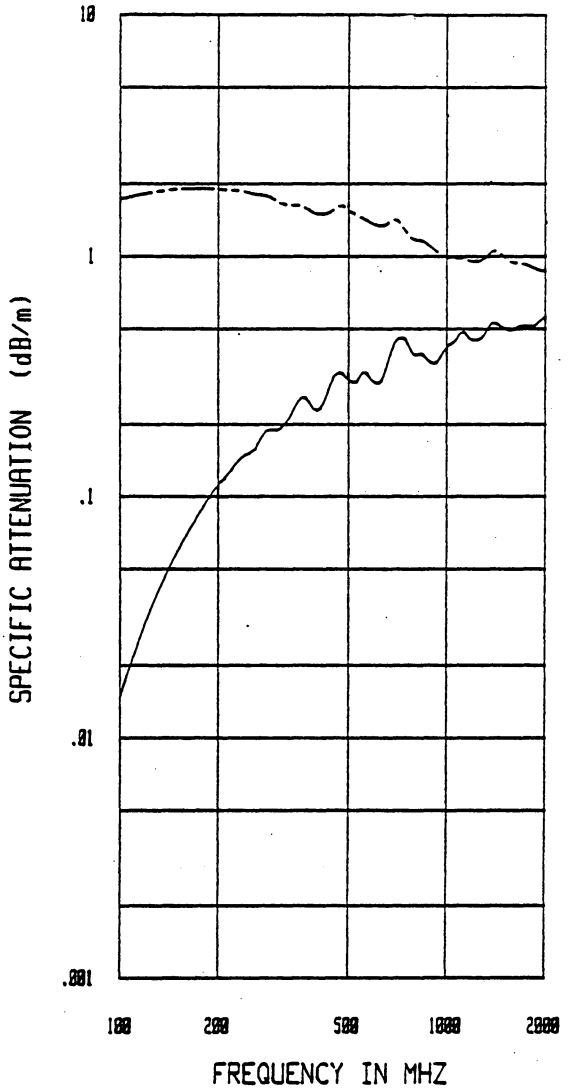

Figure 5.2-1 Specific attenuation vs frequency for a forest of trunks with exponentially distributed diameters (mean = 6.35 cm).

——— — — ——— vertical polarization

——————————— horizontal polarization

From Lang et al.[46]

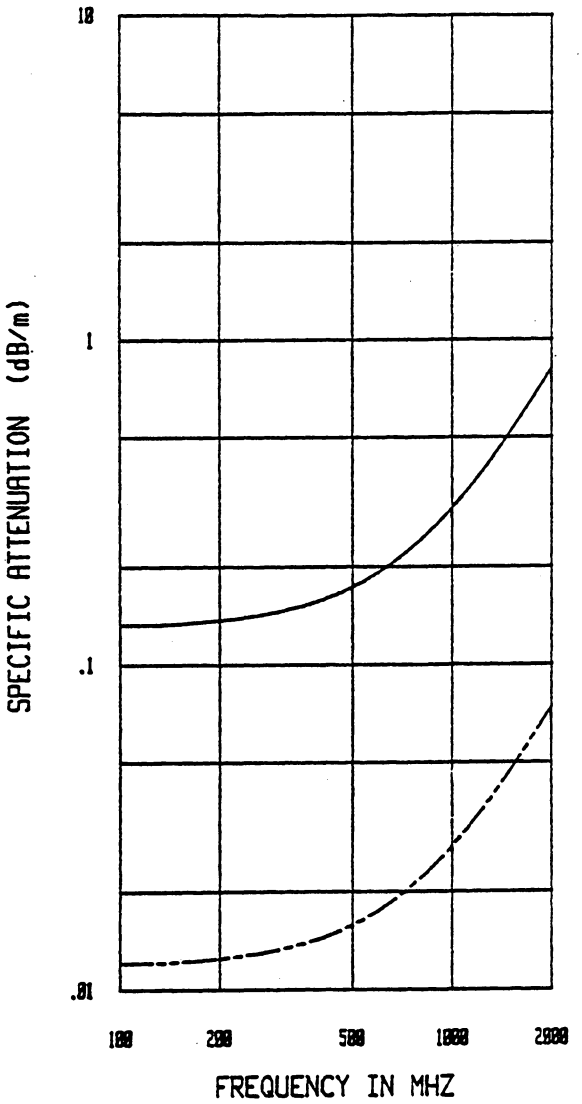

Figure 5.2-2 Specific attenuation vs frequency for a forest of leaves, fractional volume of 0.1%
——— — — ——— vertical polarization
——————————— horizontal polarization
From Lang et al, [46]

coefficient is nearly zero for incident angles above 10°; consequently, there will be little or no reflection, and the wave will propagate through the vegetation.

Refinement of this model should continue with the addition of planned experimental measurements. Currently more detailed knowledge about the medium is required before this model can be practically applied. CyberCom's second report [46] includes some preliminary analysis of the electrical and physical properties of forest constituents to address this problem. Also, a unified expression (including all tree components) for specific attenuation for the whole forest would be helpful to make the model more realistic.

5.2.2 BROWN AND CURRY "REV" MODEL

The second effort is that of Gary Brown and William Curry [9], as summarized in their paper titled "A theory and model for wave propagation through foliage". A more detailed treatment is given in [8]. Brown and Curry used Foldy-Twersky theory for coherent wave propagation through a sparsely populated, discrete random media to derive an expression for the complex propagation constant, and subsequently specific attenuation. Their results relied heavily on the observation from measurements by Stutzman et al. [70] that attenuation due to foliage was most highly correlated with that portion of foliage having a diameter of less than one-half a free-space wavelength. Consequently, the results were dependent upon an effective fractional volume of wood. For this reason,

Brown and Curry named the theory the Rayleigh effective volume (REV) model.

The final, simplified equation for specific attenuation from the REV model is given as:

$$\alpha' = k_o\{\rho\ V_p\}_{ew}\ q[\varepsilon'' + (\varepsilon'-1)/10] \qquad (5.2\text{-}1)$$

$$\alpha = 4.34\ \alpha' \qquad (5.2\text{-}2)$$

where α' = the imaginary portion of the complex propagation constant in m^{-1}

α = the specific attenuation in dB/m

k_o = the free-space wave number

$\{\rho\ V_p\}_{ew}$ = the effective fractional volume of wood

q = factor describing wood orientation distribution

$\varepsilon', \varepsilon''$ = real and imaginary parts of complex dielectric constant

Leaf effects were ignored because of their small fractional volume. Brown and Curry reasoned that branches would dominate propagation above 500 MHz. Assuming a uniform, random orientation of branches, specific attenuation then would be insensitive to polarization effects at UHF frequencies. Curves for specific attenuation versus frequency were given using estimates of the effective fractional volume and the complex dielectric constants. A curve including absorption and scattering effects is shown

in Figure 5.2-3. Note the convergence of the different polarization curves and a value for specific attenuation of about 0.30 dB/m at 850 MHz. Brown and Curry reported qualitative agreement of these curves with five sets of reported measurement data.

Direct application of the REV model would require statistical knowledge of the effective volume of foliage and a knowledge of its complex dielectric constant. Such information is generally not available. Furthermore, the conclusion that trunk and leaf effects are negligible contradicts the results of the CyberCom study. Brown and Curry especially suggest that more research be done to isolate and identify the vegetation components which are most significant in the attenuation process.

5.2.3 DIFFRACTION MODELS

Diffraction models have been applied to describe propagation loss on terrestrial paths by Head [33], Lagrone [44], Saxton and Lane [67], Reudink [58], and others (see Weissberger [79]) namely because trees were considered to be opaque obstacles and propagation was assumed to be over or around vegetation rather than through it. These models are sensitive to the clearance between the line of sight transmission path and the shadowing obstacle. This can be seen from Bullington's [11] graphical description of diffraction loss in Figure 5.2-4. The clearance, given in multiples of the first Fresnel zone radius, is the abscissa value. This normalized clearance value is in turn sensitive to the setback

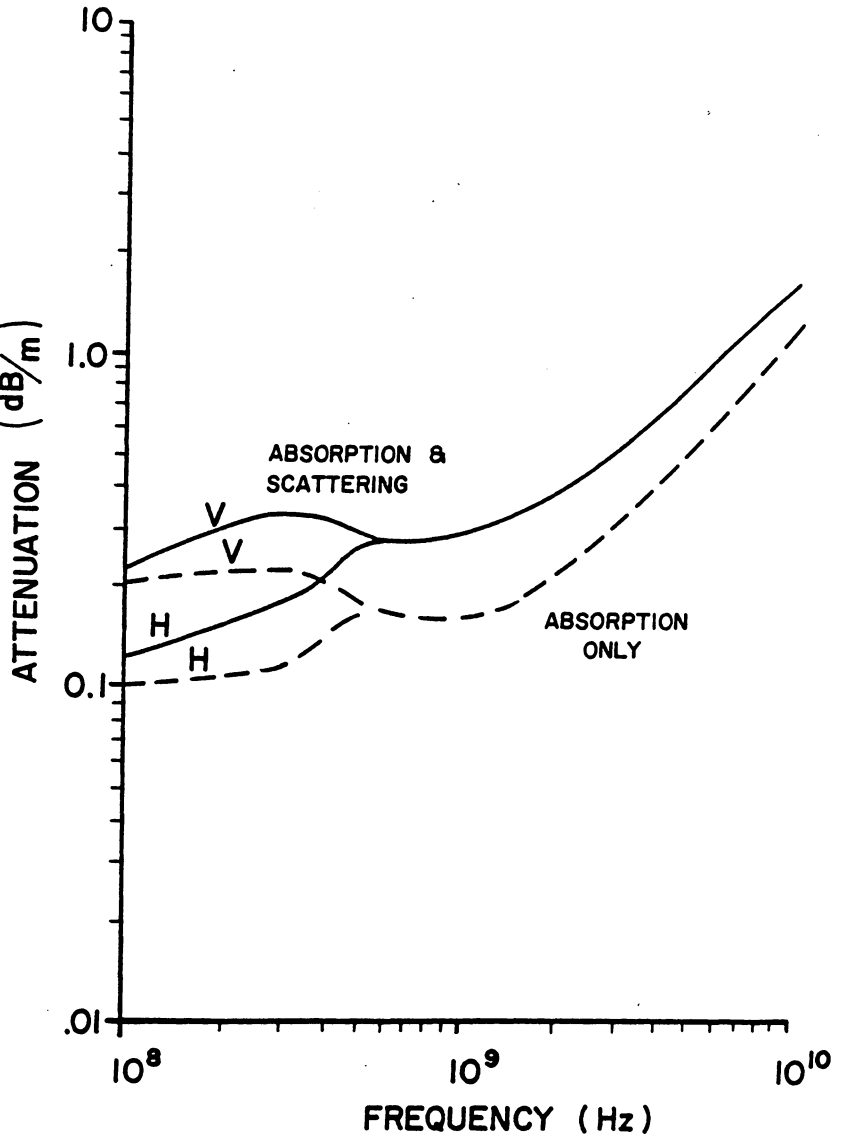

Figure 5.2-3 Specific attenuation vs frequency from the REV model including absorption and scattering effects for vertical (V) and horizontal (H) polarizations. From Brown and Curry [9]

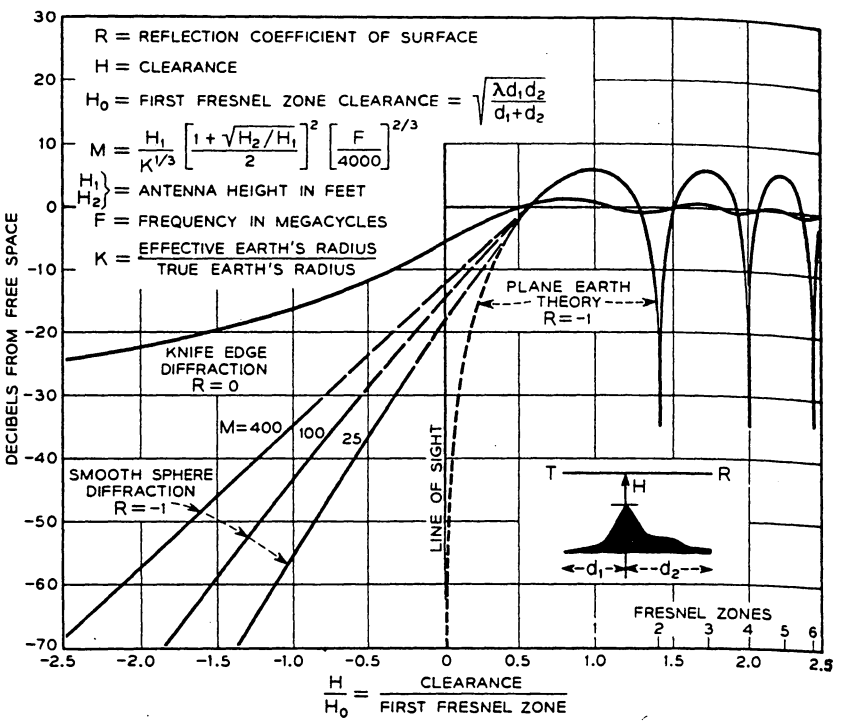

Figure 5.2-4 Graphical computation of loss from diffraction over opaque obstacles. From Bullington [11]

distance between the receiver and the shadowing obstacle since the size of the first Fresnel zone increases with increasing setback distance. The size of the first Fresnel zone is given by the equation in Figure 5.2-4. Since $d_1 >> d_2$ for a satellite path, the first Fresnel zone size, H_o, may be approximated as:

$$H_o \simeq \sqrt{\lambda d_2} \qquad (5.2\text{-}3)$$

where d_2 is the distance of the receiver to the shadowing obstacle. Assuming a frequency of 850 MHz, a clearing size of 50 m, and an angle from the receiver to the top of the vegetation of 45°, the resulting value of H_o will be 5 m. For LMSS operation, clearing sizes on the order of 0 to 50 m are expected so the first Fresnel zone radius is expected to be 5 m or less. Assuming knife edge diffraction, diffraction losses would be on the order 5 dB as the transmission path just clears the trees and increase to 20 dB as the transmission path dips 15 m down into the vegetation. These values are larger than the expected vegetation loss under the same conditions.

Weissberger's [79] study of diffraction models suggested that best results are obtained for setback distances greater than 16 to 35 m and for angles from horizontal between the receiver and the top of the vegetation of less than 8 to 26°. The 16 m clearing size and 26° vegetation clearance angle criteria were taken from Head's paper [33] which also added the constraint that the normalized transmission path clearance, H/H_o, had to be greater than -1.0. For LMSS applications, this

normalized clearance describes transmission paths passing through the very top of the trees. The other efforts ([44], [67], [58], [79]) that successfully used diffraction modeling typically had clearing sizes greater than 35 to 50 m and vegetation clearing angles of 8 to 12° or smaller. Consequently, diffraction modeling is not recommended as a good predictor of mean path loss for LMSS operation except perhaps for setback distances greater than 50 m and low elevation angles.

5.3 REVIEW OF EMPIRICAL MODELING AND EXPERIMENTAL EFFORTS

5.3.1 WEISSBERGER MED MODEL (CCIR MODEL)

Mark Weissberger's report [79] presents a review of 50 papers and reports on prediction models and available measurement data. He found that current exponential decay models tends to overpredict path loss, especially on longer paths. Weissberger proposed the MED (Modified Exponential Decay) model for predicting mean path loss and specific attenuation for propagation through vegetation as a function of both frequency and path length. It was based upon curve fits of measurement data by McQuate [50]. This model has been adopted by the CCIR [18]. The MED model is expressed as:

$$\alpha = 1.33 \; F^{0.284} \; d_v^{-0.412} \qquad 14 \le d_v \le 400\text{m} \qquad (5.3\text{-}1)$$
$$= 0.45 \; F^{0.284} \qquad 0 \le d_v < 14$$

and $L = \alpha d_v$ (5.3-2)

where α = specific attenuation in dB/m

F = frequency in GHz

d_v = the path length through vegetation in m

L = loss in dB

The unique feature of the model is the dependence of specific attenuation on path length; it accounts for the tendency observed in reported data for specific attenuation to decrease with distance. Previous exponential decay models gave specific attenuation as a constant value for a specific frequency. This model was claimed to work over a wide range of frequencies, 0.23 to 95 GHz, and for propagation paths through a dense grove of trees typical of mid-latitude woodlands; the receiver is assumed to be near the vegetation. Model performance was validated by comparison to several other sets of measurement data. The MED model consistently predicted mean path loss with smaller error than existing exponential decay models.

5.3.2 CRC STATIC VEGETATION MEASUREMENTS

The Communications Research Centre of Canada began their propagation measurement program in support of MSAT-X with a set of static vegetation measurements [13]. An 870 MHz circularly polarized transmitter was mounted on a 64 m tower and attenuation measurements were made around the tower at seven sites shadowed by deciduous trees. The elevation angles for the paths ranged from 15 to 24°. Five readings were taken at

half-wavelength spacings at each site and then averaged to cancel any multipath effects. Measurements were made from late April to early November, and Figure 5.3-1 shows the seasonal variation in vegetative attenuation. The smoothed curves are polynomial fits of the data with the outer curves bounding 95% of the data points. A cumulative probability distribution curve of three weeks of unaveraged readings, shown in Figure 5.3-2, indicates that vegetation loss follows a lognormal distribution. For the summer months a mean path loss of 7 dB was observed with 95% of the fades below 10.4 dB. The mean path length was 24 m thus giving a specific attenuation of 0.29 dB/m.

5.3.3 ARMY WIDEBAND MEASUREMENTS

Interest in the effect of vegetation on wideband military communication systems has resulted in several recent measurement programs. The major results of these are reported by Weissberger [79]. The most active program appears to be the Army effort designed to complement the CyberCom theoretical effort. The first phase of the program has been reported by Hufford et al. [38]. Wideband measurements were made in the mixed deciduous and coniferous forests of southern Tennessee using a pseudo-random noise (PN) probe to measure the power impulse response of the channel. The center frequencies used were 600, 1200, and 1800 MHz. The use of the PN probe gave insight into the multipath effects as well as basic transmission loss. Vegetative path loss was observed to be generally proportional to distance. Values of specific attenuation for a 290 m path were found to 0.13 dB/m at 600 MHz and 0.19 dB/m at 1200 MHz.

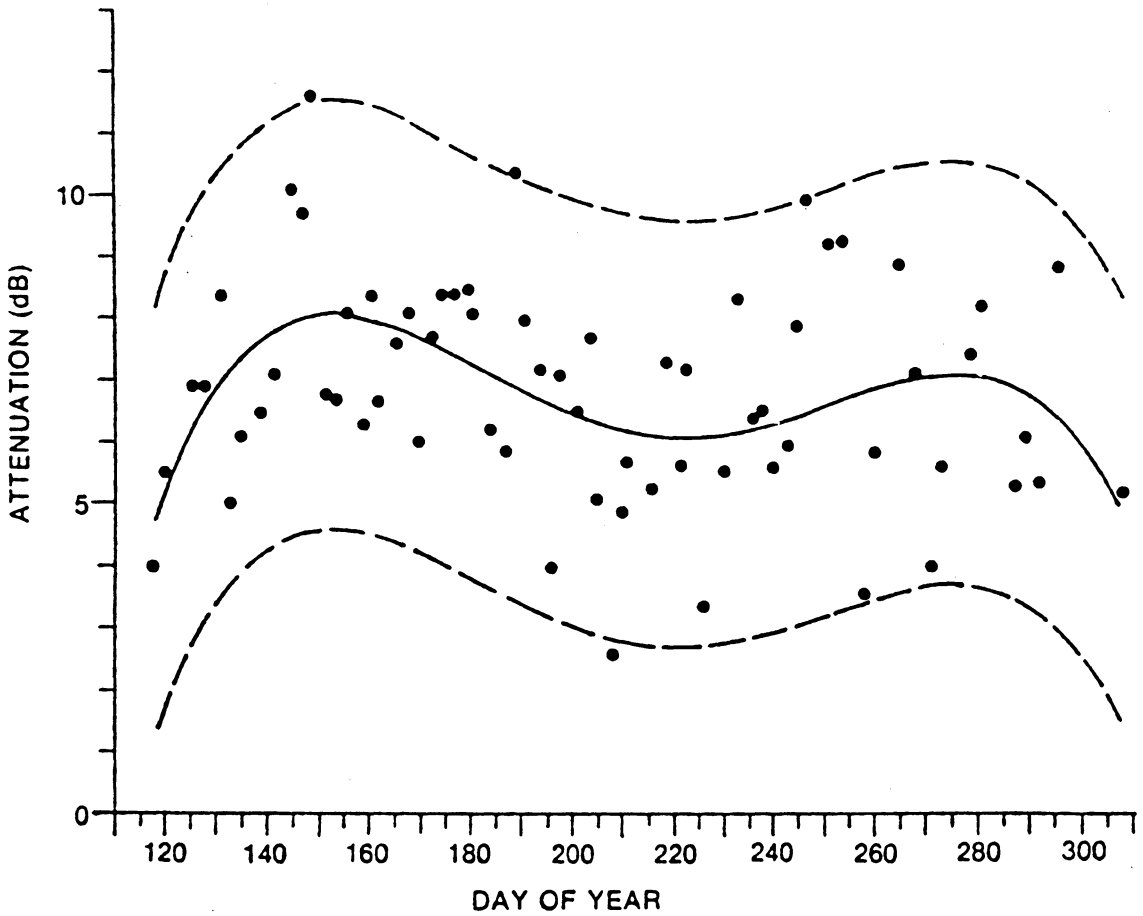

Figure 5.3-1. Vegetative attenuation measurements from late April to early November showing seasonal variation. From Butterworth [13]

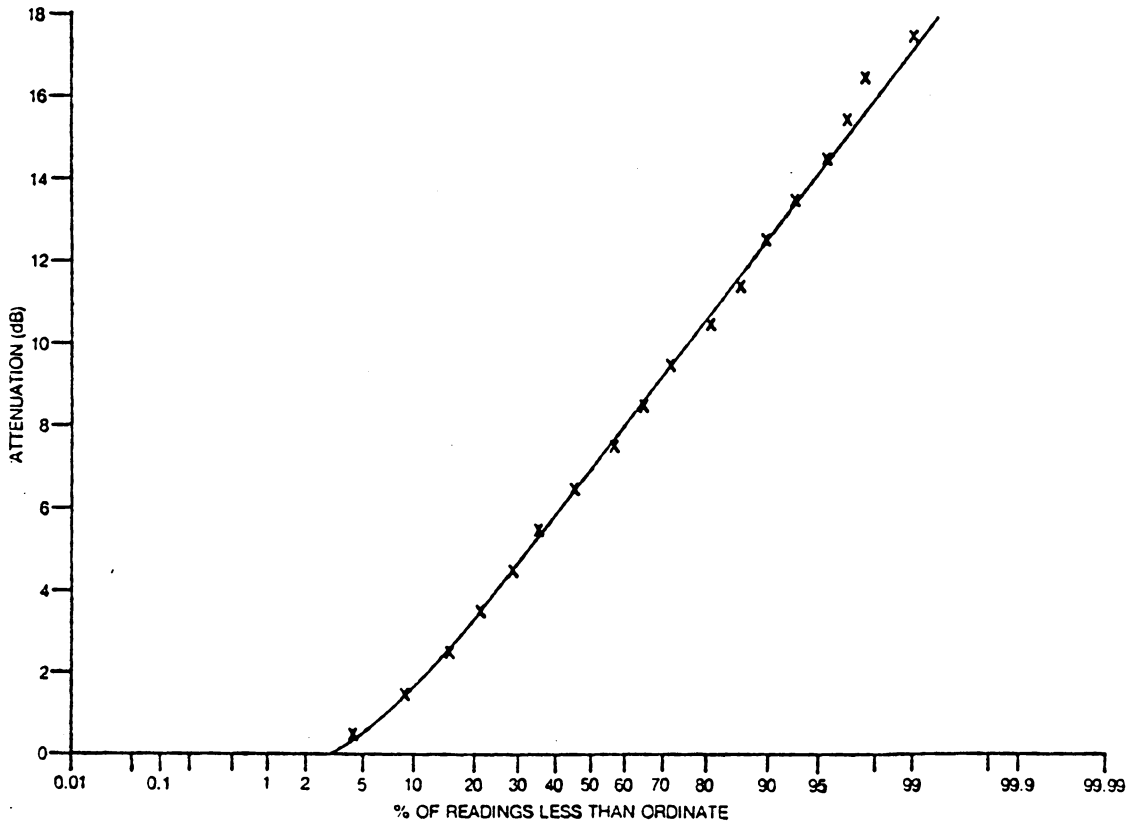

Figure 5.3-2 Cumulative distribution of vegetative attenuation readings for a three week period in June. From Butterworth [13]

Presnell [57], in a similar wideband experiment, also reported a specific attenuation of 0.19 dB/m over the same path.

The mean wideband received signal level showed little variation with time. However, the spectral response at a single frequency was widely variable. Hufford et al. [38] concluded that the time average of received signal level for a CW system would approach that observed for the wideband case. The report also cited results from Frankel's 1850 MHz wideband measurements [29] (specific attenuation of 0.17 dB/m) and comparable results from CW measurements reported by other experimenters to add confidence to their assertion that wideband data could be applied to the CW case.

Other tests were made to check multipath sensitivity to polarization. Vertically polarized signals consistently showed longer delay spreads; horizontally polarized signals tended to show a larger line-of-sight pulse. Generally the delay spread was less than 400 nsec.

An extensive effort is planned to continue these wideband measurements. A twenty-six month measurement period is expected in order to develop a channel model based on a minimal set of parameters [73]. The proposed experiments will include measurement of specific attenuation and depolarization for a trunk dominated forest.

5.4 SUMMARY OF PARAMETER DEPENDENCES

5.4.1 SPECIFIC ATTENUATION

Specific attenuation is the popular measure for the magnitude of vegetative path loss. The curves for specific attenuation versus frequency from the analytical models by CyberCom and Brown and Curry have been given in Section 5.2. At 850 MHz, the CyberCom theory predicts specific attenuations for trunks only on the order of 1.0 dB/m, depending upon trunk size distributions; for branches, about 0.03 dB/m; and for leaves, 0.025 to 0.25 dB/m, depending upon polarization. At 850 MHz, Brown and Curry's model predicts a specific attenuation of 0.30 dB/m. Previous empirical exponential decay models by Rice [61], and the CCIR [17] give values of 0.30 dB/m and 0.17 dB/m, respectively, at 850 MHz. The Weissberger MED and CCIR model gives specific attenuations ranging from 0.43 to 0.11 dB/m at 850 MHz, depending upon path length.

The MED model currently appears to be the most attractive model for specific attenuation because of its simplicity and the good case Weissberger has made for its prediction accuracy. However, the MED model was developed for a wide range of frequencies and path lengths whereas the LMSS problem involves a narrow frequency range and short path lengths. We examined the performance of the MED model for the LMSS situation by using measurement data in the UHF frequency range over path lengths typical of LMSS operation, about 0 to 150 m. The data were scaled to 850

MHz using the MED model frequency dependence. The scaling relation used was:

$$\alpha' = (850/f)^{0.284} \quad \alpha \qquad (5.4\text{-}1)$$

where α = unscaled specific attenuation

α' = scaled specific attenuation

f = measurement frequency in MHz

A table of the applicable unscaled measurement values are given in Table 5.4-1. The corresponding scaled values are plotted along with the MED model in Figure 5.4-1, which shows that there is generally good agreement. However, the drawback of the MED model is that it does not accomodate some of the parameter variations discussed in the next few sections such as vegetation density or type and elevation angle.

5.4.2 POLARIZATION DEPENDENCE

Information on polarization effects is available through analytical modeling efforts and measurements using different polarizations.

The CyberCom analysis revealed the polarization dependence of specific attenuation for various parts of the tree: trunks, leaves, or branches. The trunk model showed that specific attenuation converged to the same value for increasing frequency as previously shown in Figure 5.2-1. Convergence was more rapid for increasing trunk diameter. The leaf only

TABLE 5.4-1

SPECIFIC ATTENUATION MEASUREMENT VALUES

Experimenter	Freq.(MHz)	Foliage Depth(m)	Specific 1 Attenuation (dB/m)	Vegetation Type
Trevor [72]	500	152 m	.12 H ≃ V	deciduous trees with leaves, near Phila.
			.098 V .079 H	same path - no leaves
Saxton & Lane [67]	540	85	.20 V .18 H	mostly deciduous trees; in England
		24	.25 V .15 H	
	1200	24	.35 H ≃ V	
Frankel [29] [2,4]	1850	50-150	.24-.13 V	Oak,madrone,pine,redwood. Dense underbrush and tree tops
		50-150	.18-.14 V	Same as above,different path
		50-150	.18-.19 V	Dense underbrush to 6 m. Tall redwood and fir trees to 24 m
		50-150	.24-.16 V	Dense underbrush of mostly eucalyptus trees, 6 m high
		150	.085 V	Sparse vegetation; 3-5 m trunk separation with no underbrush
McQuate [50] [4]	751 910 1846	14	$.59\ H\left(\frac{.55}{.50}\right)^3$ $.49\ \left(\frac{.50}{.21}\right)$ $.50$	Cottonwood trees, 9 m tall with 12 m clearing
	910 1846	15	$.20\ H\left(\frac{.13}{.25}\right)^3$ $.30$	Cottonwood trees, 15 m tall with 9 m clearing
	751 910 1846	45	$.24\ H\left(\frac{.17}{.29}\right)^3$ $.36\ \left(\frac{.29}{.38}\right)$ $.39$	Cottonwood trees, 12 m tall with 6 m clearing
	751 910 1846	60	$.18\ H\left(\frac{.28}{.23}\right)^3$ $.18\ \left(\frac{.23}{.47}\right)$ $.51$	Dense cottonwood trees, 3 m clearing

TABLE 5.4-1 (continued)

Experimenter	Freq.(MHz)	Foliage Depth(m)	Specific Attenuation (dB/m) [1]	Vegetation Type
McQuate (con'd)	751 910 1846	60	.41 H $\left(\begin{matrix}.28\\.40\\.35\end{matrix}\right)^3$ .12 .33	Cottonwood trees, 12 m tall
	751 910 1846	91	.12 H $\left(\begin{matrix}.15\\.11\\.21\end{matrix}\right)^3$ .14 .21	Dense cottonwoods, 14 m tall with 3 m clearing
	751 910	---	Average loss: 2.5 dB 2.5 dB	Branches of single deciduous tree
Hufford et al.[2] [38]	60 1200	290 290	.13 .19	Oak,hickory,and pine forests of southern Tennessee
Butterworth (CRC) [13]	870	24	.29 C	Deciduous forest near Ottawa

Notes:

1. Specific attenuation values accompanied by signal polarization
2. Measuements made with wideband channel probe.
3. Values in parentheses are for case when remote antenna was elevated 13 m.
4. Results taken from report by Weissberger [79].

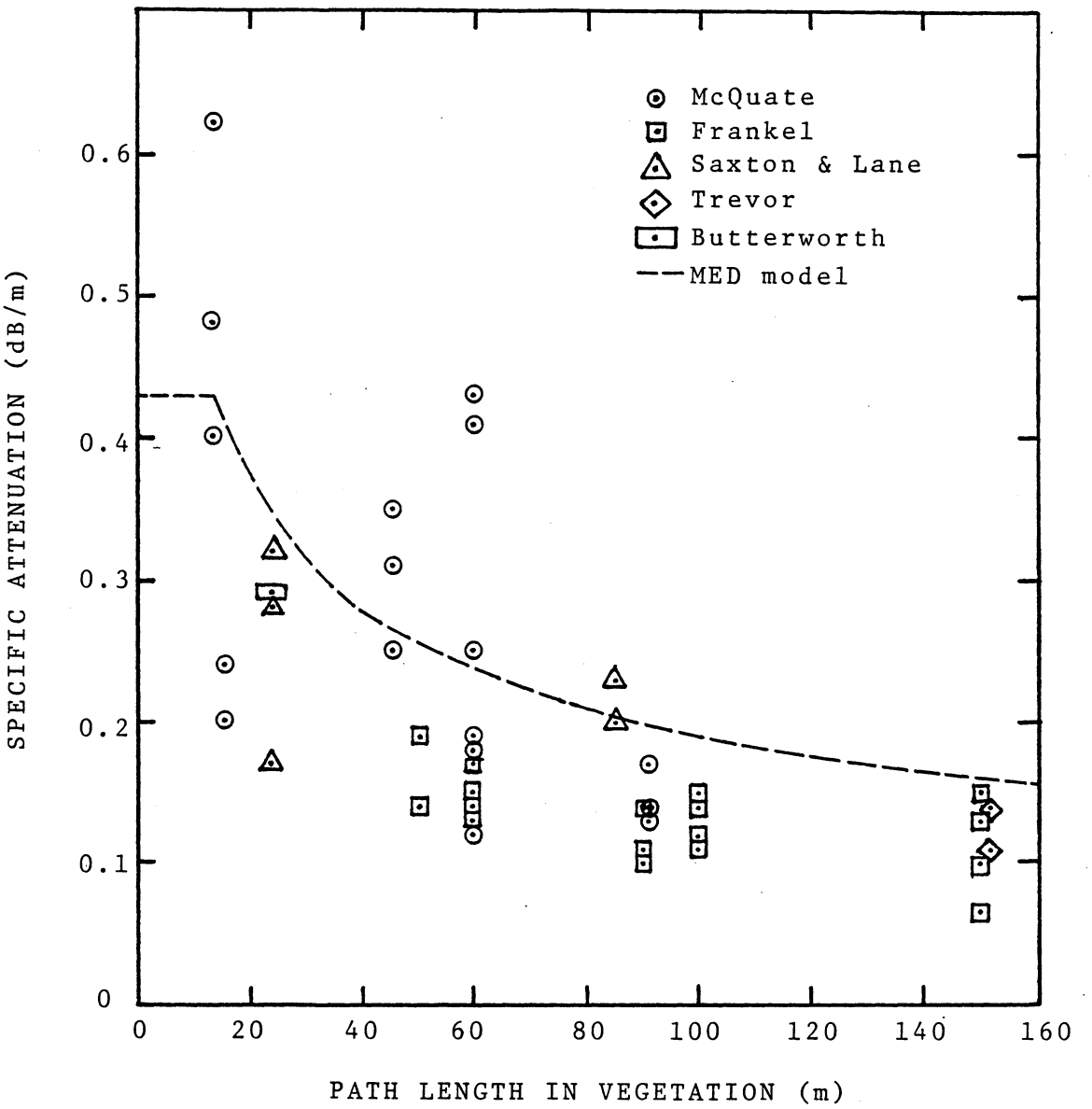

Figure 5.4-1 Scaled specific attenuation values and the MED model predictions vs path length for the data of Table 5.4-1.

model showed more loss for horizontally polarized waves than for vertically polarized waves. The polarization difference was constant with increasing frequency. The branch model showed polarization dependence similar to the leaf model. No uniform model was included so the overall effects of polarization were not studied.

The Brown and Curry REV model showed no polarization dependence for frequencies above 500 MHz. Their model assumed that branches dominate propagation and have a random, uniform orientation. Consequently, polarization effects average out for increasing frequency. Leaf effects were not discussed.

Measured data have generally shown polarization dependence to be small. Table 5.4-1 summarizes several measurements made in the UHF band and the polarization used. Trevor [72] noticed no difference between horizontal and vertical polarizations for measurements at 500 MHz in July; a repeated test in November showed only a 3 dB polarization difference with the vertical polarization being more strongly attenuated. Saxton and Lane's [67] data showed vertically polarized signals attenuated 2 dB more than horizontal at 540 MHz, but there was no difference between polarizations observed at 1200 MHz. Hughes measurements at 1 GHz reported by Weissberger [79] showed an average difference between polarizations of 1.5 dB with vertical polarization more strongly attenuated. Also, Weissberger's MED model was based upon horizontally polarized data, but worked equally well for vertically polarized data.

Thus, theory and measurement are in agreement for polarization effects on vegetative mean path loss. In most cases, little or no polarization dependence was observed for frequencies above 800 MHz. In those cases where some polarization differences were observed, vertically polarized signals were attenuated slightly more.

5.4.3 FREQUENCY DEPENDENCE

Both theory and measurement reveal that vegetative loss increases with increasing frequency. However, exact quantitative dependence is not apparent. Early empirical models based on Saxton and Lane's data expressed loss (from Weissberger [79]) as:

$$L = 0.26\ F^{0.77}\ d_v \qquad (5.4\text{-}2)$$

where L = loss in dB

F = frequency in GHz

d_v = path length through vegetation

The above relation means that loss at 1500 MHz would be 55% greater than at 850 MHz under the same conditions. The MED model equation, (5.3-1), gives a different exponent for frequency dependence; it predicts about a 20% increase in loss from 850 to 1500 MHz. The 1978 CCIR model [17], a graphical representation of specific attenuation vs frequency, also shows a 20% increase between those two frequencies. The MED model equation is based on a measurement data over a wider frequency band than the Saxton

and Lane equation so it probably is more representative of the actual frequency dependence.

5.4.4 ELEVATION ANGLE DEPENDENCE

Elevation angle dependence has proven to be especially difficult to determine since the majority of theoretical and experimental efforts have concentrated on terrestrial communications. In most experiments either both the transmitter and the receiver were immersed in the vegetation, or the transmitter was elevated but the separation distance was so large that the elevation angle was smaller than one degree.

One would expect some elevation angle dependence because for varying angles the path would pass through the different components of the vegetation (ie. trunks, branches, and leaves) in varying proportions. Analytical efforts by CyberCom and Brown and Curry have already shown that the various parts of the tree will affect propagation to different degrees. The CyberCom effort touched on this very briefly and included a graph of the oscillatory effect of elevation angle on specific attenuation for the trunk only model. This graph is given in Figure 5.4-2.

Measurement has shown some conflicting results. A graph given in Weissberger's report showed a 20 dB increase (at 9 GHz) in loss as the receiving antenna was raised so that the transmission path passed through trunks and then branches. Data by McQuate in Table 5.4-1 generally showed

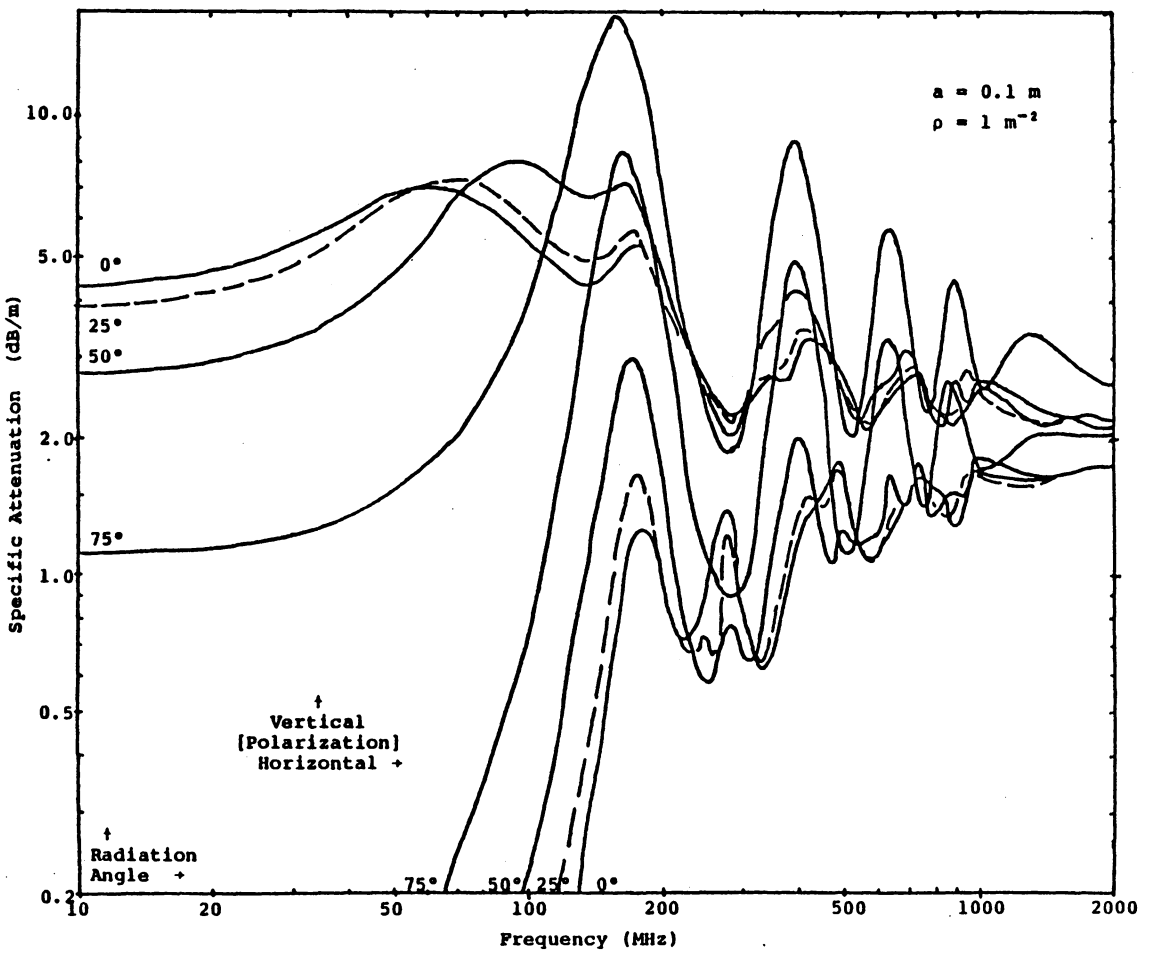

Figure 5.4-2 Specific attenuation vs frequency for different elevation (radiation) angles assuming the trunk only model. From Lang et al. [45]

a decrease in specific attenuation when the remote antenna was raised 13 m. The path loss measurements by Hess showed very little correlation to elevation angle while Vogel's data shows a decrease in path loss with increasing elevation angle, except for the anomaly between 20° and 25°. The CRC static vegetation measurements for elevation angles between 15 and 24°, (see Section 5.3.2) yielded a specific attenuation consistent with the small angle terrestrial measurements of Table 5.4-1.

Based on this information, it is difficult to make any definite conclusions about elevation angle dependence. There is evidence to support the conclusion that the tree canopy is a higher loss region than trunk region. However, more information is needed about the canopy structure and its loss properties before an elevation angle parameter can be added. At present it appears that reasonable results can be obtained by assuming vegetative path loss to be independent of elevation angle.

5.4.5 DEPTH OF VEGETATION

The dependence of specific attenuation on the depth of vegetation has also not had wide agreement. Traditionally, specific attenuation, the rate of vegetative path loss with distance, has been assumed to be a function only of the medium properties and frequency for vegetation depths below a few hundred meters. The analytical models discussed earlier do not suggest anything different. However, the MED model asserts that specific attenuation is a function of the path length through vegetation, based on trends observed in several data sets. Head [33] also reported that

specific attenuation tended to decrease with vegetation depth. Weissberger [79] offers no formal explanation for this behavior. He does though hypothesize that the tree canopy is a high loss region and that the signal energy will leak into the lower loss regions over distance. Low loss regions are considered as the trunk region or in free space at the tree tops. This effect will decrease the average rate of attenuation over distance.

Very short path lengths, less than about 20 m, have proven to be more difficult for predicting the rate of mean path loss. Here the vegetation may be a single tree or a single row of trees. Consequently, the medium does not look as homogeneous as it might for deeper vegetation. Loss measurements by Lagrone and Chapman [43] for a single tree and observations by Saxton and Lane [67] indicate that a single tree or row of trees can cause significant deviations in signal level. Thus, the rate of loss would be sensitive to the exact transmission path through a particular tree. Measurements in this range of path lengths, as displayed in Figure 5.4-1, show a wide variety in specific attenuations, as expected. An average value for attenuation is probably the best assumption to make. The MED model assumes a constant specific attenuation of 0.43 dB/m for path lengths shorter than 14 m which Figure 5.4-1 shows to be adequate.

5.4.6 VEGETATION TYPE AND DENSITY

One would expect to see some difference in mean path loss for various types of vegetation: deciduous, coniferous, or mixed. CyberCom reported data that indicated higher electrical susceptibilities for deciduous trees and leaves than for coniferous trees and needles. This would imply more loss for deciduous trees than for conifers. However, there is currently not enough data to make any quantitative conclusions.

One would also expect to see variations in vegetative path loss proportional to the vegetation density. The empirical models discussed in this chapter assumed dense vegetation. Weissberger showed overprediction by the MED model on measurements of sparse vegetation. The CyberCom effort considered trunk density to be synonymous with vegetation density. However, the trunk density measure ignores the properties of the canopy, which are probably more important.

5.4.7 OTHER EFFECTS

Seasonal variability in path loss has been observed by several experimenters [13], [72], [79]. The loss of leaves and changes in the moisture content of wood account for these effects. Generally the difference in loss for trees without leaves was found to be on the order of 3 to 5 dB.

Another interest is wet vegetation due to a rainstorm. Weissberger [79] reported Hughes measurements at 1 GHz showing that rain on trees increased specific attenuation by 0.1 dB/m. He also reported measurements at much higher frequencies that showed a 4 to 6 fold increase in path loss for wet trees in leaf.

5.5 SPATIAL VARIATION

As mentioned in the introduction, a receiver moving in the presence of vegetation will experience fluctuations in signal strength due to multipath effects or to fluctuations in the properties of the medium. Wide variations have been observed for both a grove of trees by Saxton and Lane [67] and for a single tree by Lagrone and Chapman [43]. However, no formal theoretical work has been sufficiently developed to fully describe these phenomena. Most of the knowledge on any statistical description of spatial variation is based on inferences from the probability distributions of measurement data for both land mobile terrestrial and satellite paths. To further discuss these results, the distinction between short term and long term variation must again be made. Short term variation refers to the instantaneous, rapid fluctuations around the mean signal level. Long term variation refers to the slower changes of the mean signal level over several wavelengths or several tens of wavelengths. A time plot of the CRC data given in Figure 3.2-14 shows the composite effect of both of these variations.

The following theoretical explanation to describe short term variation is taken from Lang et al. [45] and Weissberger [79]. Since vegetation both absorbs and scatters, the received field at any given point will consist of an attenuated, coherent component and a noncoherent diffuse component. The diffuse component is the resultant of many multipath components from both the vegetation and the ground that arrive at a variety of angles and delay times. For the same argument as presented in Section 2.3.2, the diffuse component will have a Rayleigh distributed amplitude with uniformly distributed phase and the resultant amplitude of the coherent and diffuse components will be Rice distributed, assuming a constant coherent component. For terrestrial paths Weissberger [79] reports measurements at 150 MHz in jungle vegetation that included both Rayleigh and Rice distributions, depending upon the polarization and location. Short term distributions reported by Okumura et al. [55] at 920 MHz, in or behind forests, appeared Rayleigh in some cases but lognormal in others, with a standard deviation of 6 to 7 dB.

Long term variation has no underlying theoretical description, but has been inferred from measurement results. It is caused primarily by changes in the medium as the receiver is moved. For terrestrial paths, the measurements of Okumura et al. [55] in suburban areas, which included vegetation and houses, showed long term variation to resemble a lognormal distribution with a predicted standard deviation of 8.25 dB at 850 MHz. Terrestrial measurements by Reudink and Wazowicz [58] at 836 MHz in suburban and rural areas also yielded long term variation distributions that appeared lognormal with standard deviations of 7 to 8 dB or higher,

depending upon distance from the transmitter. Reudink [59] has also noted that lognormal distributions have consistently been observed for a variety of environment classes and system parameters on terrestrial paths.

The signal level distribution function from measurement data will include both short and long term variation behavior provided that sampling was performed often enough to resolve short term variations. Okumura et al. [55] refer to this distribution as the composite distribution of short and long term variations. They predicted that the composite distribution for terrestrial paths through suburban environments (houses and vegetation) would be lognormal; the standard deviation of the composite distribution would be larger than the ones for the short term and long term distributions. For the satellite case, Hess was the first to report the lognormal behavior of shadowing as shown in Figure 3.4-1 except that it was for an urban environment. However, he did use the lognormal assumption when modeling loss in rural regions. The best measurements of spatial variation in the presence of vegetative shadowing alone are the early CRC measurements discussed in Sections 3.2 and 5.3.2. Figure 3.2-2 gives the distribution functions of signal levels shadowed by the different groves of trees from the CRC tethered balloon experiment. Each one appears to be mostly lognormal with means and standard deviations of (-10.5, 4.5), (-7, 3), and (-8, 6.5) dB. Figure 5.3-2 gives the distribution function of total path loss from the static vegetation measurements discussed in Section 5.3.2. It shows an underlying lognormal distribution, but it does not fully include short term variation effects

because of the small sample size of the data. The other satellite path measurements by the CRC and Vogel discussed in Sections 3.2 and 3.3 also confirm the lognormal nature of spatial variation by vegetative shadowing. However, these distribution functions are mixed with data from clear, unshadowed regions and do not show the spatial variation characteristics of vegetative shadowing alone.

If the lognormal and Rayleigh distribution are used to describe the signal level statistics in the presence of vegetative shadowing, then knowledge of the mean, standard deviation, and average diffuse power is required. Available path loss measurements have given some insight into finding the mean but much less for the other two parameters. One would expect the standard deviation to depend upon the vegetation density and the mean path loss. For dense vegetation, one would not expect large variations due to medium fluctuations. For less dense vegetation such as a single tree or row of trees, the signal level will then vary from a near LOS level to a minimum level for the transmission path through the tree center. This type of behavior has been observed earlier in the time plots of Figure 3.2-14. Consequently, the standard deviation for dense vegetation may be 40% to 50% of the mean path loss while for less dense vegetation it may be larger or 80% to 90% of the mean. An estimate for the diffuse component power from vegetative scattering is not as clear.

5.6 SUMMARY OF FINDINGS

Characterizing propagation through vegetation has proven to be very difficult due to the complex nature of the medium. In many cases, the quantitative effect of various parameters was not apparent.

These rather pessimistic findings were echoed in an earlier study by Nelson [53]. Nelson reports insufficient quantitative experimental data to form a realistic characterization of the medium that would allow quantitative predictions to be made; a guide to the order of magnitude of medium effects is the best that can be expected.

At present, the best model for predicting mean path loss seems to be the MED (Modified Exponential Decay) model proposed by Weissberger. The applicability of the model to LMSS operation was checked by comparing model predictions to measurement data in the UHF band over path lengths typical of LMSS operation (0 to 150 m); see Figure 5.4-1. Agreement to the data was fairly good, but the model does have some drawbacks. It applies primarily to dense groves of trees and does not account for parameters other than frequency and path length.

The review of parameter dependences important to vegetative shadowing for LMSS operation yielded the following information:

1. Polarization effects are minimal at LMSS frequencies, 800 to 900 MHz, and at L-band.

2. The MED model frequency dependence appears to be consistent with the majority of reported measurement data. Approximately a 20% increase (in dB) in loss is expected at 1500 MHz over loss at 850 MHz.

3. The MED model path length dependence also seems consistent with measurement data, but contradicts theoretical prediction. Mean path loss for very short paths, less than 15 m, seems to be more unpredictable than for longer paths probably due to increased non-uniformity of the vegetation or increased multipath effects.

4. Elevation angle effects are not well understood because the bulk of propagation work on vegetation has been performed for terrestrial links with elevation angles typically less than one degree. Both theory and measurement indicate that propagation loss is different for paths through tree trunks and for paths through the canopy. However, no further effort has been done to quantify elevation angle dependence.

5. Vegetation type and density have been observed to affect mean path loss, but only limited preliminary work has been done to correlate these parameters with path loss measurements.

Since elevation angle, vegetation type, and vegetation density parameters require further study, no corrections to the MED model to account for these factors can be recommended. It seems best to assume that specific attenuation is uniform over elevation angle and that MED prediction values

are the average over vegetation types and an upper bound in terms of density. Further study is suggested particularly to understand elevation angle effects better.

Measurements on terrestrial and satellite paths have given some insight to the statistics of vegetative shadowing for a mobile receiver. Short term or instantaneous variation is predicted to be Rician for large signal levels, or Rayleigh for very small LOS signals. Terrestrial measurements generally confirm this result. Slower, long term variations have been observed to be lognormally distributed. Measurements from actual or simulated satellite paths have shown the composite to behave lognormally; however, many of these measurements have included routes through cleared areas so the statistics for vegetation shadowing alone have not been isolated. Future measurements should attempt to isolate vegetative shadowing effects similar to the CRC balloon measurements discussed in Section 3.2 in order to determine the actual signal level statistics more accurately. Tests should be made to study the effects of elevation angle, vegetation type, and vegetation density on the parameters of the signal level distributions, i.e. mean, standard deviation, and diffuse component power.

VI. PROPOSED MODELING APPROACH

6.1 MODELING PHILOSOPHY

One of the primary goals of this study was to model the effects of vegetative shadowing on land mobile satellite communications. The preceding five chapters have given a review of propagation impairments, presented measurement data that included vegetative shadowing effects, summarized earlier modeling and simulation efforts, and discussed various aspects of propagation through vegetation. This chapter pulls together many of these ideas to describe the effects of vegetative shadowing.

Usually measurement routes will include shadowed and unshadowed regions in various proportions; thus, the final results are a composite of many parameters influencing propagation and subsequently the received signal level. A suggested approach then is to break the problem into two parts so that the propagation phenomena for vegetatively shadowed and unshadowed regions may be isolated and studied separately. Section 6.2 presents a simple model using basic probability theory to describe the overall signal level statistics from a knowledge of the signal level statistics for shadowing and no shadowing and of the fraction of locations where shadowing is present. The model can also be used to estimate the signal level statistics in the presence of shadowing if the overall statistics are known and a distribution is assumed for the unshadowed statistics.

With the form of the statistical distributions established, the next step is to assign physical significance to the parameters that define those statistical distributions like mean, standard deviation, or the power in a diffuse component. For the unshadowed case, the diffuse ground scatter is the principal source of interference, and its magnitude may be estimated by the methods described in Chapter 2. For vegetative shadowing, the complexity of the parameters influencing propagation suggested that an empirical type approach be taken. Specifically, the results of Chapter 5 indicated that the empirical MED model may be used to estimate vegetative path loss. Section 6.3 presents a deterministic model using the path geometry and the MED model equations to predict mean vegetative path loss. Section 6.4 shows how this model may be useful for predicting the mean of the vegetative shadowing distribution. It would also be desirable to have similar empirical, deterministic models for standard deviation and the diffuse, scattered power in the presence of vegetation; however, estimation of these parameters will require a larger data base of measurement results.

The statistical model is examined further in Section 6.4. The results are shown for the synthesis of overall signal level statistics from shadowed and unshadowed distributions, and the sensitivity to the model parameters is discussed. Then vegetative shadowing distributions are taken from measurement data and compared with the results of the deterministic path loss model.

6.2 OVERALL STATISTICAL MODEL

A reasonable way to estimate the overall signal level statistics for partially shadowed routes is to divide the problem into two cases according to the physical situation: 1) shadowing of the LOS signal by vegetation; and 2) no shadowing by vegetation. The two cases are mutually exclusive, and the signal statistics for each one are expected to be different. The statistics for the overall result can then be found by combining the statistics for each case using a total probability argument and the fraction of locations that vegetative shadowing will occur.

To start, let the probability density function of the received signal amplitude, f(r), be defined as follows using the properties of total probability:

$$f(r) = f(r|vs)p + f(r|\overline{vs})\ (1-p) \qquad (6.2\text{-}1)$$

where $f(r|vs)$ and $f(r|\overline{vs})$ are the conditional density functions of the received signal for vegetative shadowing (vs) and no vegetative shadowing ($\overline{vs}$), respectively, and p is the fraction of locations where shadowing by vegetation will occur along the propagation path. Note that the density functions are assumed to remain the same or spatially stationary over the measurement route. The cumulative distribution function, G(R) is found from f(r) as follows:

$$G(R) = P\{r > R\} = \int_R^\infty f(r)\ dr \qquad (6.2\text{-}2)$$

Integrating (6.2-1) yields a corresponding CDF equation:

$$G(R) = G(R|vs)p + G(R|\overline{vs})\ (1-p) \qquad (6.2\text{-}3)$$

where $G(R|vs)$ and $G(R|\overline{vs})$ represent the cumulative distribution functions in the presence of vegetative shadowing and when no shadowing is present, respectively. This type of approach was first reported (although not in explicit mathematical terms) by the CRC, as discussed in Section 4.2 with the concatenation of shadowed and unshadowed data in various proportions. The significance of the relationship given in (6.2-3) is that it isolates the statistics of vegetative shadowing. Consequently, the effects of vegetative shadowing alone can be simply applied to describe the statistics along routes that are only partially shadowed.

The overall level crossing rate statistics can be found using the same argument. As previously defined in Chapter 2 the level crossing rate is given by:

$$N(R) = \int_0^\infty \dot{r}\ f(R, \dot{r})\ d\dot{r} \qquad (6.2\text{-}4)$$

where $N(R)$ is the number of positive level crossings at threshold R, $\dot{r}$ is the time rate of change of the received signal amplitude, and $f(R, \dot{r})$ is the joint density function of the signal amplitude and its time rate

of change. As before, $f(R, \dot{r})$ can be expressed using the property of total probability for shadowing and no shadowing:

$$f(R, \dot{r}) = f(R, \dot{r}|vs)p + f(R, \dot{r}|\overline{vs})\ (1-p) \qquad (6.2\text{-}5)$$

where $f(R, \dot{r}|vs)$ and $f(R, \dot{r}|\overline{vs})$ are conditional densities for shadowing and no shadowing. Inserting (6.2-5) into (6.2-4) gives the following results:

$$N(R) = N(R|vs)p + N(R|\overline{vs})\ (1-p) \qquad (6.2\text{-}6)$$

where $N(R|vs)$ and $N(R|\overline{vs})$ represent the level crossing rate at threshold R in the presence of vegetative shadowing and no shadowing respectively. Equation (6.2-6) shows that the overall level crossing rate can be found for partially shadowed routes from the separate level crossing rates for vegetative shadowing and no shadowing.

The overall average fade duration statistics though cannot be found using the previous total probability argument. As defined earlier, the average fade duration below a threshold R is given as:

$$D(R) = F(R)/N(R) \qquad (6.2\text{-}7)$$

where $$F(R) = P\{r \leq R\} = 1 - G(R) \qquad (6.2\text{-}8)$$

and N(R) is the level crossing rate. Since F(R) can be expanded in the same manner as (6.2-2), and N(R) can be expanded according to (6.2-6), then (6.2-7) can be expressed as:

$$D(R) = \frac{F(R|vs)p + F(R|\overline{vs})\ (1-p)}{N(R|vs)p + N(R|\overline{vs})\ (1-p)} \qquad (6.2\text{-}9)$$

which is not the linear combination of D(R|vs) and D(R|$\overline{vs}$), the average fade duration for shadowing and no shadowing. Instead, the following relationship may be used:

$$D(R) = \frac{D(R|vs)\ N(R|vs)p + D(R|\overline{vs})\ N(R|\overline{vs})\ (1-p)}{N(R|vs)p + N(R|\overline{vs})\ (1-p)} \qquad (6.2\text{-}10)$$

$$= D(R|vs)\frac{N(R|vs)p}{N(R)} + D(R|\overline{vs})\frac{N(R|\overline{vs})\ (1-p)}{N(R)} \qquad (6.2\text{-}11)$$

Consequently, computation of the overall average fade duration statistics, D(R), from the individual average fade durations for shadowing and no shadowing requires knowledge of the level crossing rate statistics.

The total probability argument can also be extended to more than the two cases presented here. If several distinct shadowed and unshadowed regions exist and the fraction of locations for the occurrence of each region is known, then (6.2-1) can be generalized to:

$$f(r) = \sum_i f_i(r|vs)p_i + \sum_j f_j(r|\overline{vs})q_j \qquad (6.2\text{-}12)$$

$$\sum_i p_i + \sum_j q_j = 1 \qquad (6.2\text{-}13)$$

where $f_i(r|vs)$ and $f_j(r|\overline{vs})$ are the conditional density functions of the received signal in each of the shadowed and unshadowed regions with p_i and q_j denoting the fraction of locations for the occurrence of each shadowing region.

To summarize, the fading statistics under partial shadowing conditions can be found from the separate fading statistics for clear and shadowed conditions using a total probability argument. In practical applications, this model is useful for two reasons. First, it breaks down the problem of predicting the signal fading statistics when some proportion of shadowing is present; it includes a measure of the amount of shadowing and accommodates the different fading statistics expected for shadowed and unshadowed conditions. Previous statistical modeling efforts have suggested a single distribution to predict the signal fading statistics with little regard to the particular effects of shadowing. Since the statistics for unshadowed conditions are better understood, this model suggests further study be done to isolate and determine the fading statistics for shadowing alone. Second, if Rician properties are assumed for the unshadowed statistics and the p parameter, the amount of shadowing, is known, then an estimate of the fading statistics from shadowing alone can be estimated from field measurements over partially shadowed routes. Both of these aspects of the proposed model is considered in Section 6.4.

6.3 THE DETERMINISTIC PATH MODEL

The discussion of Chapter 5 has shown that a non-electromagnetic model, namely the MED model, is adequate for estimating mean path loss per meter for propagation through vegetation. This section presents a simple deterministic model using geometrical parameters to compute path length and then path loss from the MED loss equations.

Shown in Figure 6.3-1 is a simple diagram that illustrates geometric parameters for vegetative shadowing of the direct or LOS satellite signal. The vegetation is assumed to be a uniform slab with average height, H, and removed from the mobile by an average setback distance, W. Note that W is the setback of the dense portion of the tree canopy and not the tree trunks. The satellite is at an elevation angle, ε, and the mobile is traveling perpendicular to the satellite azimuth; this condition will give the longest and consequently worst case vegetative path lengths. Also, the terrain is assumed to be smooth. From simple trigonometric relations, the vegetative path length, denoted as d_v, can be calculated from:

$$d_v = H \csc \varepsilon - W \sec \varepsilon \qquad (6.3\text{-}1)$$

Alternately, d_v may be expressed in terms of γ, the vegetation clearance angle, and either H or W using (6.3-1). γ is related to the average tree height, H, and setback, W, by

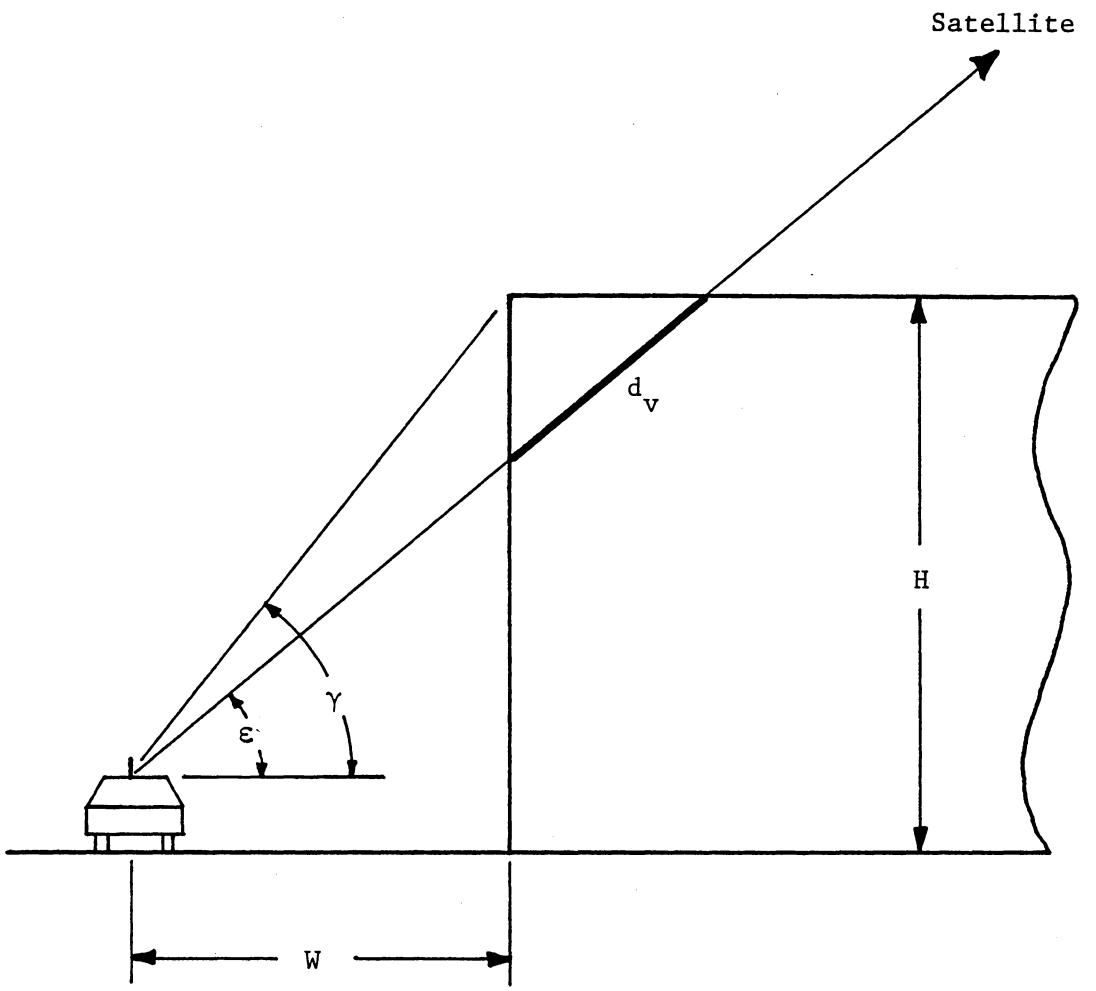

Figure 6.3-1 Simple path model for vegetative shadowing.

$$\tan \gamma = H/W \qquad (6.3\text{-}2)$$

A more precise expression for d_v would include the height of the mobile antenna. This parameter will typically be 2 to 3 m, but the actual tree heights will exhibit fluctuations on that order and thus antenna height is not included as a parameter.

The MED model loss equation, (5.3-1), is now used to find path loss. If a signal frequency of 850 MHz is assumed, then vegetative loss, L_v, in dB may be computed as:

$$L_v = 1.27\, d_v^{0.588} \quad , d_v \geq 14\text{m} \qquad (6.3\text{-}3)$$
$$L_v = 0.43\, d_v \quad , d_v < 14\text{m}$$

where d_v is given in (6.3-1).

Average tree heights are expected to vary widely with location. However, a brief study of tree heights using Cannell [16] and Elias [27] showed that the majority of species of North American trees will grow to heights between 10 and 30 m. Similarly, average vegetation setbacks will vary with the road type and terrain at a given location. The AASHTO [1] policy for highway design gave the following recommendations for the clearances between roadside obstructions and the center of the roadway: 6.5 m for local rural streets, 13 m for rural two lane arterials, and 20 m for four lane freeways. For travel on the opposite side of a divided freeway, an

approximate setback of 50 m would be expected. These values were used to compute expected pathlengths from (6.3-1) and then to compute the corresponding vegetative path loss from (6.3-3) over elevation angles from 15 to 60°. (Note that elevation angles in the continental U.S. (CONUS) for a mid-latitude satellite will vary from about 20 to 60°.) The results are displayed in Figures 6.3-2 through 6.3-5 which give path loss for a single average tree height and four different setbacks. Figure 6.3-6 summarizes by giving the loss for the following combinations of setback and tree height: a worst case, a midrange and a low range loss curve.

For the worst case curve, the longest path length through vegetation was 110m. The knee observed in some curves are due to the change in the MED loss equation for paths shorter than 14m. Also, the no loss condition was assumed when the elevation angle was greater than the vegetation clearance angle.

The simple geometric model of Figure 6.3-1 can be extended to include any direction of travel with respect to the satellite azimuth if the parameter β is included as shown in Figure 6.3-7. β may be called the bearing angle and is defined as the acute angle between the satellite azimuth and the centerline of the roadway. The only change required to incorporate the bearing angle is in (6.3-1)

$$d_v = H \csc \varepsilon - W \csc \beta \sec \varepsilon \qquad (6.3\text{-}4)$$

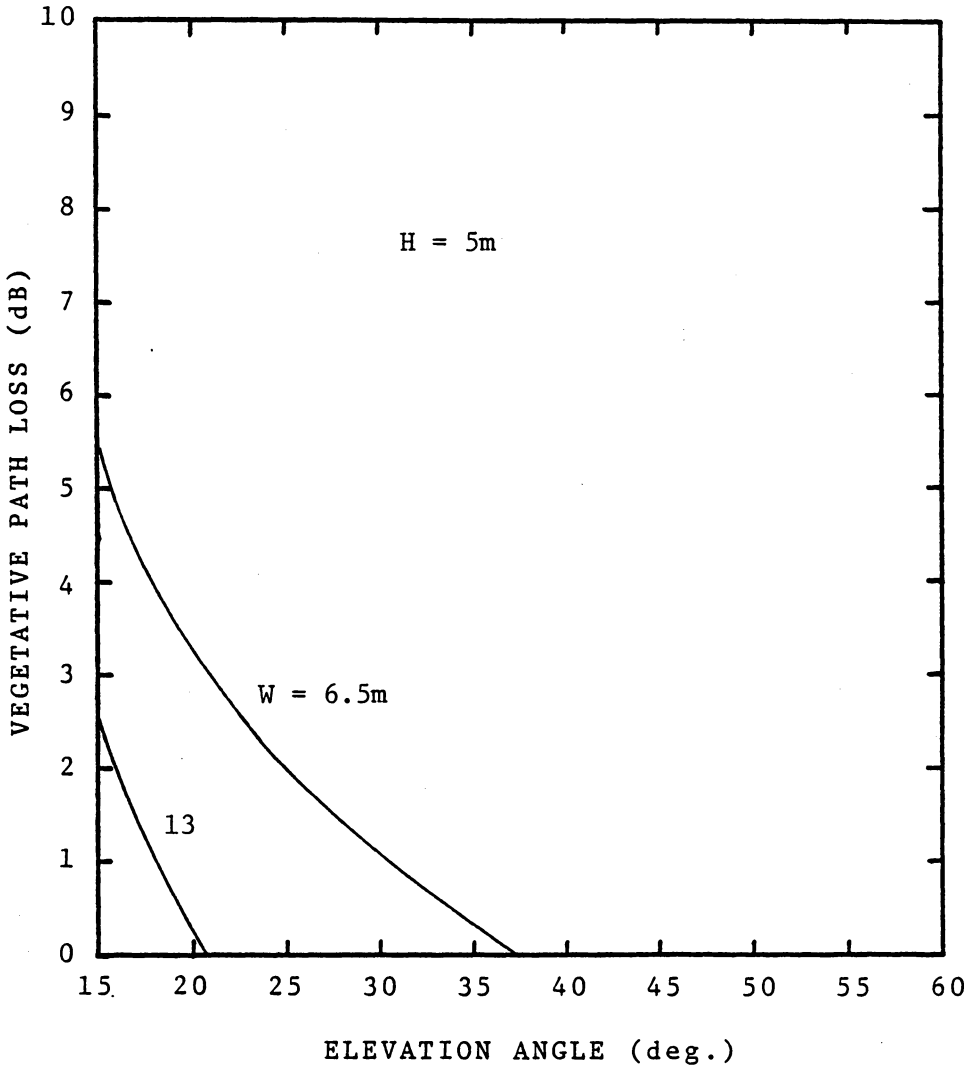

Figure 6.3-2 Vegetative path loss curves for a tree height of 5m and various setbacks.

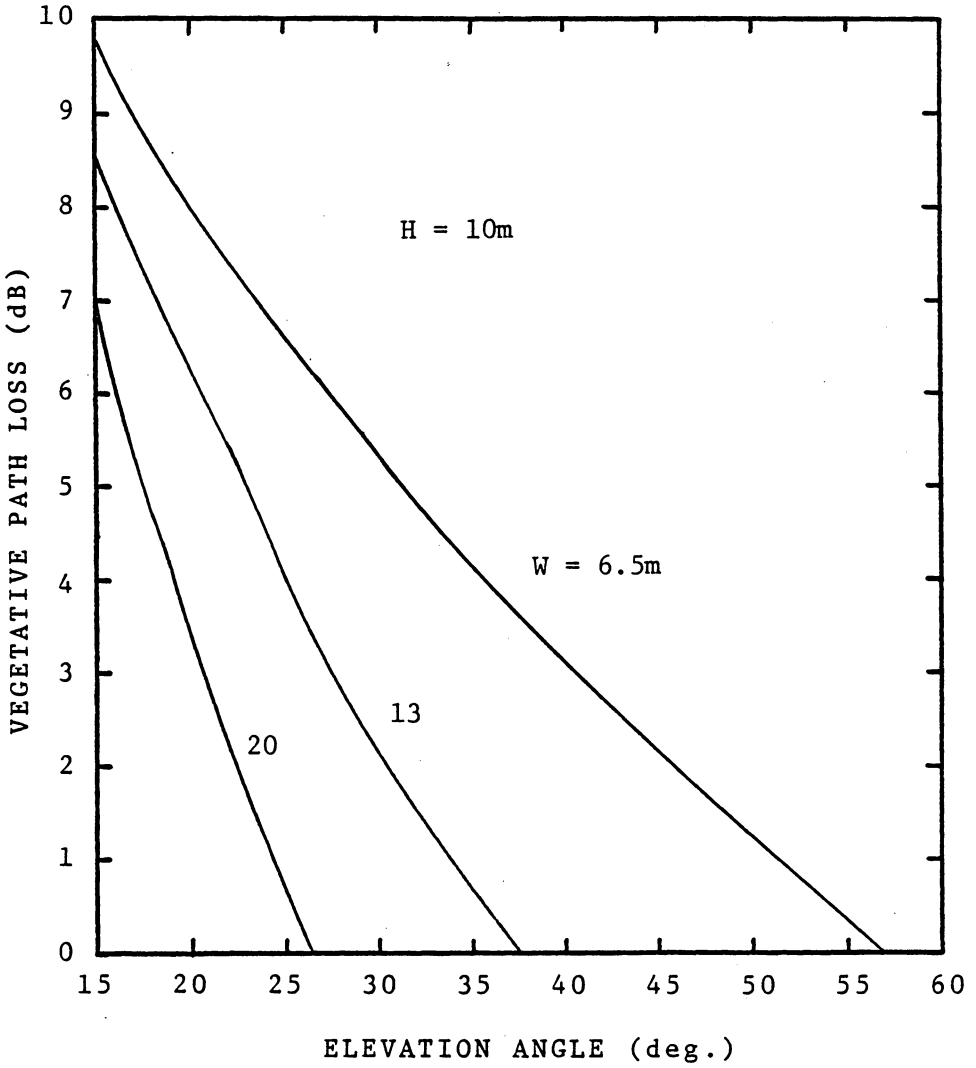

Figure 6.3-3 Vegetative path loss curves for a tree height of 10m and various setbacks.

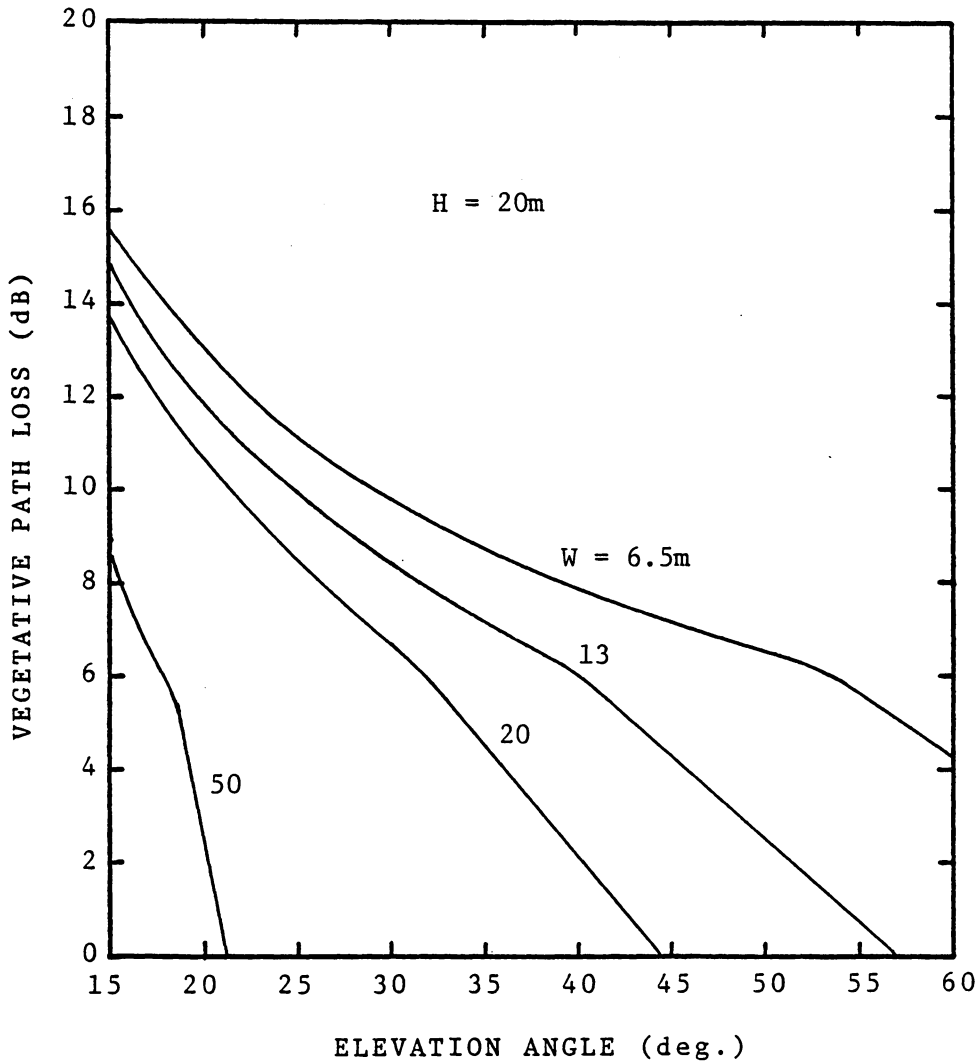

Figure 6.3-4 Vegetative path loss curves for a tree height of 20m and various setbacks.

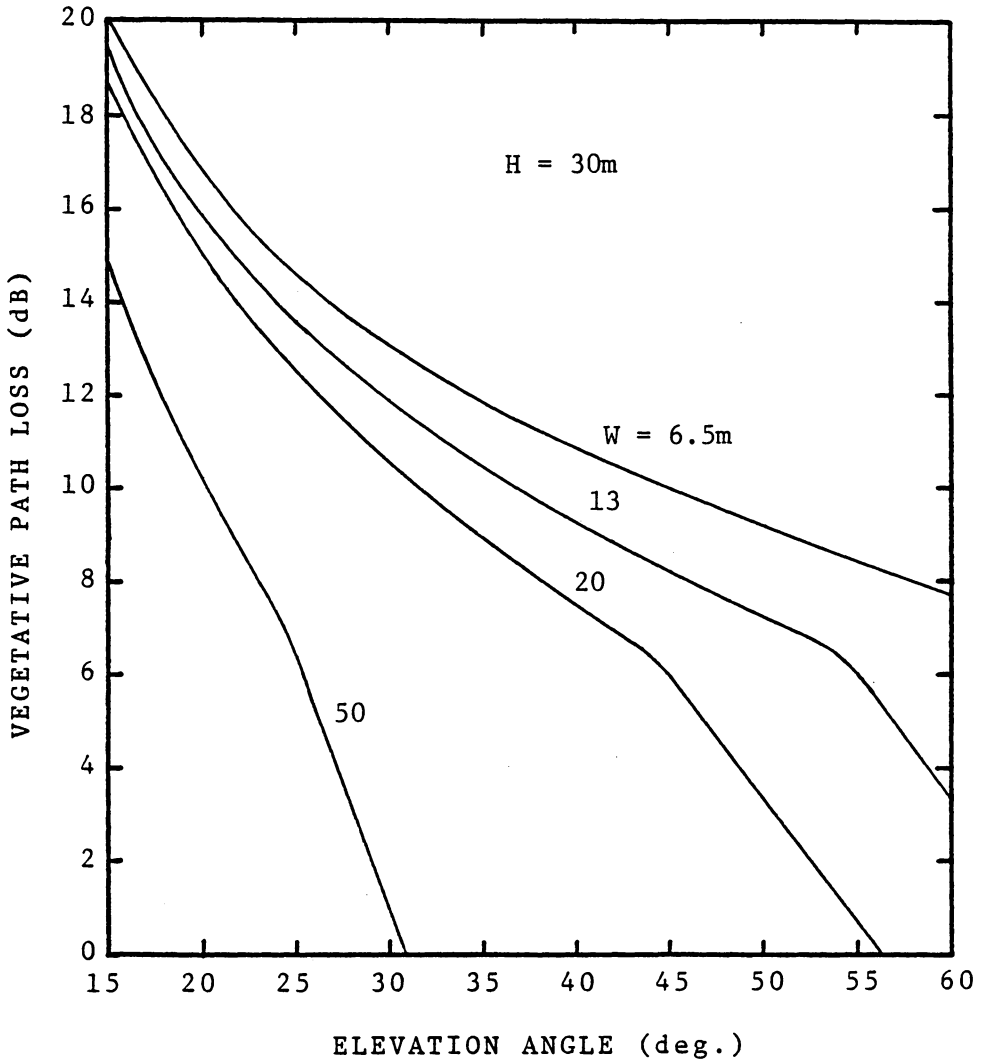

Figure 6.3-5 Vegetative path loss curves for a tree height of 30m and various setbacks.

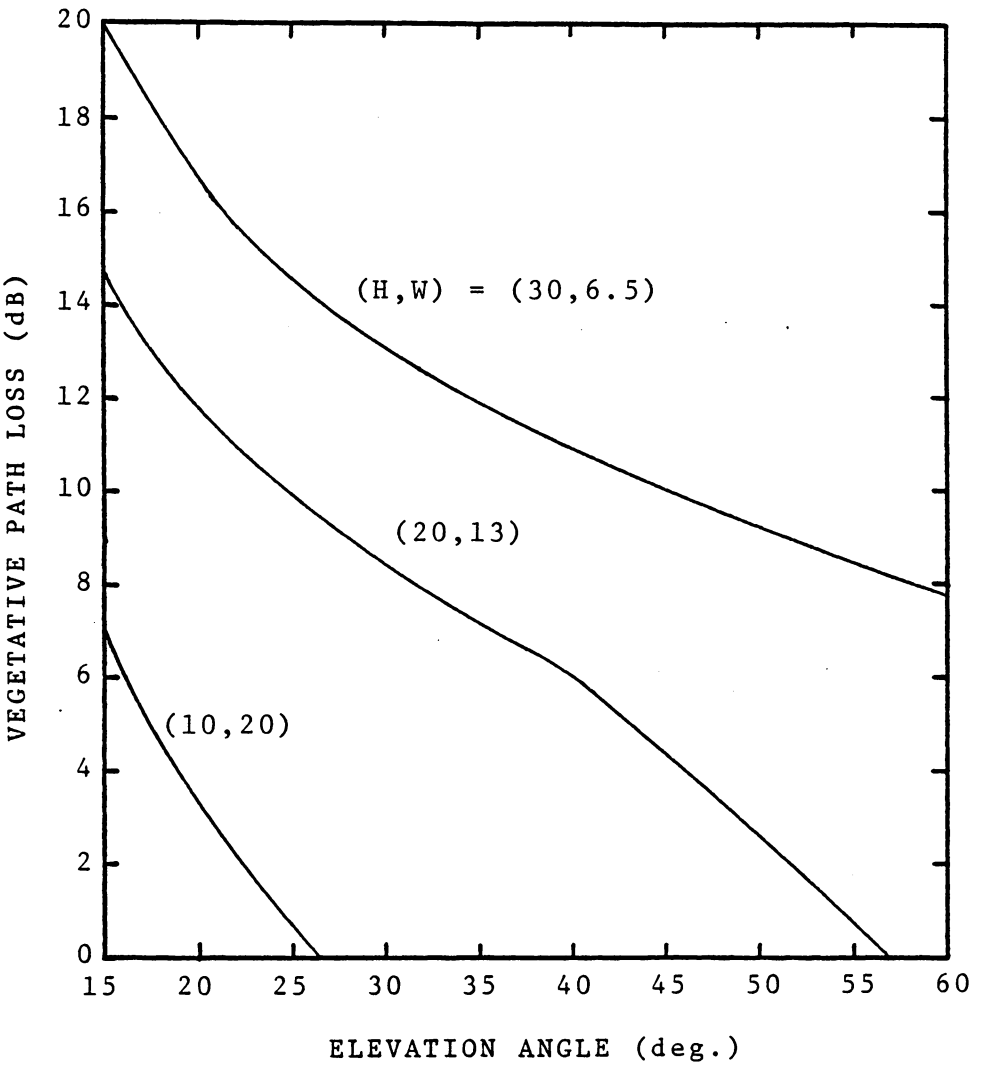

Figure 6.3-6 Summary of vegetative path loss curves showing worst case, midrange, and low range values.

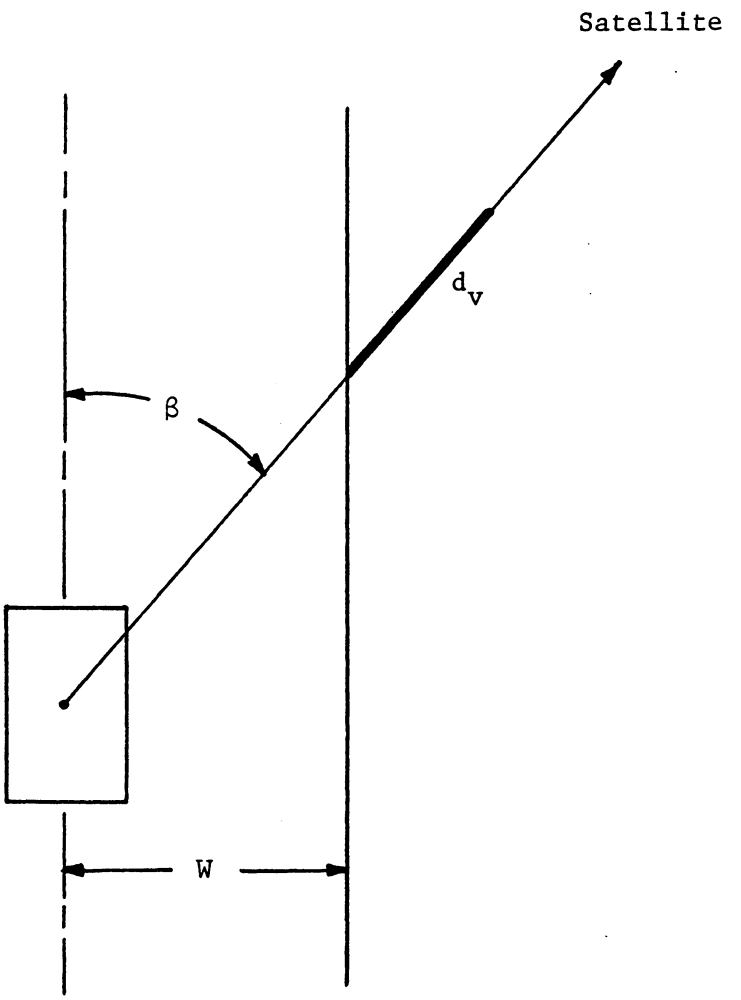

Figure 6.3-7 Simple path model for vegetative shadowing including the bearing angle.

Figure 6.3-8 shows the change in vegetative path loss for bearing angles of 30° and 60° on the path loss curves of Figure 6.3-6, where β is 90°. There is only a moderate reduction in path loss as β goes from 90° to 30°, but there is a rapid reduction as β approaches 0° where there is no vegetative path loss because the satellite appears to be directly ahead or behind the vehicle.

As discussed in Chapter 5, the MED predictions for vegetative path loss are for dense vegetation, and thus represent worst case conditions. Further corrections are desirable for lighter vegetation densities, varying vegetation types, and any further elevation angle dependence born out by theory or measurement.

This model is deterministic, and it reveals nothing about the form of statistical variations in signal level for a mobile travelling through a region of vegetative shadowing. However, this model can provide insight to the magnitude of the statistical parameters. If a lognormal type distribution is assumed, then L_v, the vegetative path loss, can serve as the mean of the signal level distribution function.

Unfortunately, this model reveals little about the standard deviation. Again, lack of information about the standard deviation suggests that additional measurements of vegetative shadowing be made. Then an empirical modeling approach like that of Hess could be used to account for parameter variations.

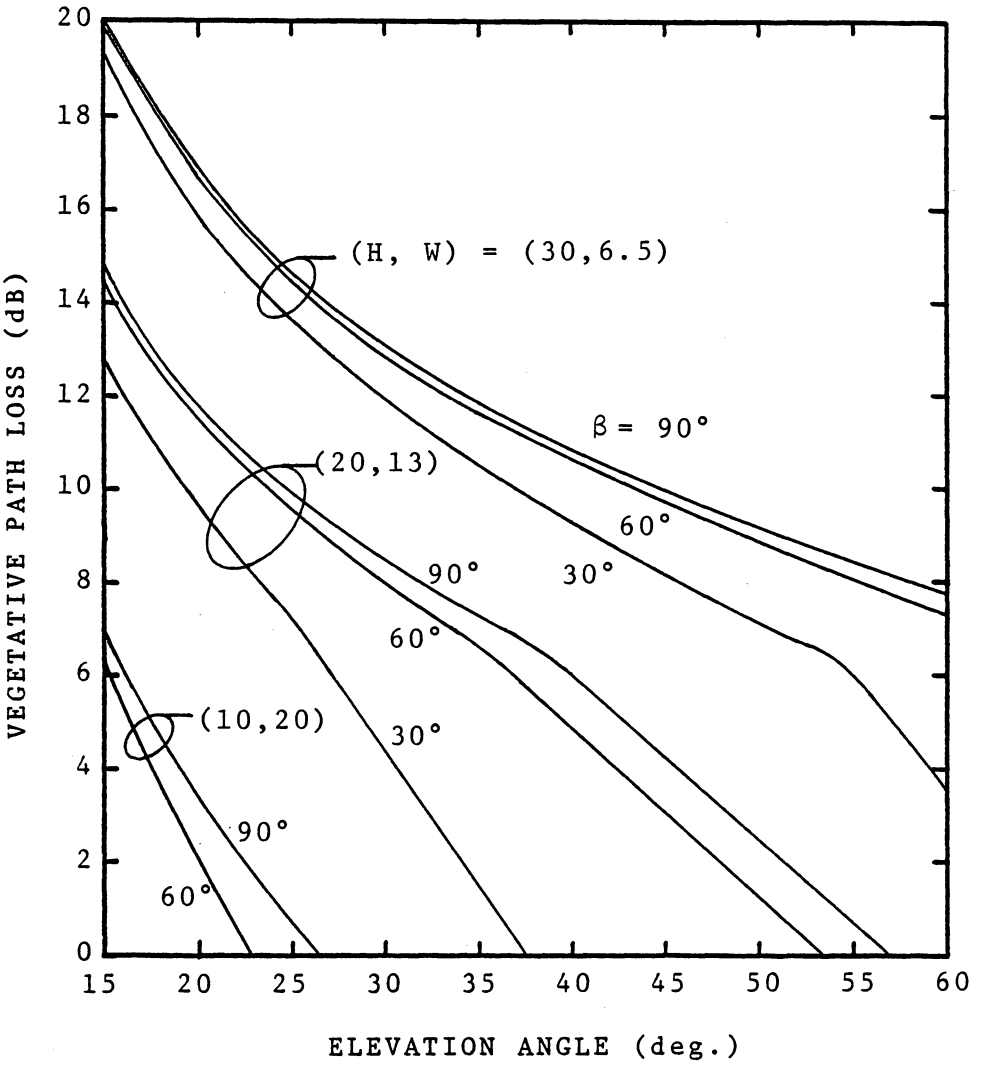

Figure 6.3-8 Vegetative path loss curves showing the effects of bearing angle.

6.4 MODEL EVALUATION

6.4.1 FORM OF THE DISTRIBUTIONS

The equations from Section 6.2 combine the fading statistics from shadowed and unshadowed situations in varying proportions. Consequently, evaluation of this method must begin by assuming some form for the signal level probability distributions.

In the unshadowed situation, a clear choice for the signal level distribution is the Rice distribution if the effects of a specular component are neglected. The discussion of Chapter 2 reviewed the theoretical predictions of a Rice distribution, and this theory was supported by the measurement results presented in Chapter 3. The following discussion then will assume a Rice distribution for the signal level statistics conditioned on no shadowing (vs). The particular Rice distribution used will be specified by the value of K, the dB ratio of the constant component power to the diffuse multipath power. Values for K are expected to range from -8 to -14 dB; typical values used in the subsequent sections are -10 or -11 dB.

The form of the signal level distribution for the vegetatively shadowed case is still not well established. As the measurements discussed in Chapter 3 and 5 have shown, the long term signal variation for shadowed signals appear to be lognormal. The diffuse multipath interference, which will cause the finer, more rapid variations, is still expected to be

Rayleigh distributed but not necessarily at the same power level for unshadowed sites. Consequently, a reasonable assumption for the signal level distribution would be the resulting distribution from the sum of lognormal and Rayleigh random variables. Beckmann [6] and Loo [49] have derived the exact form for this probability density function (pdf), which was given in (4.2-1). Evaluation of that equation must be done numerically and has proven to be a formidable exercise. As a simple first approximation, the signal level distribution for vegetative shadowing (vs) was taken to be lognormal. The effects of diffuse multipath are ignored, but a plain lognormal distribution is much easier to work with and can still offer insight into the performance of the overall statistical model. The lognormal distributions used in the subsequent discussion are specified by their mean and standard deviation in dB.

6.4.2 RICE AND LOGNORMAL

As just mentioned, the shadowed signal was first approximated by a lognormal distribution and the unshadowed signal by a Rice distribution. These two distributions are shown in Figure 6.4-1 for a Rice K of -11 dB and lognormal mean and standard deviation of -7 dB and 6 dB respectively. The lognormal distribution is truncated at the 0 dB level; this was done on the assumption that in the presence of shadowing the signal level would always be less than the LOS value. Also included in Figure 6.4-1 are two distributions mixed from the Rice and lognormal distributions: one is for 5% shadowing, and the other is for 35%. These values of p were reported by the CRC for their MARECS-A data.

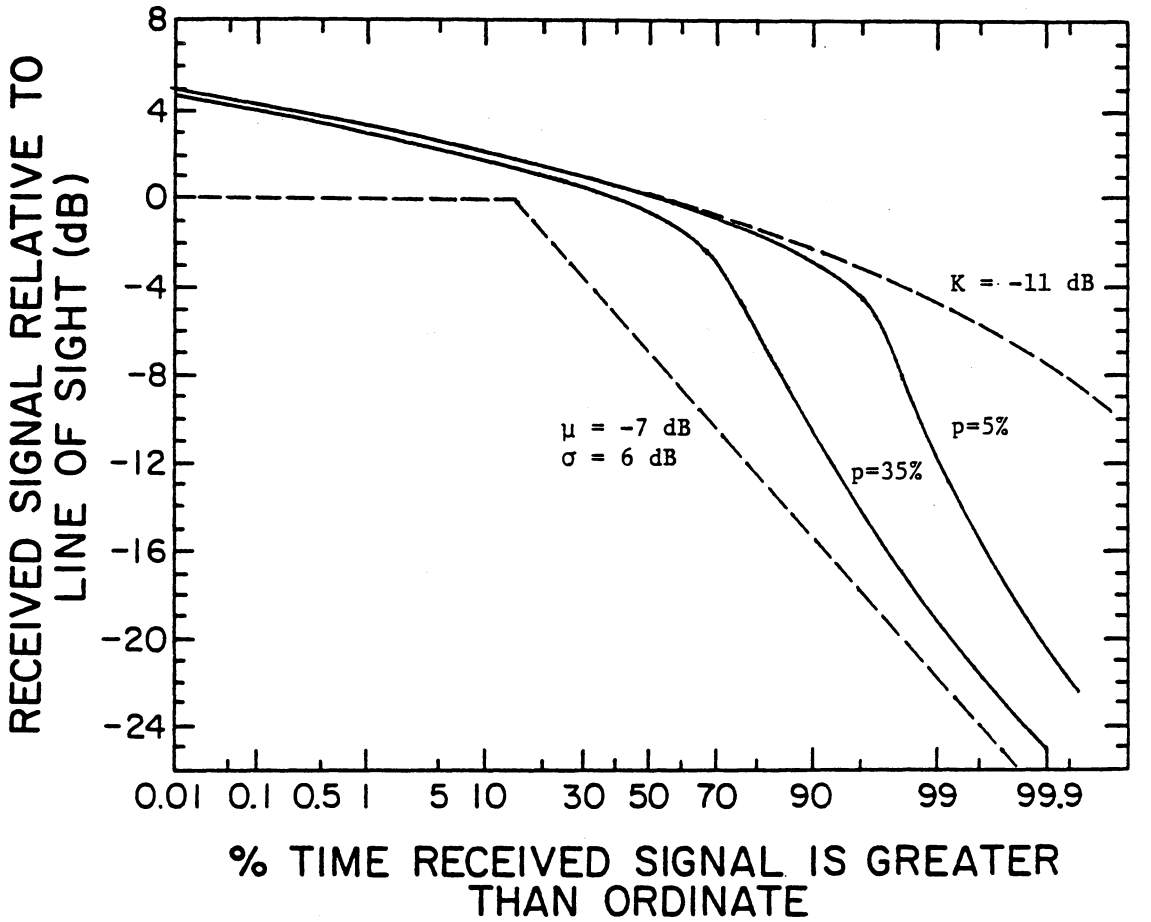

Figure 6.4-1 Rice and lognormal distributions with the overall distribution functions for two proportions of shadowing.

Figure 6.4-2 shows the two mixed distributions of Figure 6.4-1 with the CRC MARECS-A measurement data. This figure indicates that a mixed distribution may be able to model the signal level distribution function with some success or at least with better results than either a Rice or lognormal distribution function alone. Note that the mixed distribution curves exhibit the same pronounced "knee" as the measurement data. The only irregularity in these results is the slight inward slope of the distribution function tails to the right of the knee. This behavior may be attributed to the initial lognormal only assumption; the addition of diffuse multipath effects to the shadowed distribution function should straighten out the tails further and closer resemble the experimental distribution curves.

Next the overall distribution was checked for sensitivity to the parameter K of the Rice distribution. The same lognormal distribution (mean of -7 dB, standard deviation of 6 dB) was mixed with Rice distributions for K of -8 to -14 dB. The results are shown in Figure 6.4-3, 6.4-4, and 6.4-5. These figures show that the distribution functions are moderately insensitive to K especially for the deep fade probabilities. The largest deviation is at the "knee" where it is 3 dB between K of -8 and -14 dB; this deviation reduces for increased shadowing.

The sensitivity of the overall statistics to the amount of shadowing, p, was investigated in a similar manner. The same lognormal and Rice distributions were combined for values of p from 0 to 100%. The distribution function for a p of 0% is the Rice distribution and for a p

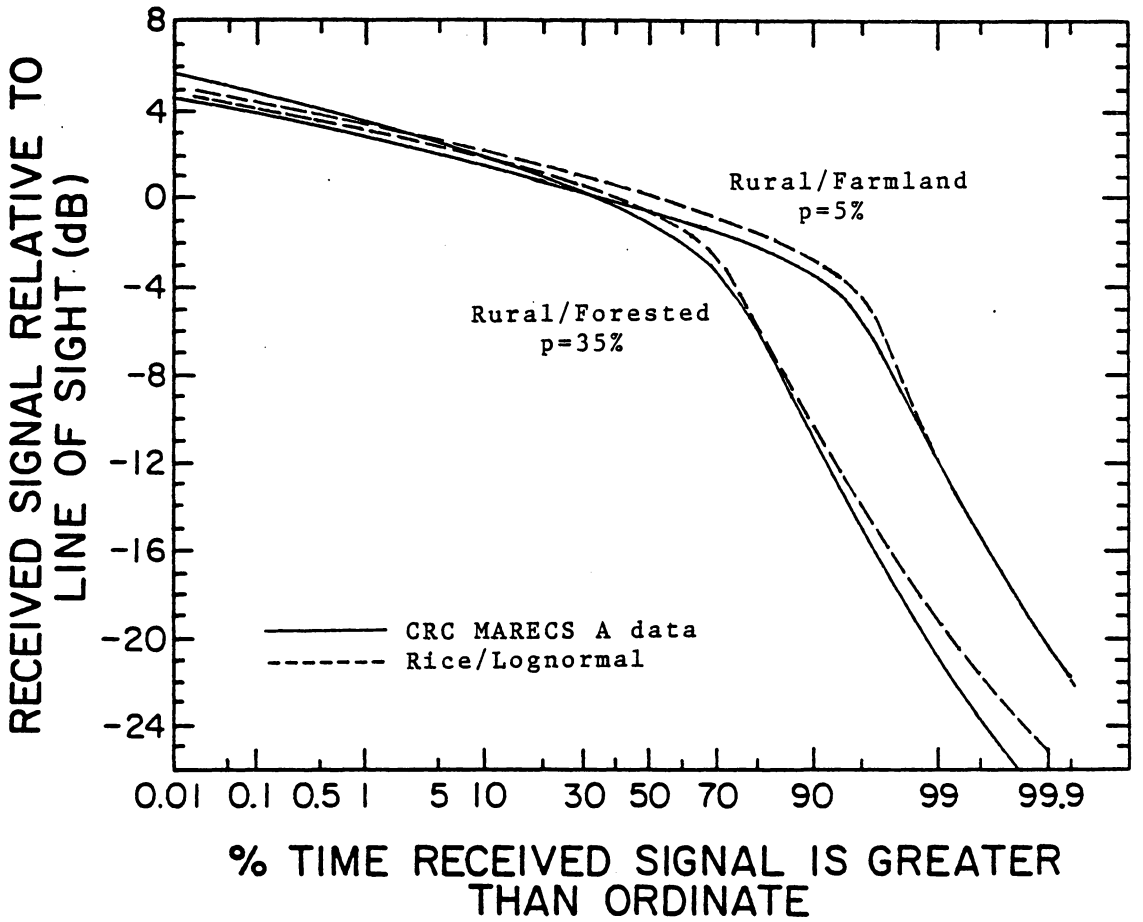

Figure 6.4-2 Distribution functions of measurement data compared to the mixed distributions from Figure 6.4-1.

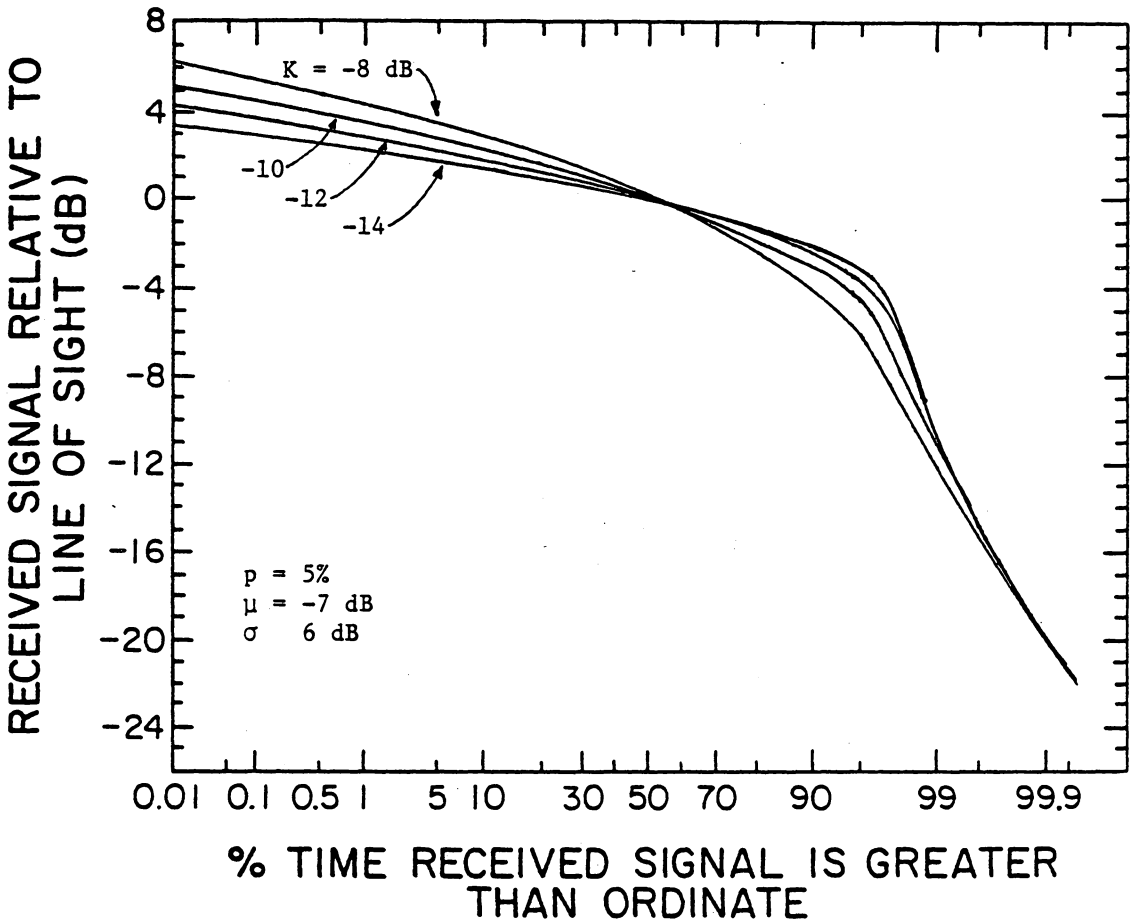

Figure 6.4-3 Variation of the mixed distribution function with K, p = 5%.

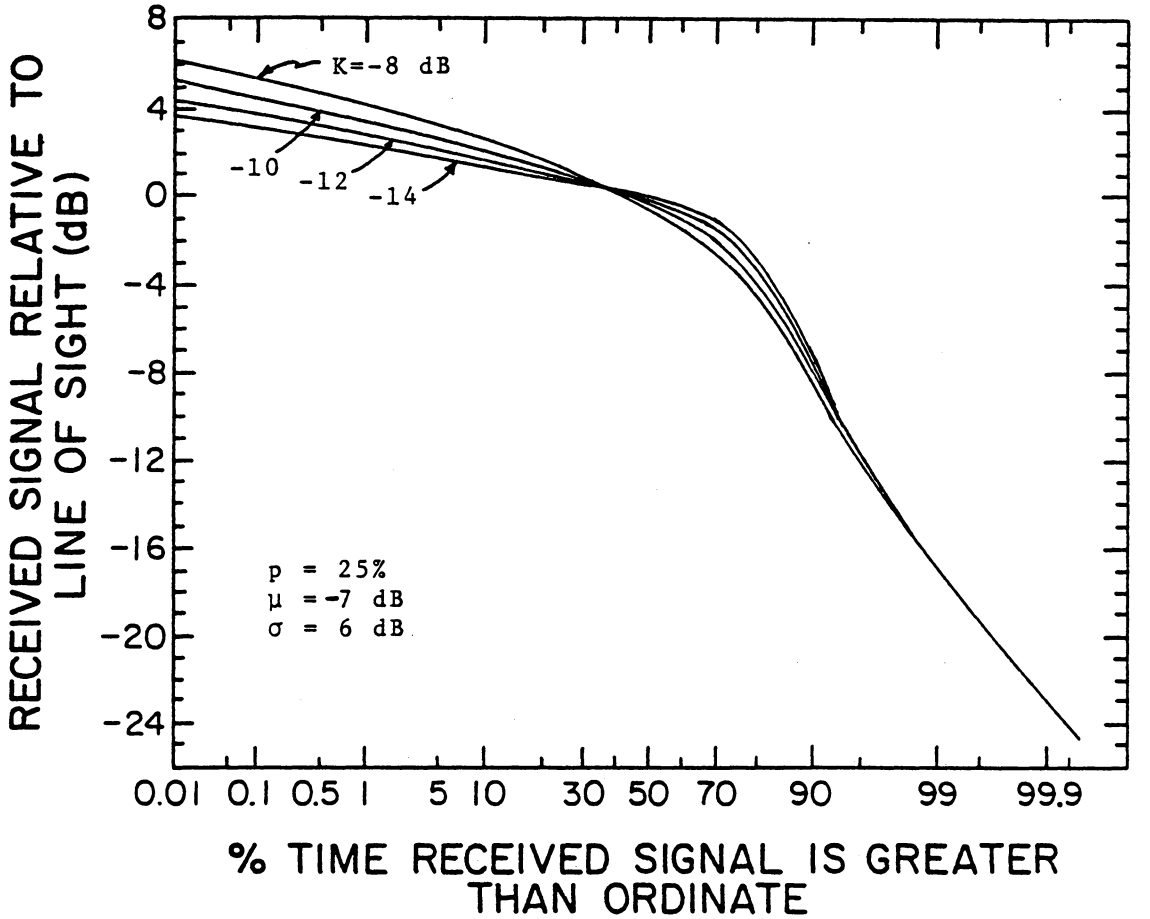

Figure 6.4-4 Variation of the mixed distribution function with K, p = 25%.

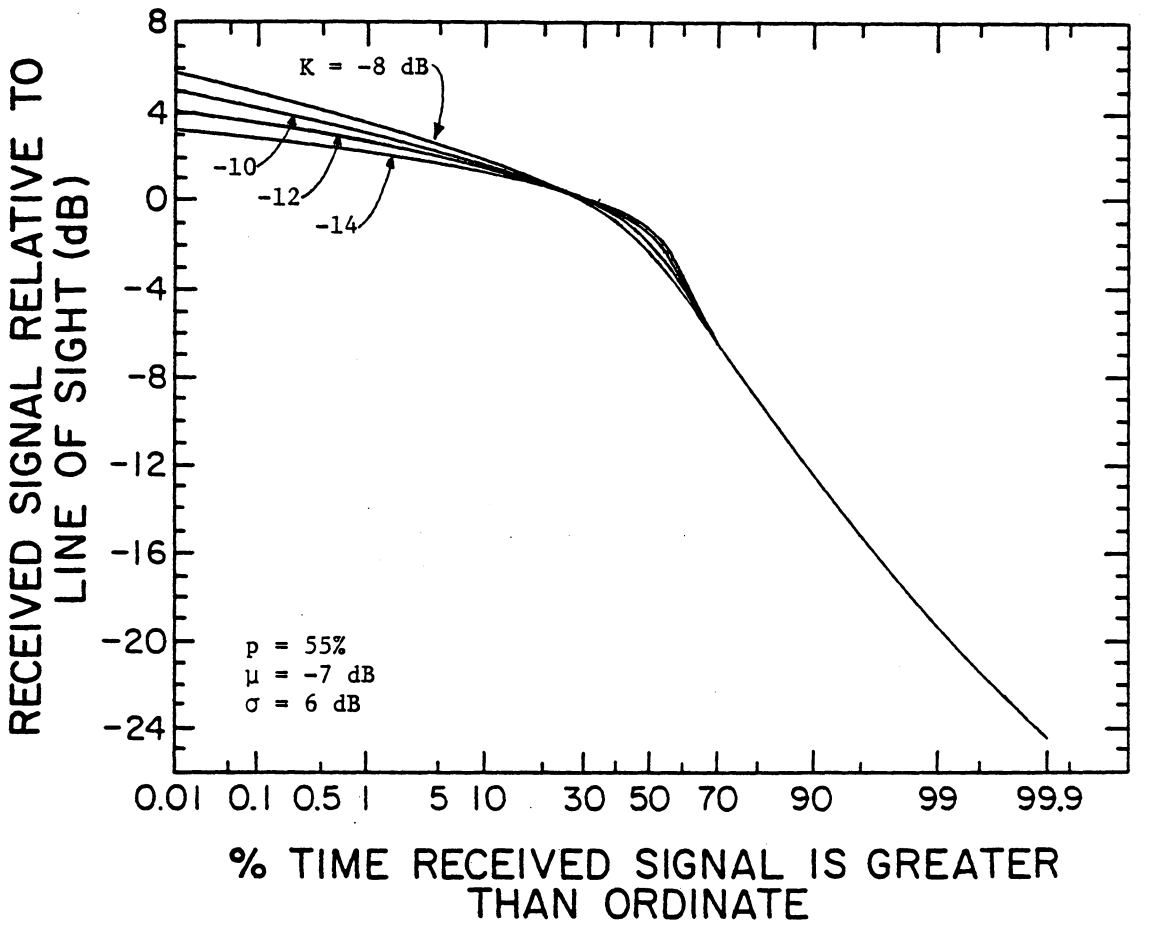

Figure 6.4-5 Variation of the mixed distribution function with K, p = 55%.

of 100% is the truncated lognormal distribution. These results are plotted in Figure 6.4-6. Several observations can be made from this figure. First it shows that even small percentages of shadowing can require significantly larger margins over that needed for 98-99% reliability on unshadowed links. Second, the left hand portion of the distribution function is nearly unaffected by increases in the amount of shadowing except for large p. This same type of behavior was noted in the measurement data discussed in Chapter 3. Third, the "knee" moves to the left with increasing p, the amount of shadowing. Similar behavior was also observed in the measured data. For small p, the "knee" is located at approximately 100%-p%.

6.4.3 VEGETATIVE SHADOWING DISTRIBUTIONS

The previous section synthesized overall signal level distributions from the assumed distributions for shadowed and unshadowed conditions. This section examines the signal level distributions for shadowing solved from the overall distribution functions of measured data and from the Rice distribution used for unshadowed conditions.

This approach was first tried on the CRC MARECS-A rural/forested distribution function because the estimate of tree cover, 35%, was reported. The vegetative shadowing distributions were solved for using several different values of K for the Rice distribution. The results are shown in Figure 6.4-7.

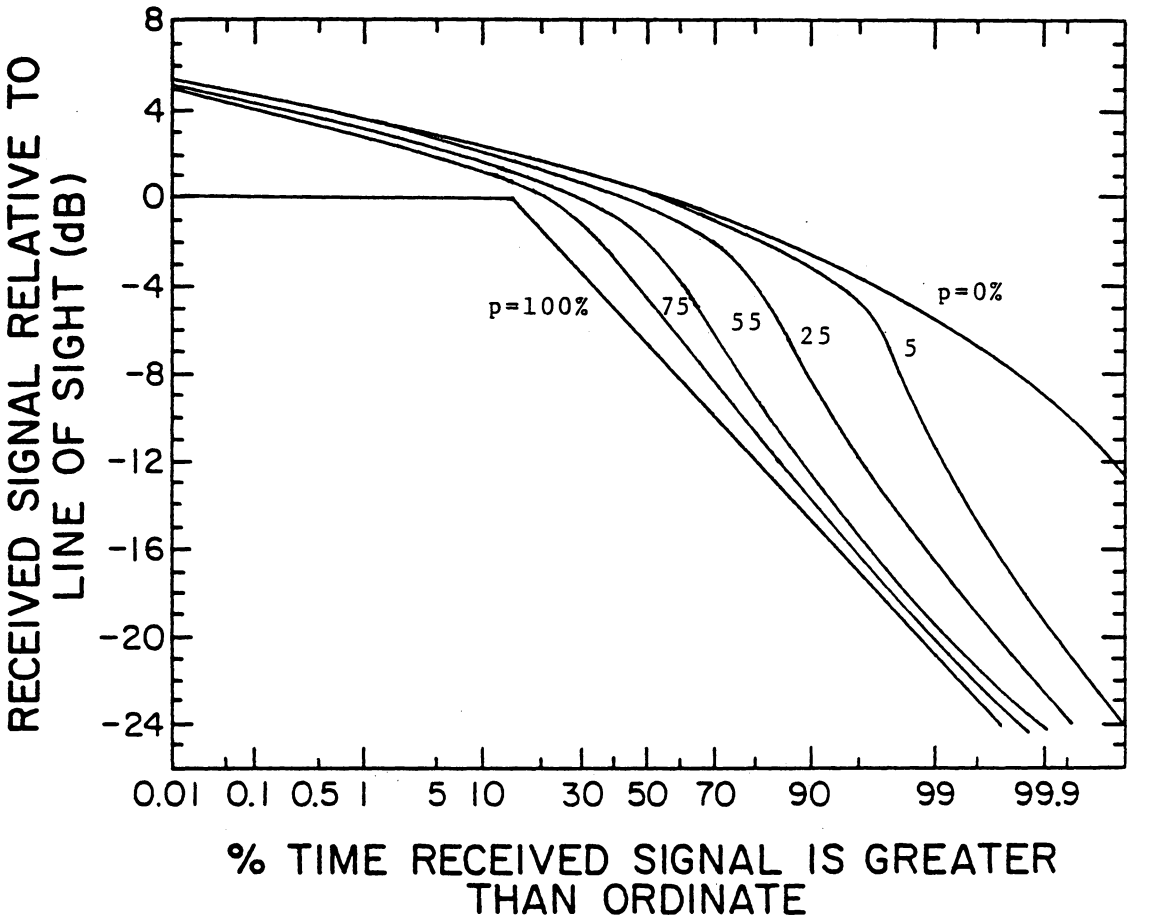

Figure 6.4-6 Variation of the mixed distribution function with p.

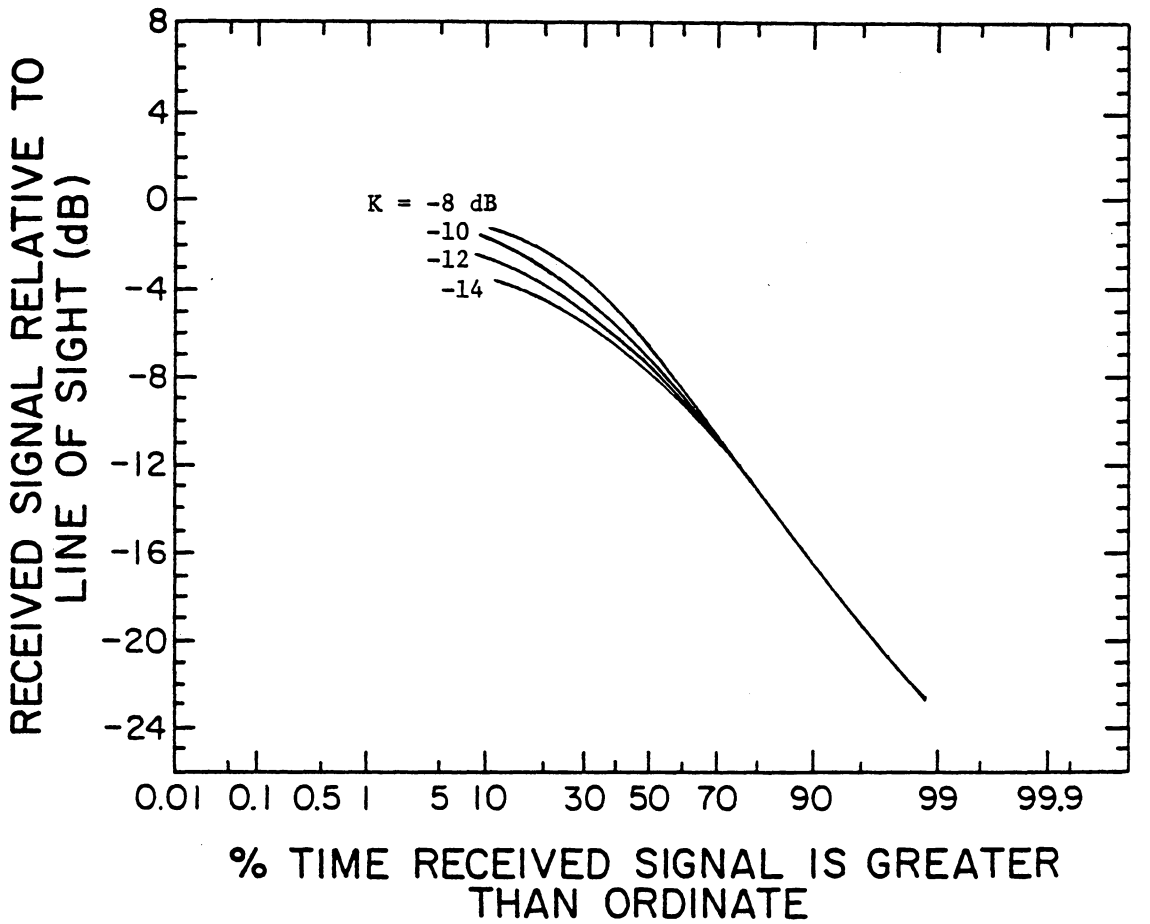

Figure 6.4-7 Vegetative shadowing distribution functions for the CRC MARECS-A rural/forested (6/83) data with Rice distributions removed.

The variation in the results was minimal so the curve for K of -10 dB was chosen. The same method was successfully used on the CRC MARECS-A rural/farmland distribution function. For the 15 to 20° balloon data of Vogel [76], no estimate of the percentage of shadowing was given; an assumption of 25% was used. The vegetative shadowing distributions for these three data sets is given in Figure 6.4-8. A shadowing distribution from the first CRC helicopter experiment is not included because the above method produced poor results.

These vegetative shadowing distribution curves look similar to the ones measured by the CRC in Figure 3.2-2. For comparison, the six distribution curves are overlayed in Figure 6.4-8.

A correlation of these curves to the deterministic model of Section 6.3 can be made by considering the 50% point or median of the distributions. If the distribution is mostly lognormal, then the median may be taken as the mean. Consequently, the path loss model of Section 6.3 may be used to estimate the 50% of the distribution. Most of the data were taken for elevation angles of 20° and travel perpendicular to the source. If an average setback distance of 13 m is assumed with an average tree height of 10 to 20 m, then the mean vegetative path loss is predicted to range from 6.3 dB to 11.8 dB. This range is shown in Figure 6.4-8 by the vertical bar. The agreement appears rather promising.

Another observation to make from Figure 6.4-8 is that the shadowing distribution curves are not perfect straight lines; they deviate from a

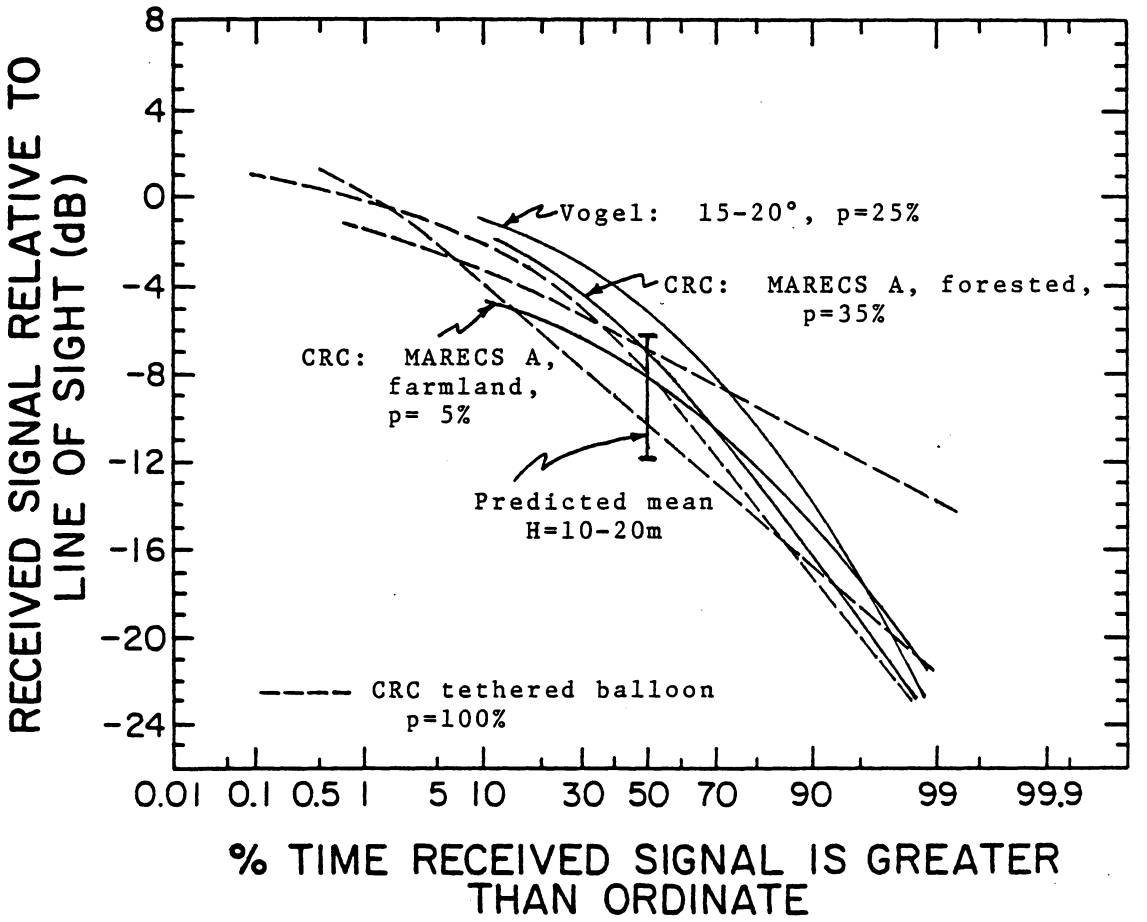

Figure 6.4-8 Vegetative shadowing distributions obtained from measurement data and the CRC tethered balloon measurements (p=100%) compared to the estimated mean vegetative path loss.

true lognormal or truncated lognormal distribution. The deviation may be explained by the influence of the additive Rayleigh multipath interference. These curves look somewhat like the distribution functions that Loo [49] generated for his lognormal plus Rayleigh statistical model shown earlier in Figure 4.2-1. Some preliminary work has been done to numerically evaluate the integral of (4.2-1) to describe the signal level pdf, but standard IMSL integration routines have been inadequate due to the complicated nature of the integrand.

VII CONCLUSIONS

Knowledge of propagation effects on LMSS channels is important for system design and evaluation. The problem is a complex one because of the large number of parameters influencing propagation. This study started with a general look at the whole propagation problem by reviewing the literature for available experimental data and related modeling efforts. The focus then narrowed to analyzing the effects of vegetative shadowing.

The most significant results of this study are:

1. A total probability approach has been proposed to describe the signal fade depth statistics in which

$$G(R) = G(R|vs)p + G(R|\overline{vs})(1-p)$$

and $G(R|vs)$ and $G(R|\overline{vs})$ are examined separately. $G(R|\overline{vs})$ has been predicted by theory and verified by measurement to follow a Rice distribution with a K of approximately -10 dB. The form of $G(R|vs)$ is not as well defined. Measurement indicates that its behavior is lognormal. The total probability approach can be applied to the level crossing rate statistics as well.

2. Mean vegetative loss can be computed using a deterministic path model and the MED model attenuation formula. Calculation of this value can be used to help determine G(R|vs).

Recommendations for future efforts to continue the work of this study would be to:

1. Examine G(R|vs) further as well as the secondary fading statistics, both analytically and experimentally.

2. Expand the parameter dependence of the expression for mean attenuation.

3. Investigate the determination of standard deviation.

4. Explore the characterization of vegetation.

Analytical studies of the signal level fading statistics can be continued by statistical analyses like that of Loo [49] or by software simulation. Simulation has the advantage of being able to more easily account for factors such as Doppler shifts or antenna gain patterns.

This study has shown an obvious need for further propagation measurement data, especially to characterize the effects of vegetation. It would be desirable to build a data base that would include many of the varied conditions where LMSS users are expected to operate. Reporting of

measurement results should be done in a standardized format. This format should include graphical display of the signal level fading statistics (CDF, LCR, and AFD) like those used herein and tabular documentation for the experiment characteristics. A list of important characteristics would include a description of the vegetation in terms of type, height, setback, density, clearance angle, and percentage of locations where blockage is present along with other parameters such as frequency, polarization, antenna type, location, highway type, terrain, elevation angle, and bearing angle. This type of format would aid analytical modeling by giving insight into parameter dependences and would allow for more accurate empirical models.

REFERENCES

[1] American Association of State Highway and Transportation Officials (AASHTO), A Policy on Geometric Design of Highways and Streets, Washington, D.C., 1984.

[2] R. E. Anderson, R. L. Frey, and J. R. Lewis, "Satellite-Aided Mobile Communications Limited Operational Test in the Trucking Industry," Final Report for NASA Contract NAS5-24365 (N81-20338), June 1979.

[3] R. E. Anderson, R. L. Frey, J. R. Lewis, and R. T. Milton, "Satellite-Aided Mobile Communications: Experiments, Applications and Prospects," IEEE Trans. on Vehicular Technology, vol. VT-30, no. 2, pp. 54-61, May 1981.

[4] E. Bahar, "Full-wave solutions for the scattered radiation fields from rough surfaces with arbitrary slope and frequency," IEEE Trans. on Antennas and Propagation, vol. AP-28, pp. 11-21, Jan. 1980.

[5] P. Beckmann and A. Spizzichino, The Scattering of Electromagnetic Waves from Rough Surfaces, Pergamon Press, New York, 1963.

[6] P. Beckmann, Probability in Communication Engineering, Harcourt, Brace & World, New York, 1967.

[7] D. Bodson, G. F. McClure, and S. R. McConoughey, editors, Land-Mobile Communications Engineering, IEEE Press, New York, 1984.

[8] G. S. Brown and W. J. Curry, "An analytical study of wave propagation through foliage," Final report for contract F19618-78-C-0159, Appl. Sci. Assoc., Apex, NC, 1980.

[9] G. S. Brown and W. J. Curry, "A theory and model for wave propagation through foliage," Radio Science, vol. 17, pp. 1027-1036, Sept.-Oct. 1982.

[10] G. S. Brown, Seminar presented at VPI&SU on current research for rough surface scattering, May 10, 1985.

[11] K. Bullington, "Radio propagation fundamentals," Bell System Technical Journal, vol. 36, pp. 114-122, May 1957.

[12] J. S. Butterworth and E. E. Matt, "The characterization of propagation effects for land mobile satellite services," Proceedings of IEE International Conference on Satellite Systems for Mobile Communication and Navigation, London, pp. 51-54, June 1983.

[13] J. S. Butterworth, "Propagation Measurements for Land-Mobile Satellite Services in the 800 MHz Band," Communications Research Centre, Department of Communications, Canada, Aug. 1984.

[14] J. S. Butterworth, "Propagation Measurements for Land-Mobile Satellite Systems at 1542 MHz," Communications Research Center, Department of Communications, Canada, Aug. 1984.

[15] J. S. Butterworth, "The description and evaluation of a mobile communications channel simulator," Proceedings of the Propagation Workshop in Support of MSAT-X, JPL, Pasadena, CA, pp. 4.3-4.21, Jan. 1985.

[16] M. G. R. Cannell, World Forest Biomass and Primary Production Data, Academic Press, London, 1982.

[17] CCIR XIVth Plenary Assembly, "Influence of terrain irregularities and vegetation on tropospheric propagation," Report 236-4, Volume 5, International Telecommunications Union, Geneva, Switzerland, 1978.

[18] CCIR XVth Plenary Assembly, "Influence of terrain irregularities and vegetation on tropospheric propagation," Report 236-5, Volume 5, International Telecommunications Union, Geneva, Switzerland, 1982.

[19] CCIR XVth Plenary Assembly, "Propagation data for maritime and land-mobile satellite systems above 100 MHz," Report 884, Volume 5, International Telecommunications Union, Geneva, Switzerland, 1982.

[20] CCIR XVth Plenary Assembly, "Propagation data required by mobile services using communication or radiodetermination satellite systems," Study Programme 7C-1/5, Volume 5, International Telecommunications Union, Geneva, Switzerland, 1982.

[21] CCIR Interim Working Party 5/2, "Propagation data for land-mobile satellite systems for frequencies above 100 MHz," Document 5/12-E, Mar. 1983.

[22] R. H. Clarke, "A statistical theory of mobile-radio reception," Bell System Technical Journal, vol. 47, pp. 957-1000, July-Aug. 1978.

[23] CyberCom Corporation, "Proposed Forest Transmission Experiments," for U.S. Army Communications-Electronics Command, Ft. Monmonth, NJ, Contract DAK80-81-C-0136, June 1984.

[24] F. Davarian and J. Sumida, "Channel simulator tests digital mobile radios," Microwaves and RF, vol. 23, pp. 115-118, Aug. 1984.

[25] F. Davarian, "JPL's mobile communications channel hardware simulator," Proceedings of the Propagation Workshop in Support of MSAT-X, JPL, Pasadena, CA, pp. 2.5-2.18, Jan. 1985.

[26] D. Divsalar, "Software simulation of the LMSS propagation channel," Proceedings of the Propagation Workshop in Support of MSAT-X, JPL, Pasadena, CA, pp. 2.19-2.46, Jan. 1985.

[27] T. S. Elias, The Complete Trees of North America, Van Nostrand Reinhold Company, New York, 1980.

[28] W. L. Flock, "Propagation effects on satellite systems at frequencies below 10 GHz: A handbook for satellite system design," NASA Reference Publication 1108, Dec. 1983.

[29] M. S. Frankel, "L-band Forest Measurements," Packet Radio Temporary Note 254, SRI International, Menlo Park, CA, 1978.

[30] M. J. Gans, "A power-spectral theory of propagation in the mobile-radio environment," IEEE Trans. on Vehicular Technology, vol. 21, pp. 27-38, Feb. 1972.

[31] F. M. Gardner, "Multipath Link and Modem Design for Satellite Mobile Communications," Gardner Research Co., Palo Alto, CA, Aug. 1983.

[32] E. J. Haakinson and R. D. Jennings, "Land mobile radio system performance model for VHF and higher frequencies over irregular terrain," Proceedings of IEEE 28th Vehicular Technology Conference, pp. 512-517, 1978

[33] H. T. Head, "The influence of trees on television field strengths at ultra-high frequencies," Proceedings of the IRE, vol. 48, pp. 1016-1020, June 1960.

[34] G. C. Hess, "Land Mobile Satellite Path Loss Measurements," Third Year ATS-6 Experiment Final Report, Motorola Inc., Schaumberg,IL, Sept. 6, 1978.

[35] G. C. Hess, "Land-Mobile Satellite Excess Path Loss Measurements," IEEE Trans. on Vehicular Technology, vol. VT-29, pp. 290-297, May 1980.

[36] G. C. Hess, private communication, Nov. 15, 1984.

[37] R. W. Huck, J. S. Butterworth, and E. E. Matt, "Propagation Measurements for Land Mobile Satellite Services," Proceedings of IEEE 33rd Vehicular Technology Conference, pp. 265-268, 1983.

[38] G. A. Hufford, R. W. Hubbard, P. F. Sass, L. E. Pratt, J. E. Adams, and S. J. Paulson, "Wideband Propagation Measurements in the Presence of Forests," U.S. Army Communications Electronics Command, Ft. Monmonth, NJ, Tech. Rep. 82-CS029-F, Jan. 1982.

[39] W. C. Jakes, Microwave Mobile Communications, Wiley, New York, 1974.

[40] V. Jamnejad, "Ground multipath in TOPEX's precision orbit determination tracking system," JPL Interoffice Memorandum 3365-84-003, Jet Propulsion Lab., Pasadena, CA, Jan. 9, 1985.

[41] G. H. Knouse, "Terrestrial/land mobile satellite considerations, NASA plans, and critical issues," IEEE Trans. on Vehicular Technology, vol. VT-29, pp. 370-374, Nov. 1980.

[42] G. H. Knouse and P. A. Castruccio, "The concept of an integrated terrestrial/land mobile satellite system," IEEE Trans. on Vehicular Technology, vol. VT-30, pp. 97-101, Aug. 1981.

[43] A. H. Lagrone and C. W. Chapman, "Some propagation characteristics of high UHF signals in the immediate vicinity of trees," IRE Trans. on Antennas and Propagation, vol. AP-9, pp. 487-491, Sept. 1961.

[44] A. H. Lagrone, "Propagation of VHF and UHF electromagnetic waves over a grove of trees in full leaf," IEEE Trans. on Antennas and Propagation, vol. AP-25, pp. 866-869, Nov. 1977.

[45] R. H. Lang, A. Schneider, S. Seker, and F. J. Altman, "UHF Radiowave Propagation Through Forests," CyberCom Technical Report CTR-108-01, Sept. 1982.

[46] R. H. Lang, A. Schneider, F. J. Altman, and K. Truang, "UHF Radiowave Propagation Through Forests," CyberCom Technical Report CTR-108-06, May 1984.

[47] W. C. Y. Lee, Mobile Communications Engineering, McGraw Hill, New York, 1982.

[48] S. H. Lin, "Statistical behavior of a fading signal," Bell System Technical Journal, vol. 50, pp. 3211-3270, Dec. 1971.

[49] C. Loo, "A statistical model for a land mobile satellite link," Proceedings of the 1984 IEEE International Communications Conference, pp. 588-594, 1984.

[50] P. L. McQuate et al, "Tabulations of Propagation Data Over Irregular Terrain in the 230-9200 MHz Frequency Range, Part I, Gunbarrel Hill Receiver Site," ESSA TR ERL 65-ITS 58-1, Institute for Telecommunications Sciences (ITS), Boulder, CO, Mar. 1968.

[51] "MSAT-X Quarterly," Jet Propulsion Lab., Pasadena, CA, no. 1, Oct. 1984.

[52] F. Naderi, W. J. Weber, and G. H. Knouse, "NASA's mobile satellite communications program; ground and space segment technologies," Proceedings of the 35th Congress of the International Astronautical Federation, Lausanne, Switzerland, Oct. 1984.

[53] R. A. Nelson, "UHF Propagation in Vegetative Media," Final report for project 8998, SRI International, Apr. 1980.

[54] K. A. Norton, L. E. Vogler, W. V. Mansfield, and P. J. Short, "The probability distribution of the amplitude of a constant vector plus a Rayleigh distributed vector," Proceedings of the IRE, Vol. 43, pp. 1354-1361, Oct. 1955.

[55] Y. Okumura, E. Ohmori, T. Kawano, and K. Fukuda, "Field strength and its variability in VHF and UHF land-mobile radio service," Rev. Elec. Commun. Lab., vol. 16, pp. 825-873, Sept.-Oct. 1968. (reprinted in [7])

[56] A. Papoulis, Probability, Random Variables, and Stochastic Processes, McGraw-Hill, New York, 1965.

[57] R. I. Presnell, "JTIDS Ground-to-Ground Propagation Measurements," SRI International for U.S. Army CORADCOM, Final Rep., contract MDA903-78-C-0126, June 1980.

[58] D. O. Reudink and M. F. Wazowicz, "Some propagation experiments relating foliage loss and diffraction loss at X-band and UHF frequencies," IEEE Trans. on Vehicular Technology, vol. VT-22, pp. 114-122, Nov. 1973.

[59] D. O. Reudink, "Properties of mobile radio propagation above 400 MHz," IEEE Trans. on Vehicular Technology, vol. VT-23, pp. 143-159, Nov. 1974. (reprinted in [7])

[60] D. O. Reudink, "Estimates of path loss and radiated power for UHF mobile satellite systems," Bell System Technical Journal, vol. 62, pp. 2493-2512, Oct. 1983.

[61] P. L. Rice, "Some effects of buildings and vegetation on VHF/UHF propagation," IEEE Mountain West EMC Conference Record, pp. 1-10, Nov. 1971.

[62] A. B. Salmasi, "Land mobile satellite system channel simulation and propagation study," Minutes of the Propagation/MSAT-X Meeting: Attachment D, Jet Propulsion Lab., Pasadena, CA, July 1983.

[63] A. B. Salmasi, "Multipath fading references," JPL Interoffice Memo 3391-84-27, Jet Propulsion Lab., Pasadena, CA, Feb. 1984.

[64] A. B. Salmasi, A. B. Springett, J. C. Sumida, and J. J. Richter, "Land Mobile Satellite Service (LMSS) Channel Simulator: An End-to-End Hardware Simulation and Study of the LMSS Communications Link," Jet Propulsion Lab., Pasadena, CA, NASA-CR-173744, May 1984.

[65] W. A. Sandrin, "Land-mobile satellite start-up systems," COMSAT Technical Review, vol. 14, pp. 137-164, Spring 1984.

[66] P. F. Sass, "Propagation measurements for UHF spread spectrum mobile communications," IEEE Trans. on Vehicular Technology, vol. VT-32, pp. 168-176, May 1983.

[67] J. A. Saxton and J. A. Lane, "VHF and UHF reception and effects of trees and other obstacles," Wireless World, vol. 61, pp. 229-232, May 1955.

[68] A. Schneider and F. Altman, "Proposed Forest Transmission Experiments," CyberCom Technical Report CTR-108-07, Contract DAAK80-81-C-0136, June 1984.

[69] E. K. Smith, J. F. Cavanagh, and W. L. Flock, "Propagation effects for land mobile satellite systems," Proceedings of the National Radio Science Meeting, Jan. 1983.

[70] W. L. Stutzman, F. W. Colliver, and H. S. Crawford, "Microwave transmission measurements for estimation of the weight of standing pine trees," IEEE Trans. on Antennas and Propagation, vol. AP-27, pp. 22-26, Jan. 1979.

[71] T. Tamir, "On radio wave propagation in forest environments", IEEE Trans. on Antennas and Propagation, vol. AP-15, pp. 806-817, Nov. 1967.

[72] B. Trevor, "Ultra-high frequency propagation through woods and underbrush," RCA Review, vol. 5, pp. 97-100, July 1940.

[73] U. S. Army Communications - Electronics Command, "Statement of Work: Experiment Planning and Engineering Direction For A Wideband Propagation Measurement Program," Solicitation No. DAAB07-85-R-K520, Apr. 30, 1984

[74] W. J. Vogel, "PELMOSS balloon experiment at 869 MHz (status report)," Minutes of the Propagation/MSAT-X Meeting: Attachment B, Jet Propulsion Lab., Pasadena, CA, July 1983.

[75] W. J. Vogel and G. W. Torrence, "Measurement Results From a Balloon Experiment Simulating Land Mobile Satellite Transmissions," MSAT-X Report No. 101, (submitted for JPL Contract 956520), Apr. 1984.

[76] W. J. Vogel and E. K. Smith, "Propagation considerations in land-mobile satellite transmission," MSAT-X Report No. 105, NASA-JPL, Pasadena, CA, pp. 1.5-1.18, Jan. 1985.

[77] W. J. Vogel, "PELMOSS Balloon Experiments," Proceedings of the Propagation Workshop in Support of MSAT-X , JPL, Pasadena, CA, pp. 1.5-1.18, Jan. 1985.

[78] M. A. Weissberger et al, "Radio Wave Propagation: A Handbook of Practical Techniques for Computing Basic Transmission Loss and Field Strength," Electromagnetic Compatability Analysis Center, Report No. ECAC-HDBK-82-049, Sept. 1982.

[79] M. A. Weissberger, "An Initial Critical Summary of Models for Predicting the Attenuation of Radio Waves by Trees," ESD-TR-81-101, Electromagnetic Compatibility Analysis Center, Annapolis, MD, July 1982.

The vita has been removed from the scanned document